

AFRL-SN-RS-TM-2000-2
In-House Technical Memorandum
August 2000



**THE DESIGN, FABRICATION AND TEST OF
FEEDS, RADIATING ELEMENTS AND LINEAR
SUBARRAYS FOR A SMALL PROTOTYPE
PLANAR ARRAY ANTENNA**

Michael J. Callahan

APPROVED FOR PUBLIC RELEASE; DISTRIBUTION UNLIMITED.

20001121 021

**AIR FORCE RESEARCH LABORATORY
SENSORS DIRECTORATE
ROME RESEARCH SITE
ROME, NEW YORK**

DTIC QUALITY INSPECTED 4

This report has been reviewed by the Air Force Research Laboratory, Information Directorate, Public Affairs Office (IFOIPA) and is releasable to the National Technical Information Service (NTIS). At NTIS it will be releasable to the general public, including foreign nations.

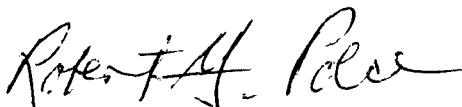
AFRL-SN-RS-TM-2000-2 has been reviewed and is approved for publication.

APPROVED:



GERARD J. GENELLO
Chief, Radar Signal Processing Branch
Sensors Directorate

FOR THE DIRECTOR:



ROBERT G. POLCE
Chief, Rome Operations Office
Sensors Directorate

If your address has changed or if you wish to be removed from the Air Force Research Laboratory Rome Research Site mailing list, or if the addressee is no longer employed by your organization, please notify AFRL/SNRT, 26 Electronic Pky, Rome, NY 13441-4514. This will assist us in maintaining a current mailing list.

Do not return copies of this report unless contractual obligations or notices on a specific document require that it be returned.

REPORT DOCUMENTATION PAGE			Form Approved OMB No. 0704-0188	
Public reporting burden for this collection of information is estimated to average 1 hour per response, including the time for reviewing instructions, searching existing data sources, gathering and maintaining the data needed, and completing and reviewing the collection of information. Send comments regarding this burden estimate or any other aspect of this collection of information, including suggestions for reducing this burden, to Washington Headquarters Services, Directorate for Information Operations and Reports, 1215 Jefferson Davis Highway, Suite 1204, Arlington, VA 22202-4302, and to the Office of Management and Budget, Paperwork Reduction Project (0704-0188), Washington, DC 20503.				
1. AGENCY USE ONLY (Leave blank)		2. REPORT DATE August 2000		3. REPORT TYPE AND DATES COVERED In-House, 1992-1994, Additions Made In 1997
4. TITLE AND SUBTITLE The Design, Fabrication and Test of Feeds, Radiating Elements and Linear Subarrays for a Small Prototype Planar Array Antenna			5. FUNDING NUMBERS PR: 4506 TA: 14 WU: P9	
6. AUTHOR(S) Michael J. Callahan				
7. PERFORMING ORGANIZATION NAME(S) AND ADDRESS(ES) AFRL/SNRT 26 Electronic Parkway Rome, NY 13441-4514			8. PERFORMING ORGANIZATION REPORT NUMBER AFRL-SN-RS-TM-2000-2	
9. SPONSORING/MONITORING AGENCY NAME(S) AND ADDRESS(ES) AFRL/SNRT 26 Electronic Parkway Rome, NY 13441-4514			10. SPONSORING/MONITORING AGENCY REPORT NUMBER AFRL-SN-RS-TM-2000-2	
11. SUPPLEMENTARY NOTES F30602-92-C-0056 Integrated Sensors, Inc. (ISI), 502 Court Street, Suite 210, Utica, NY 13502. Christofer Wilder, Ronald Gauss & Jerry Olmstead of ISI taught/assisted Virginia Ross, Jeffrey Carlo, Lorraine Flanders, Clifford Tsao & Michael Callahan (author) of Rome Laboratory (now part of AFRL). John McNamara (AFRL) also provided key technical guidance.				
12a. DISTRIBUTION AVAILABILITY STATEMENT APPROVED FOR PUBLIC RELEASE; DISTRIBUTION UNLIMITED.			12b. DISTRIBUTION CODE	
13. ABSTRACT (Maximum 200 words) A few years ago, a team of people at Rome Laboratory (now part of Air Force Research Laboratory) designed, fabricated and tested feeds, radiating elements and linear subarrays for a small prototype planar array antenna of the sort envisioned for someday growing into a notional full-sized antenna for a notional radar system to fit within a notional unmanned aerial vehicle (UAV). The author of this document was a member of that team. We started small, with several limiting qualifications imposed for simplicity's sake. The prototype array that we intended to design was considerably smaller and simpler than the larger, more complex model of a kind that might form part of a radar system inside a UAV someday. The prototype array was planar, linearly polarized, had a rectangular aperture, operated at X-band (roughly 10 Ghz) with a very narrow (50 Mhz) 3 dB bandwidth, had a fixed beam (no electronic beamsteering capability), was receive-only (not capable of handling high power) and possessed a microstrip corporate/series feed structure with rectangular microstrip patch radiating elements having inset feed points. Only one design iteration was attempted, so the final results were understandably poor. Though the objectives of this project weren't met, the team members feel that if the work had been continued through another design iteration, better results could have been achieved.				
14. SUBJECT TERMS Microstrip Patch Radiating Elements, Microstrip Patch Antennas, Antenna Arrays			15. NUMBER OF PAGES 160	
			16. PRICE CODE	
17. SECURITY CLASSIFICATION OF REPORT UNCLASSIFIED	18. SECURITY CLASSIFICATION OF THIS PAGE UNCLASSIFIED	19. SECURITY CLASSIFICATION OF ABSTRACT UNCLASSIFIED	20. LIMITATION OF ABSTRACT UL	

TABLE OF CONTENTS

LIST OF FIGURES	iii
ACKNOWLEDGEMENTS	vii
FORWARD	viii
CHAPTER 1 DOWNSELECTION OF RADAR MISSIONS, RADAR REQUIREMENTS AND SIMPLIFYING ASSUMPTIONS, AND ANTENNA REQUIREMENTS	1
CHAPTER 2 ANTENNA SIZING, LATTICE STRUCTURE AND ELEMENT CHOICE	8
CHAPTER 3 DESIGN OF THE PROTOTYPE ARRAY AZIMUTH AND ELEVATION FEED NETWORKS	11
CHAPTER 4 TEST CIRCUIT FABRICATION	20
CHAPTER 5 S-PARAMETER MEASUREMENT CAMPAIGN RESULTS	23
CHAPTER 6 FARFIELD ANTENNA PATTERN MEASUREMENT RESULTS	25
CHAPTER 7 SUMMARY	27
REFERENCES	28
APPENDIX A COMMONLY ENCOUNTERED DISCONTINUITIES IN MICROSTRIP LINES - THEIR USES, PHYSICAL AND ELECTRICAL IMPACT ON CIRCUITS, AND LUMPED ELEMENT EQUIVALENT CIRCUITS	29
APPENDIX B CAVITY MODEL FOR A MICROSTRIP PATCH ANTENNA	45
APPENDIX C TEST PLAN	48
APPENDIX D DETAILED DRAWINGS OF THE IMAGES SENT TO MPC FOR ETCHING ON THE TMM-3 AND TMM-6 SUBSTRATE BOARDS	51
APPENDIX E COLOR COPIED PHOTOGRAPHS OF SELECTED TEST CIRCUITS AS THEY LOOKED AFTER THE TESTING AND TUNING PHASE WAS COMPLETED	58
APPENDIX F PLOTS ILLUSTRATING THE MEASURED AND SIMULATED S21 DATA COMPILED FOR THE HALF AZIMUTH AND HALF ELEVATION FEED OUTPUT PORTS VERSUS FREQUENCY	67
APPENDIX G PLOTS ILLUSTRATING THE MEASURED S21 DATA COMPILED FOR THE HALF ELEVATION FEEDS AT BAND CENTER AND AT THE BAND EDGES, ALONG WITH SIMULATED AND THEORETICAL S21 DATA AT BAND CENTER	72
APPENDIX H SELECTED SMITH CHARTS SHOWING RESONANCE LOOPS FOR ISOLATED MICROSTRIP PATCH ELEMENTS MEASURED WITH AN HP 8510C NETWORK ANALYZER	75

APPENDIX I SELECTED PLOTS SHOWING S11 VERSUS FREQUENCY FOR THE TMM-3 ELEVATION ARRAY AND FOR AN ISOLATED TMM-6 MICROSTRIP PATCH MEASURED ON THE HP 8510C NETWORK ANALYZER	80
APPENDIX J ISOLATED MICROSTRIP PATCH FARFIELD ANTENNA PATTERNS MEASURED WITH AN HP 8510C NETWORK ANALYZER	83
APPENDIX K FARFIELD ANTENNA PATTERNS MEASURED IN THE ANECHOIC CHAMBER AT TANNER HILL	86
APPENDIX L MODELING AN ISOLATED, RECTANGULAR, INSET FED TMM-6 MICROSTRIP PATCH AND ITS FEEDLINE BY MEANS OF TRIANGULAR BASIS FUNCTIONS PREDICTED LARGE VSWR VALUES (GROSS IMPEDANCE MISMATCH BETWEEN THE FEEDLINE AND THE PATCH)	109

LIST OF FIGURES

Figure 1. Sketch Of A Single Wilkinson Power Splitter (Divider)	17
Figure 2. Basic Half Elevation Feed Structure Employed In Both The TMM-3 And TMM-6 Designs	18
Figure 3. Drawing Of A Microstrip Patch Element Having An Inset Feed	19
Figure 4. Sketch Of A Mitered Bend With Important Dimensions Indicated	33
Figure 5. Current Distribution On A Microstrip Meander Line	34
Figure 6. Tangential Electric Field Distribution Over A Microstrip Meander Line	35
Figure 7. The Geometry Of Right Angle And Mitered Bend Discontinuities As Utilized In Figure 8 For A Mitered Bend	36
Figure 8. Magnitude Of Electric Surface Currents At A Mitered Bend	37
Figure 9. Sketch Of A Microstrip T-Junction With Important Dimensions Indicated	38
Figure 10. The Geometry Of A Mitered T-Junction As Utilized In Figure 11	39
Figure 11. Magnitude Of Electric Surface Currents On A Mitered T-Junction	40
Figure 12. A Step In Line Width For A Microstrip Line With Charge Buildup Indicated By Dots In The Corners	41
Figure 13. An Open End Discontinuity, With Charge Buildup At The End Shown As Dots, Forming An Open Circuit Matching Stub Much Like The Ones Used In The Plated Through Via Hole Test Circuits	42
Figure 14. Geometry Of Unmitered And Mitered Open End Discontinuities As Utilized In Figure 15 For The Mitered Open End Discontinuity	43
Figure 15. Magnitude Of Electric Surface Currents On A Mitered Open End Discontinuity	44
Figure 16. Development Of The Cavity Model Of A Microstrip Element	46
Figure 17. Rectangular Microstrip Patch Antenna (No Inset Feed)	47
Figure 18. TMM-3 Board 1	52
Figure 19. TMM-3 Board 1 – Half Azimuth Feed	53
Figure 20. TMM-3 Board 1 – Full Elevation Feed And Microstrip Patches	54
Figure 21. TMM-3 Board 2	55
Figure 22. TMM-6 Board	56
Figure 23. TMM-6 Board – Full Elevation Feed And Microstrip Patches	57

Figure 24. Four Isolated Patch Circuits In Their Test Fixtures	59
Figure 25. Tuned TMM-3 Full Elevation Array	60
Figure 26. 3 dB Power Divider And Plated Through Via Hole Circuits	61
Figure 27. Elevation Feedline-Only Test Circuits	62
Figure 28. E-Plane Patch Array Test Circuits	63
Figure 29. H-Plane Patch Array Test Circuits	64
Figure 30. TMM-3 Half Azimuth Feed	65
Figure 31. TMM-6 Full Elevation Array	66
Figure 32. Measured TMM-3 Half Azimuth Feed S21 Magnitudes Versus Frequency, Ports 1-16	68
Figure 33. Measured TMM-3 Half Elevation Feed S21 Magnitudes Versus Frequency, Ports 1-8	69
Figure 34. Measured TMM-6 Half Elevation Feed S21 Magnitudes Versus Frequency, Ports 1-8	70
Figure 35. Simulated TMM-6 Half Elevation Feed S21 Magnitudes Versus Frequency, Ports 1-8	71
Figure 36. S21 Magnitudes Versus Port Number For The TMM-3 Half Elevation Feed	73
Figure 37. S21 Magnitudes Versus Port Number For The TMM-6 Half Elevation Feed	74
Figure 38. Resonance Loop For An Isolated, Nominal, Unmodified TMM-3 Patch Circuit As A Function Of Frequency, Plotted In Smith Chart Form	76
Figure 39. Resonance Loop For An Isolated, Nominal, Painted TMM-3 Patch Circuit As A Function Of Frequency, Plotted In Smith Chart Form	77
Figure 40. Resonance Loop For An Isolated, Nominal, Unmodified TMM-6 Patch Circuit As A Function Of Frequency, Plotted In Smith Chart Form	78
Figure 41. Resonance Loop For An Isolated, Nominal, Trimmed And Painted TMM-6 Patch Circuit As A Function Of Frequency, Plotted In Smith Chart Form	79
Figure 42. S11 Versus Frequency For The Unmodified TMM-3 Elevation Array	81
Figure 43. S11 Versus Frequency For An Isolated, Nominal, Unmodified TMM-6 Patch Circuit	82
Figure 44. E-Plane Principal Polarization Antenna Pattern Cuts For Two Isolated TMM-3 Rectangular Microstrip Patch Elements With Inset Feeds, Frequency = 9.825 GHz, Measured Using An HP 8510C	84

Figure 45. E-Plane Principal Polarization Antenna Pattern Cut For An Isolated, Trimmed And Painted TMM-6 Rectangular Microstrip Patch Element With An Inset Feed, Frequency = 9.985 GHz, Measured Using An HP 8510C	85
Figure 46. Measured Noise In The Newport Anechoic Chamber Prior To Farfield Antenna Pattern Cut Measurements, Frequency = 9.830 GHz	87
Figure 47. Measured Farfield Antenna Pattern Cut For An AEL 5300 Standard Gain Horn, Frequency = 9.830 GHz	88
Figure 48. Measured E-Plane Principal Polarization Farfield Antenna Pattern Cut For An Isolated TMM-3 Rectangular Microstrip Patch Element With An Inset Feed, Frequency = 9.830 GHz	89
Figure 49. Measured E-Plane Cross Polarization Farfield Antenna Pattern Cut For An Isolated TMM-3 Rectangular Microstrip Patch Element With An Inset Feed, Frequency = 9.830 GHz	90
Figure 50. Measured H-Plane Principal Polarization Farfield Antenna Pattern Cut For An Isolated TMM-3 Rectangular Microstrip Patch Element With An Inset Feed, Frequency = 9.830 GHz	91
Figure 51. Measured H-Plane Cross Polarization Farfield Antenna Pattern Cut For An Isolated TMM-3 Rectangular Microstrip Patch Element With An Inset Feed, Frequency = 9.830 GHz	92
Figure 52. Measured E-Plane Principal Polarization Farfield Antenna Pattern Cut For An Array Of TMM-3 Rectangular Microstrip Patch Elements With Inset Feeds Arrayed In The H-Plane, Frequency = 9.830 GHz	93
Figure 53. Measured E-Plane Cross Polarization Farfield Antenna Pattern Cut For An Array Of TMM-3 Rectangular Microstrip Patch Elements With Inset Feeds Arrayed In The H-Plane, Frequency = 9.830 GHz	94
Figure 54. Measured H-Plane Principal Polarization Farfield Antenna Pattern Cut For An Array Of TMM-3 Rectangular Microstrip Patch Elements With Inset Feeds Arrayed In The H-Plane, Frequency = 9.830 GHz	95
Figure 55. Measured H-Plane Cross Polarization Farfield Antenna Pattern Cut For An Array Of TMM-3 Rectangular Microstrip Patch Elements With Inset Feeds Arrayed In The H-Plane, Frequency = 9.830 GHz	96
Figure 56. Measured E-Plane Principal Polarization Farfield Antenna Pattern Cut For An Array Of TMM-3 Rectangular Microstrip Patch Elements With Inset Feeds Arrayed In The H-Plane, Gain Not Calibrated, Frequency = 10.000 GHz	97
Figure 57. Measured E-Plane Cross Polarization Farfield Antenna Pattern Cut For An Array Of TMM-3 Rectangular Microstrip Patch Elements With Inset Feeds Arrayed In The H-Plane, Gain Not Calibrated, Frequency = 10.000 GHz	98
Figure 58. Measured H-Plane Principal Polarization Farfield Antenna Pattern Cut For An Array Of TMM-3 Rectangular Microstrip Patch Elements With Inset Feeds Arrayed In The H-Plane, Gain Not Calibrated, Frequency = 10.000 GHz	99

Figure 59. Measured H-Plane Cross Polarization Farfield Antenna Pattern Cut For An Array Of TMM-3 Rectangular Microstrip Patch Elements With Inset Feeds Arrayed In The H-Plane, Gain Not Calibrated, Frequency = 10.000 GHz	100
Figure 60. Measured E-Plane Principal Polarization Farfield Antenna Pattern Cut For An Isolated, Trimmed And Painted TMM-3 Rectangular Microstrip Patch Element With An Inset Feed, Gain Not Calibrated, Frequency = 9.975 GHz	101
Figure 61. Measured E-Plane Cross Polarization Farfield Antenna Pattern Cut For An Isolated, Trimmed And Painted TMM-3 Rectangular Microstrip Patch Element With An Inset Feed, Gain Not Calibrated, Frequency = 9.975 GHz	102
Figure 62. Measured H-Plane Principal Polarization Farfield Antenna Pattern Cut For An Isolated, Trimmed And Painted TMM-3 Rectangular Microstrip Patch Element With An Inset Feed, Gain Not Calibrated, Frequency = 9.975 GHz	103
Figure 63. Measured H-Plane Cross Polarization Farfield Antenna Pattern Cut For An Isolated, Trimmed And Painted TMM-3 Rectangular Microstrip Patch Element With An Inset Feed, Gain Not Calibrated, Frequency = 9.975 GHz	104
Figure 64. Measured E-Plane Principal Polarization Farfield Antenna Pattern Cut For An Isolated, Trimmed And Painted TMM-6 Rectangular Microstrip Patch Element With An Inset Feed, Gain Not Calibrated, Frequency = 10.135 GHz	105
Figure 65. Measured E-Plane Cross Polarization Farfield Antenna Pattern Cut For An Isolated, Trimmed And Painted TMM-6 Rectangular Microstrip Patch Element With An Inset Feed, Gain Not Calibrated, Frequency = 10.135 GHz	106
Figure 66. Measured H-Plane Principal Polarization Farfield Antenna Pattern Cut For An Isolated, Trimmed And Painted TMM-6 Rectangular Microstrip Patch Element With An Inset Feed, Gain Not Calibrated, Frequency = 10.135 GHz	107
Figure 67. Measured H-Plane Cross Polarization Farfield Antenna Pattern Cut For An Isolated, Trimmed And Painted TMM-6 Rectangular Microstrip Patch Element With An Inset Feed, Gain Not Calibrated, Frequency = 10.135 GHz	108
Figure 68. Longitudinal Current Along The 100 Ohm Feedline Leading Up To An Isolated Microstrip Patch With An Inset Feed Fabricated On TMM-6 Substrate At 10.00 GHz	110
Figure 69. Longitudinal Current Along The 100 Ohm Feedline Leading Up To An Isolated Microstrip Patch With An Inset Feed Fabricated On TMM-6 Substrate At 9.68 GHz	111

ACKNOWLEDGEMENTS

This work would not have been possible without the support of the management chain within the Surveillance and Photonics Directorate of Rome Laboratory (RL/OC) in 1992-1994, in particular, John McNamara, Richard Schneible, Joseph Polniaszek, Joseph Simons, Fred Demma and Dr. Donald Hanson, and without the guidance and help of Christofer Wilder and Ronald Gauss of Integrated Sensors, Inc. (ISI).

The work was performed by a team of individuals from Rome Laboratory (Virginia W. Ross, Lorraine E. Flanders, Clifford T. Tsao, Jeffrey T. Carlo and Michael J. Callahan). The whole team was involved in the overall first-order system level design, in the initial circuit fabrication attempt, and in the testing phase. The circuit and test fixture design tasks, however, were parceled out to individual team members. The author designed and laid out a corporate/series feed with each feed output port terminated in a rectangular, inset fed microstrip patch, forming a linear antenna array with an intended -35 dB taper applied across it. This tapered linear antenna array was intended to be used as an elevation subarray in a small prototype antenna array. Thirty-two elevation subarrays would be laid side by side, each one fed from an output port of an azimuth feed that had a taper applied across it as well. The author's circuitry used Rogers TMM-6 material as the substrate. Lorraine Flanders and Clifford Tsao designed and laid out a similar tapered linear antenna elevation subarray, but used Rogers TMM-3 material as the substrate. Jeffrey Carlo designed and laid out the azimuth feed on Rogers TMM-3 substrate. Other assorted test circuits were developed as well by Jeffrey, Lorraine and Clifford. Virginia Ross designed the test fixtures that the circuits were mounted in. The Rome Laboratory machine shop people built and machined the test fixtures. Microwave Printed Circuits (MPC) etched the circuits. Jerry Olmstead of ISI mounted the circuits in the test fixtures for us.

Christofer Wilder provided us with a MathCad worksheet (PATCHANT) to use in arriving at dimensions for our inset fed microstrip patches, and an antenna pattern program (PATT) that he had written that we used to generate the weights to produce the desired tapers across the elevation and azimuth feeds. John McNamara provided creative and valuable insights and ideas throughout this project. Mark Pugh of Rome Laboratory was instrumental in starting us on this project. Michael Little of Rome Laboratory actively encouraged us to use the software (Libra/Touchstone) and equipment (HP 8510C, a Sun workstation, special printers) in his laboratory. The people of ARL (Army Research Laboratory) were extremely generous and helpful in letting us use their etch facility in our attempt to etch the circuits ourselves. Microwave Printed Circuits (MPC), who etched the circuits that we used in the testing and measurement phase, did a fine job against challenging requirements. John Rooks of Rome Laboratory instructed us in the proper use of the HP 8510C vector network analyzer to take S-parameter measurements. The people who operate the anechoic chamber at Tanner Hill, Newport Test Site (a Rome Laboratory facility) helped us measure the antenna patterns produced by the radiators in some of our test fixtures. Our photo shop people did a wonderful job of capturing our circuits on film. Michael Wicks of Rome Laboratory provided advice and encouragement. Syracuse University EE graduate school professors taught the author how to use their software to model circuits by means of triangular basis functions, enabling him to write Appendix L. Special thanks go to the computer support people, arts and graphics people, clerical, administrative and contracting people without whom we could never have started, worked on, or finished this project.

The contents of Appendix A came from a host of references (References 2,3,4, 7,8,9,10,and 11), and the material in Appendix B came primarily from Reference 12. Clifford Tsao originally wrote what has been included as Appendix B after consulting the open literature, in particular, Reference 12.^{† ‡ §}

[†] The Surveillance and Photonics Directorate was dissolved when Rome Laboratory was formally integrated into Air Force Research Laboratory (AFRL). All former RL/OC personnel were reassigned to either the Information Directorate or the Sensors Directorate of AFRL (i.e. AFRL/IF or AFRL/SN).

[‡] Christofer Wilder has since left ISI to found his own corporation, Millennium Antenna.

[§] Lorraine E. Flanders and Clifford T. Tsao have since left the former Rome Laboratory.

FORWARD

More so now than ever before, the United States finds itself faced with the dilemma of projecting its military power to trouble spots throughout the globe in an era of force restructuring, pullback and drawdown. Because of this, global surveillance and warning has come to be of paramount importance to military commanders.

Wide area surveillance, and particularly downlooking radar wide area surveillance, presents an attractive means of fulfilling the mission of global surveillance and warning. This, as well as the lean budget years ahead make it desirable to upgrade sensor suites already in the field.

An airborne early warning aircraft sent to a hostile region will typically fly over friendly territory well behind the battle lines for safety reasons, conducting long range surveillance of the battle area from there. These aircraft are prime targets for an enemy, and must be preserved from harm.

It would be beneficial to extend the coverage region of airborne early warning aircraft by means of auxiliary radars mounted aboard unmanned aerial vehicles (UAVs). These aircraft can fly deep within enemy territory without danger to any personnel (since the UAVs are, by definition, unmanned) at high altitudes while staying on station for a long time. Detection and track files can be transmitted back for integration with the reports from other UAVs and with the data gathered directly from the controlling airborne early warning aircraft itself.

We undertook this project to design, fabricate and test planar antenna arrays of the sort envisioned for a radar system that we might someday consider mounting within a UAV. Because this was our first design iteration, we started small, with several qualifications imposed for simplicity's sake. The prototype array that we intended to design was considerably smaller than the larger model that we hoped to field in a UAV someday. The prototype array was planar, linearly polarized, had a rectangular aperture, operated at X-band (roughly 10 Ghz) with a very narrow (50 Mhz) 3 dB bandwidth, had a fixed beam (no electronic beamsteering capability), was not capable of handling high power and possessed a microstrip corporate/series feed structure with rectangular microstrip patch radiating elements having inset feed points.

CHAPTER 1 DOWNSELECTION OF RADAR MISSIONS, RADAR REQUIREMENTS AND SIMPLIFYING ASSUMPTIONS, AND ANTENNA REQUIREMENTS

The postulated mission for the downlooking radar mounted in a UAV is to perform wide area surveillance from a sidelooking position (antenna boresight orthogonal to the platform velocity vector) against both ground and air targets. More specifically, mission requirements are to perform wide area surveillance, ground moving target surveillance, imaging, and foliage penetrating blob detection with a sensor mounted aboard a UAV platform.

Mission requirements drive the radar requirements. Based on the postulated mission requirements, four basic modes of radar operation are required. These four are: 1) airborne early warning (AEW) capability against aircraft and cruise missiles; 2) low velocity ground target detection; 3) synthetic aperture radar (SAR) imaging capability against armor, artillery, missile launchers, etc. that are in the clear; and 4) foliage penetration (FOPEN) "blob detection" against armor, artillery, missile launchers, etc. that are hidden beneath forest canopies.

SAR and FOPEN are important, but they introduce a great degree of complexity into the antenna design and into the signal processor, and in the interest of keeping things relatively simple the first time around, we omitted these modes from our consideration for the following reasons.

If we were to incorporate both SAR and foliage penetration capabilities into our design, we would need to design a dual band system, since SAR will tend to drive operating frequency upward to achieve better resolution, and foliage penetration will tend to drive operating frequency downward so that leaves etc. are electrically small. A good SAR design could be implemented at X-band, while VHF to UHF would probably be best for blob detection under foliage given that ultra-wide bandwidth is also necessary in addition to low frequency. Wide bandwidth in its own right presents difficulties to the antenna designer. If we confine our attentions to detecting slow ground movers and fast airborne vehicles, are not trying to achieve a high degree of range resolution, and assume that we will be able to adaptively place antenna nulls in the direction of jammers, we can work over a fairly narrow instantaneous bandwidth in a single frequency band. This is not at all realistic, but it gives us a simple starting point from which to develop a more complex design at a later date.

For our first design iteration, we assume that the antenna can be no more than 5 meters long if it is to fit within the UAV, and that the UAV cruises at an altitude of 60,000 feet above mean sea level at about 200 knots (102 meters/second).

Area search rate dictates the size of the mainbeam, and X-band seems to be a good choice of operating frequency since it offers us the beamwidth that we need given the physical dimensions of the array that the antenna platform imposes upon us. Therefore, we will design our antenna at a center frequency of 10.0 Ghz. We will set our azimuth scan limits from -45 to +45 degrees because these limits are felt to be achievable.

A variety of PRF modes must be employed if we wish to detect both slow moving ground targets and fast moving airborne ones. If we want to keep things simple for now, we can focus in on one mode and perform our calculations for that mode alone. We will focus in on a low PRF mode, because a low PRF mode requires less average power handling capability from the radar equipment and from the antenna. Later on, we will see that the antenna design concept that we came up with wasn't robust enough to handle high average power waveforms, limiting us to low duty cycle waveforms and forcing us to employ a low PRF scheme.

We thus have eliminated another potential mission from our list, leaving us with only slow ground moving target detection. This is much too limiting for a system that must be fielded; however the object of this

project is to build a simple prototype antenna, not an operational system. Therefore, we can afford to sacrifice capability to achieve simplicity of design. Our hope is to one day revisit this analysis with much more rigor, designing an antenna for the multimode usage envisioned in our radar requirements listed above.

A low PRF eliminates range ambiguities. Low PRFs usually fall in the range of a few hundred to a few thousand pulses per second. Here we will use a PRF of 1500 Hz to yield an unambiguous range of 100 km or 54 nm. In all likelihood, we will not have to contend with ambiguities in range given the low amount of average power that we can reasonably expect to transmit with our design, so 1500 Hz should be a good choice. We can employ simple pulse delay ranging techniques, and if range ambiguities do give us problems, we can use staggered PRFs to eliminate them.

We next determine whether or not some form of adaptive space time processing must be used. If we assume that the radar must detect ground moving targets with a minimum discernible velocity of 5 knots (2.572 m/s) for a 5 sq m target, then the approach we must take is as follows.

First we must determine the mainlobe clutter spectrum when the beam is pointed orthogonal to the platform velocity vector. This spectrum is broadened by the intrinsic motion of the clutter background, which we will take to be that of leaves blowing in a 20 knot wind. A normal probability density function for the blowing leaves is assumed, with a mean of 0.0 and a standard deviation as given below on the left. The standard deviation due to platform motion is given below on the right [1].

INTERNAL CLUTTER MOTION

$$\sigma_M = \frac{2\sigma_V}{\lambda} \text{ Hz}$$

where:

$$\sigma_V = 0.13 \text{ m/s in a 20 knot wind}$$

$$\sigma_M = \frac{2(0.13)}{0.03} = 8.7 \text{ Hz}$$

PLATFORM MOTION

$$\sigma_{PM} \equiv \frac{0.7V}{D} \sin(\alpha)$$

where:

$$\alpha = 90^\circ$$

$$\begin{aligned} V &= \text{platform speed} \\ &= 200 \text{ kt} = 102 \text{ m/s} \end{aligned}$$

$$\begin{aligned} D &= \text{antenna length} = 5 \text{ meters} \\ &= 5 \text{ meters} \end{aligned}$$

$$\sigma_{PM} = \frac{0.7(102)}{5} \sin(90^\circ) = 14.3 \text{ Hz}$$

$$\sigma_{CLUTTER} = (\sigma_M^2 + \sigma_{PM}^2)^{\frac{1}{2}} = 16.7 \text{ Hz}$$

Here we made use of the fact that the total variance of the leaf clutter spectrum due to impressed effects (wind) and due to platform motion is equal to the sum of the variances from each individual effect. The standard deviation of the mainlobe clutter spectrum when the mainlobe is pointed sideways with respect to the platform velocity vector is equal to the square root of the total variance of the leaf clutter.

Assume that we only need 16 filters in our Doppler filter bank. Reasons for this choice are: 1) each filter will span approximately a 2.5-3.0 kt velocity step, which is enough velocity resolution for GMTI purposes; 2) we won't have to correct for Doppler walk due to minor target accelerations or decelerations; 3) we can coherently dwell over 16 pulses at a PRF of 1500 Hz.

The 3 dB width of each Doppler filter in the bank is equal to:

$$\frac{1500 \text{ Hz}}{16 \text{ filters}} = 93.7 \text{ Hz / filter}$$

Assume that the filters in the bank are not weighted. Also assume that the filters are arranged such that the 3 dB point where filters 8 and 9 are joined lies at zero Doppler. Arranged like so, the left mainlobe null of the 11th Doppler filter (third filter up from zero Doppler) lies at 156.60 Hz, or 9.377 times the standard deviation of the clutter spectrum about zero Doppler due to internal and platform motion effects. A radially inbound 5 kt target with a Doppler frequency of 171.47 Hz would lie in the 11th Doppler filter. If we assume the clutter backscatter is spread over Doppler in such a manner as to conform to a Gaussian distribution, we can calculate the fractional amount of clutter in each Doppler filter and find that the clutter power in the 11th Doppler filter is essentially 0. This does assume that each Doppler filter consists only of a mainlobe lying between nulls with no sidelobe structure at all. In practice, this is not the case, but here assume that no clutter will compete with a 5 kt target return. Adaptive space time processing techniques are not required. The calculation that was performed to determine the amount of clutter in the 11th Doppler filter is shown here.

$$\text{Define } \text{erf}(x) = \frac{1}{\sqrt{2\pi}} \int_0^x e^{-\frac{1}{2}t^2} dt$$

For purposes of this calculation, the following symbology and parameter values will be used.

The mean value of the clutter Doppler frequency will be denoted by μ and will equal 0.0 Hz.

The standard deviation of the clutter Doppler frequency will be denoted by σ and will equal 16.7 Hz.

Doppler filter 11 will be bounded by Doppler frequencies a and b. Doppler frequency a =

156.60 Hz, and Doppler frequency b = 311.90 Hz. The filter - 3 dB points are separated from one another by 93.7 Hz. This separation is equal to 0.603354564 times the separation between the null points. The null points are therefore separated by 155.30 Hz.

The fractional clutter lying in a Doppler filter bounded by Doppler frequencies a and b is equal to:

$$\text{erf}\left(\frac{b-\mu}{\sigma}\right) - \text{erf}\left(\frac{a-\mu}{\sigma}\right)$$

Matlab was used to perform this calculation, and to the precision available (14 decimal places) the above equation yielded $0.50000000000000 - 0.50000000000000 = 0.0$. When this result was converted to dB, Matlab complained about taking the log of zero and returned a value of - Infinity dB.

The reader must be careful in performing the above calculation for him or her self, since the Matlab definition of the error function differs slightly from what is shown above. To perform the above computation using Matlab, we would do the following.

The fractional clutter lying in a Doppler filter bounded by Doppler frequencies a and b is equal to:

$$\frac{1}{2} \text{erf}\left(\frac{1}{\sqrt{2}} \frac{b-\mu}{\sigma}\right) - \frac{1}{2} \text{erf}\left(\frac{1}{\sqrt{2}} \frac{a-\mu}{\sigma}\right)$$

$$\text{using the Matlab definition of } \text{erf}(x) = \frac{2}{\sqrt{\pi}} \int_0^x e^{-t^2} dt$$

Below is an example calculation that we would employ for our case if there were clutter power that we had to suppress [1]. It yields the (approximate) clutter suppression requirement. Here we assume that the clutter power in the 11th Doppler filter (3rd filter up from 0 Doppler) is -137 dB. We also assume a spherical, featureless 4/3 earth with terrain cover painted on the surface and the radar at an altitude of 60,000 feet above a cueball earth.

$\sigma^0 = 0.1$ = clutter cross section coefficient (relatively high assumption)

$R = 100$ km = maximum unambiguous range at a PRF of 1500 Hz

$\theta = 0.5^\circ$ = azimuth beamwidth (preliminary antenna requirement shown further down in the text)

$$\Delta R = \frac{c\tau}{2} = \frac{2.998 \times 10^8 \text{ m/s} \times 0.4 \times 10^{-6} \text{ s}}{2} = 60 \text{ m} = \text{range resolution}$$

$$\phi = -\sin^{-1} \left(\frac{R^2 - 2 \left(\frac{4}{3} \right) 6378 \left(\frac{60000}{3281} \right) - \left(\frac{60000}{3281} \right)^2}{2R \left(\frac{4}{3} \right) 6378} \right) = 10.206^\circ = \text{grazing angle (with UAV at 60,000 ft)}$$

$$(\sigma^0 (R\theta)(\Delta R \sec(\phi))) = 5320.17 \text{ m}^2 = 37.26 \text{ dBsm} = \text{clutter cross section}$$

$$\sigma_{\text{tgt}} = 5 \text{ m}^2 = 6.99 \text{ dBsm} = \text{target cross section}$$

In order to suppress clutter to a level 13 dB below the target, the required clutter suppression is $37.26 - 6.99 + 13.00 = 43.27$ dB.

Therefore, a 5 kt target is detectable in the 11th Doppler filter with a -43.27dB - (-137dB) or 93.73dB margin. Adaptive space time processing techniques are not required.

The sidelobe clutter extent for a 200 kt platform speed is ± 6860 Hz since the maximum Doppler frequency extends out to $\pm \frac{2V}{\lambda}$ Hz about the transmit frequency.

The number of sidelobe clutter ambiguities $= 4 \left(\frac{6860}{1500} \right) = 18.3 = 12.6$ dB. This accounts for both positive and negative Doppler, and for both the starboard and port sides of the aircraft.

The antenna sidelobe level necessary to ensure that the total sidelobe clutter is 10dB below mainlobe clutter is therefore defined as $12.6 \text{ dB} + 10 \text{ dB} = 22.6 \text{ dB}$ below the antenna mainlobe peak.

There is a concern over velocity ambiguity. A PRF of 1500 Hz at 10 GHz yields ambiguous velocities at multiples of $\pm 22.5 \text{ m/s}$ or $\pm 43.74 \text{ kt}$ (50.33 statute miles/hour), which may be unacceptable. An alternate waveform can be used to measure velocity.

At this point, we will assume parameters for the radar in the ground moving target mode [1].

GROUND MOVING TARGET SURVEILLANCE MODE ASSUMPTIONS¹

PRF	1500 Hz
PRI	667 microseconds
SNR required for detection	13 dB
Peak power Pt	10 kW
Duty factor	2%
Average power	200 W
Pulse width (duty factor * PRI)	13.3 microseconds
Receiver noise figure	≤ 2 dB
Pulse compression ratio 32:1 (Processing gain, Gp = 15.05 dB)	0.416 microseconds

FRAME TIME FOR ONE BAR SCAN (GROUND MOVING TARGET SURVEILLANCE MODE)¹

scan time = (number of beam positions)(dwell time)

If the beam is scanned in $\frac{1}{3}$ beamwidth steps - 45 to + 45 degrees from broadside in azimuth

number of beam positions = $3(\text{scan range} / \text{beamwidth}) = 3(90^\circ) / (0.5^\circ) = 540$

dwell time = 1 CPI = $16(1 \text{ PRI}) = 16(667 \text{ microseconds}) = 10.67 \text{ milliseconds}$

scan time = $(540)(0.01067) = 5.76 \text{ seconds}$

LOSS BUDGET *¹

La (Atmospheric loss due to water vapor and oxygen absorption)	1.3 dB
Lw (Weather loss due to 20 km of 4 mm/hour rainfall)	4.8 dB
Lp (Processing loss due to weighting, filter crossover, and thresholding plus pulse compression and A/D conversion straddle)	4.5 dB
Lm (RF loss due to duplexer, isolator, filter, receiver limiter and 0.5 dB of radome loss)	2.5 dB
Lb (Beamshape loss)	1.6 dB
 L = La + Lw + Lp + Lm + Lb =	 14.7 dB

* This loss budget came from ISI. Atmospheric and weather losses seem to have been padded to make them larger than what we have been able to cross check at RL. We will use this loss budget anyway, because the extra loss we are allowing for in the atmosphere and weather categories might offset possibly low estimates of loss in the other categories.

ANTENNA GAIN REQUIREMENTS¹

$$Ga = \left[\frac{SNR(4\pi)^3 R^4 (Fn)(kT)(\beta\tau)L}{Pt(pw)\lambda^2 \sigma Gp} \right]^{1/2}$$

$$SNR = 13 \text{ dB} = 20$$

$$R = 100 \text{ km}$$

$$Fn = 2 \text{ dB} = 1.58$$

$$kT = 3.98 * 10^{-21} \text{ Joules}$$

$$\beta\tau = 1 \text{ (matched receiver)}$$

$$Pt = 10 \text{ kW}$$

$$pw = 13.3 \text{ microseconds}$$

$$\lambda = 0.03 \text{ meters}$$

$$\sigma = 5 \text{ square meters}$$

$$Gp = 15.05 \text{ dB} = 32$$

$$L = 14.7 \text{ dB} = 29.5$$

$$Ga = 6232 = 38 \text{ dB}$$

PRELIMINARY ANTENNA REQUIREMENTS¹

Gain	
Transmit	> 38 dB
Receive	> 38 dB
-3dB Beamwidth	
Azimuth	$\cong 0.5^\circ$
Elevation	fan beam (narrow UAV body diameter)
Sidelobes	
Peak	-35 dB (emission control and jamming suppression)
RMS	-43 dB

ANTENNA SYSTEM DESIGN GOALS¹

PARAMETER	VALUE	NOTES
Frequency		
Operational	10.0 GHz	
Instantaneous	50.0 MHz	
Gain	> 38.0 dB	
Beamwidth		
Azimuth	0.5°	At broadside and 10.0 Ghz
Elevation	fan (intermediate value)	At broadside and 10.0 GHz
Scan Limits		
Azimuth	±45°	
Elevation	N/A	
Sidelobes		
Azimuth Axis		
Peak	-35 dB	
RMS	-43 dB	
Elevation Axis		
Peak	-25 dB	
RMS	-35 dB	
Polarization	Single Linear	Horizontal
VSWR	< 2:1	Nominal 50 Ω impedance
RF Input Power		
Operational		
Peak	10 kW	
Average	200 W	
Extreme	TBD kW	Recovery time < TBD s
DC Power Supply	TBD	
Weight	TBD	< TBD lbs
Temperature Range		
Operational	-55° C to +85° C	
Storage	-55° C to +125° C	
Special Functions		
Elevation Mechanical Scan	TBD	
Dynamic Calibration	TBD	
Guard Antenna	TBD	

The items marked TBD in the above were never addressed within the context of this project.

CHAPTER 2 ANTENNA SIZING, LATTICE STRUCTURE AND ELEMENT CHOICE

Under this project, we only designed, fabricated and tested a fixed beam prototype receive aperture. However, if the real receive aperture can be sized such that it meets the gain requirements, the aperture on transmit most certainly will (assuming a monostatic system). The receive aperture was sized to achieve greater than 38 dB gain while being amplitude weighted to reduce sidelobes as follows [1].

A rectangular outline was assumed.

Scan Axis Element Spacing From Scan Limits

$$dx \leq \frac{\lambda_0}{\sin(\theta) + \sin(\theta_{MAX})}$$

dx = element spacing along the x - axis

θ = maximum farfield observation angle (90°)

θ_{MAX} = maximum scan angle along the x - axis (45°)

λ_0 = wavelength in free space (1.18034 inches)

$$dx \leq \frac{1.18034}{\sin(90^\circ) + \sin(45^\circ)} = 0.691 \text{ inches}$$

Array Width From The Azimuth Beamwidth

$$W = \frac{F\lambda_0}{\sin(BW_{-3dB})} = 161.2 \text{ inches}$$

W = width (length) of array

F = excitation taper dependent beamspread factor (1.192 for Taylor -35 dB, $\bar{n} = 5$)

BW_{-3dB} = broadside beamwidth between -3 dB crossovers (0.5° in azimuth at 10 GHz)

Array Height From Directivity

$$D = 10 \log \left(\frac{4\pi WH}{\lambda_0^2} \right)$$

D = aperture directivity = 38.5 dB (a value greater than 38 dB)

W = aperture width = 161.2 inches

H = aperture height = TBD

$$H = \frac{(10^{\frac{D}{10}})\lambda_0^2}{4\pi W} = 4.87 \text{ inches (intermediate result, actual value determined below)}$$

We have budgeted 8 dB as per ISI for radome, aperture taper, radiating element efficiency, feed and interconnect losses. This loss budget is broken out as follows [1].

Radome transmission loss	0.5 dB
Taper loss for linear Taylor weighting	1.0 dB (azimuth for -35 dB wt)
	0.5 dB (elevation for -25 dB wt)
Radiating element efficiency loss	call it 1.0 dB
Feed loss	assume 4.0 dB
Interconnect loss	1.0 dB
	<hr/>
	8.0 dB

Gain = Directivity - Loss

If we want a gain of 38.5 dB, then

$$D = \frac{4\pi A}{\lambda^2} = 46.5 \text{ dB} \approx 44,668$$

$$\therefore A = \frac{D\lambda^2}{4\pi} = 4952 \text{ inches}^2$$

Since $W = 161.2$ inches

$$H = \frac{A}{W} = 30.7 \text{ inches (final value)}$$

The elevation beamwidth is

$$BW_{el} = \sin^{-1}\left[\frac{F\lambda}{H}\right] = \sin^{-1}\left[\frac{1.068(118034)}{30.7}\right] \approx 2.35^\circ \text{ (final value)}$$

F = excitation taper dependent beamspread factor (1.068 for Taylor -25 dB, $\bar{n} = 3$)

Element count

$$N_{az} = 161.2 / 0.691 \approx 233$$

$$N_{el} = 30.7 / 0.691 \approx 44$$

PATT, a computer program developed by ISI (Christofer Wilder) to compute mainlobe spread, taper efficiency, array factor and farfield pattern for a variety of common antenna aperture illumination weighting schemes was exercised in an interactive manner for a number of different tapers in the Taylor family. Theoretically derived approximations for RMS amplitude, phase and phase shifter quantization errors which degraded the pattern were considered in the analysis. Various design tapers were tried until we found one which gave us the peak and RMS sidelobe responses we were looking for. The error approximations we used and the values generated by these expressions are shown below [1].

$$\sigma_A = 10^{\frac{(\text{RMS AMPLITUDE ERROR})}{20}} - 1$$

$$\sigma_P = \frac{\pi(\text{RMS PHASE ERROR})}{180}$$

$$\sigma_Q = \frac{\pi}{\sqrt{3}(2^b)}$$

$$\sigma^2 = \sigma_A^2 + \sigma_P^2 + \sigma_Q^2$$

$$\sigma_E^2 = \frac{\sigma^2}{\eta N}$$

$$\text{Peak SLL} = 20 \log \left(10^{\frac{-\text{DESIGNSLL}}{20}} + 2\sigma_E \right)$$

If we assume an RMS amplitude error of 0.5 dB, an RMS phase error of 4.0 degrees, and 6-bit phase shifters, with a total number of elements equal to 233*44 and an efficiency of 0.808 in azimuth (due to azimuth weighting) and 0.902 in elevation (due to elevation weighting), then the effective peak sidelobe levels in azimuth and elevation can be calculated as follows.

$$\sigma_A = 10^{\frac{0.5}{20}} - 1$$

$$\sigma_P = \frac{\pi(4)}{180}$$

$$\sigma_Q = \frac{\pi}{\sqrt{3}(2^6)}$$

$$\sigma^2 = \sigma_A^2 + \sigma_P^2 + \sigma_Q^2$$

$$\sigma_E^2 = \frac{\sigma^2}{0.808(233)(44)}$$

$$\text{Peak SLL}_{az} = 20 \log \left(10^{\frac{-35}{20}} + 2\sigma_E \right) = -34.0 \text{ dB}$$

$$\begin{aligned}
\sigma_A &= 10^{\frac{0.5}{20}} - 1 \\
\sigma_P &= \frac{\pi(4)}{180} \\
\sigma_Q &= \frac{\pi}{\sqrt{3}(2^6)} \\
\sigma^2 &= \sigma_A^2 + \sigma_P^2 + \sigma_Q^2 \\
\sigma_E^2 &= \frac{\sigma^2}{0.902(233)(44)} \\
\text{Peak SLL}_1 &= 20 \log \left(10^{\frac{-25}{20}} + 2\sigma_E \right) = -24.7 \text{ dB}
\end{aligned}$$

A square lattice was employed for ease of calculation and for a few other characteristics that we intended to exploit. Though more elements are needed in a square lattice ($\approx 16\%$ more) for the same grating lobe-free scanning extent off boresight as that exhibited by a triangular lattice, we feel that the square lattice, with more elements, should be able to provide us with correspondingly greater peak and average power, and allow us to sample the illumination taper more densely and, hence, more accurately. The interelement spacing between the element centers was chosen such that a 51° scan angle off boresight in azimuth could be achieved before the peak of a grating lobe would make its appearance in real space. We felt that this would give us a comfortable margin when we scanned out to 45° since the attendant sidelobe structure of the grating lobe would be all that would creep into real space then, and we didn't think that these would cause too much trouble when multiplied by the element pattern. Note here that the element pattern drops rapidly in amplitude at angles far from zero.

Microstrip patch elements were chosen because they are: 1) cheap; 2) lightweight; 3) easily manufactured on array panels; 4) lend themselves rather readily to array use; 5) possess high radiation efficiency; and 6) are excellent choices for narrowband array use. We at RL could at one time also model their performance to first order as radiating elements in an array environment using PAAS (the Parametric Antenna Analysis Software developed by STI and ARC).

Rectangular microstrip patches of length $\lambda_g/2$ fed from feed lines inserted into a gap such that the desired impedance of the element was 100Ω in an array environment were used. A MathCad calculation worksheet (PATCHANT) developed by ISI (Christofer Wilder) was utilized in initially dimensioning the elements such that for an isolated element the fundamental mode achieved resonance at 10 GHz and the input impedance of the isolated element was approximately 100Ω . At this point in time, the best approach to sizing elements to function well in an array environment is to produce a large number of test circuits and trim the elements until the desired performance is achieved.

For the small array that we wanted to build (really just a prototype and proof of concept), our goal was to achieve -30dB peak sidelobes in azimuth and elevation. The overall dimensions of this array were roughly $21.30'' \times 10.65''$. There were 32 columns in this array with 16 elements per column.

CHAPTER 3 DESIGN OF THE PROTOTYPE ARRAY AZIMUTH AND ELEVATION FEED NETWORKS

Two array feed approaches were taken.

The first involved feeding the elements from an azimuth/elevation feed structure on the same board as the antenna array. The substrate material was to be Rogers TMM-3 with a relative dielectric constant $\epsilon_r = 3.27$, a dielectric thickness of 20 mils and 1 oz Cu metallization.

The second array feed approach involved feeding the antenna elements from an azimuth feed structure behind the board that the antenna array is printed on by means of plated through via holes to the elevation feed circuit traces which conduct power to the elements. In this approach, only the elevation feeds would be on the same board as the antenna elements.

Feedlines present on the array face will induce scattering, spoiling the antenna pattern especially at larger scan angles. To what extent our feedlines will induce this phenomenon remains to be seen, but certainly fewer feedlines on the array face is a good thing. There are two different ways that the second array feed approach could be implemented. Both involve printing the azimuth feed on TMM-3 material, with one way using TMM-3 material as the substrate for the array face and elevation feeds, and the other way using Rogers TMM-6 material ($\epsilon_r = 6.00$, substrate thickness = 25 mils, 1 oz Cu metallization) as the substrate for these.

Sought after advantages of using TMM-6 material for the array face and elevation feed substrate instead of TMM-3 were: 1) the antenna elements were smaller since λ_g is smaller for a material with a higher relative dielectric constant; 2) for a given impedance value, the microstrip line width needed to achieve that impedance is narrower; 3) $\lambda_g/4$ impedance transformer sections were shorter in length due to the higher relative dielectric constant of TMM-6. However, the power handling capability of the array and feed fabricated on TMM-6 material is less than what could be had from an array and feed fabricated on TMM-3 material because of the smaller dimensions of the TMM-6 circuitry.

All approaches to designing the elevation feed took essentially a series feed approach. Available space and power division ratios at feedline splits determined the overall geometry of the feeds. True line length equalization was not performed for the elevation feeds since there simply wasn't enough room available. Modulo 2π line length equalization was done so that at bandcenter and at boresite all the elements would be in phase (even though no phase steering capability had been implemented in the prototype). This condition deteriorates rapidly as frequency is varied, but over a very narrow bandwidth (a fraction of a percent) this isn't much of a problem and the elements are still relatively in phase.

The azimuth feed was implemented using a corporate feed approach with no isolation chip resistors in place to keep coupling between output ports down to a very low level. The chip resistors were omitted due to the need to save space. It was felt that the interport coupling would be acceptably low for our power division network, and we decided to accept whatever performance level we would achieve in terms of interport coupling performance.

A few spot checks were performed at various stages via simulation to ensure that interport coupling was down below -15 to -20 dB, which was felt to be acceptably low. This is not the best of practices, but we were terribly cramped for space.

The ISI computer program PATT was utilized in choosing a design aperture illumination function such that amplitude, phase and quantization errors did not bring our peak sidelobe level above that shown in the specifications. After a suitable design taper was found, the voltage weights for the elements were written to a file. This data file was then edited to strip off the header information and the phase associated with

each weight (which, of course, was identically 0.00 since the small test array would not be scanned electronically) and then read into Microsoft Excel as a single long column of data. Based on the information that was contained in the header section that had been deleted, the column of voltage weight data was reformatted into 32 columns, with 16 rows in each column. Each row i-column j intersection consisted of one number in a cell, representing the amplitude weight associated with element i,j in the 2-D test array.

The unnormalized voltage weights were normalized by the following process. First, the sum of the squares of all weights was computed to find the total power being output by the unnormalized array. The square root of this sum was then computed and every cell value was divided by this number. The voltage weights were now normalized in the sense that the sum of the squares of all the weight values equaled 1.00, that is, the array had unity power output. The advantage of doing it this way is that the azimuth and elevation weights, which we will determine next, are such that any linear scaling in output power for the array involves simply scaling all the voltage values by the square root of the output power scaling factor. The relative value of each voltage weight with respect to the others is fixed.

Now that the normalized voltage weights have been computed, we must calculate the azimuth and elevation feed port weights. The power output at element i,j should equal the power output from azimuth feed port j multiplied by the power output from elevation feed port i.

The sum of the squares of the 32 normalized voltage weights in each row was computed, yielding 16 sum values. The square root of each of these was taken to yield the 16 elevation feed weights. In a similar manner, the 32 azimuth feed weights were computed by taking the sum of the squares of the 16 normalized voltage weights in each column and taking the square root of each of the 32 sums.

Having computed the azimuth and elevation feed values in terms of power, we now employed the Wilkinson power division formulas in designing our power splitting networks (feeds), though we omitted the isolation chip resistors due to lack of space. A sketch of a single Wilkinson power splitter is shown in Figure 1. The equations used to calculate the line impedances and the resistance of the chip resistor are shown below. The equation to calculate the isolation chip resistor value at each split is given so that the reader might employ it in like tasks where it is practical and desirable to make use of it.

$$\begin{aligned} Z_1 &= Z_0 \sqrt{\frac{(1+k)}{k^{\frac{3}{2}}}} & Z_2 &= kZ_1 \\ Z_3 &= \frac{Z_0}{\frac{1}{k^{\frac{1}{4}}}} & Z_4 &= \sqrt{k}Z_3 \\ R &= (k+1)Z_0 \end{aligned}$$

The power splitter shown in Figure 1 works best when the k value is between 1.0 and ≈ 2.5 , or, equivalently, when $1/k$ is between 1.0 and ≈ 2.5 . No matter whether you prefer P_2/P_1 or P_1/P_2 , (it doesn't matter to the power splitter equations which arm will carry more power and which less), what matters is the ratio between the two. This is because when the k value gets much higher than 2.5, the disparity in impedance values required to implement such a power division results in the following. Some lines become so wide that the assumption made in the design equations that the line width is less than $\lambda_g/10$ is violated, the equations yield inaccurate values, and the true impedance of the wide line becomes anybody's guess; and other lines become so narrow that tolerancing problems arise where the tolerance of the process used to etch the lines in terms of undercutting, etc. contribute errors that are a significant fraction of a line width to the width of the line. Use the equations as given to find Z_1 through Z_4 , but when it comes to calculating R, make certain that you employ whichever value (k or $1/k$) is greater than or equal to 1.0.

With this guidance, we designed the power division networks. By mentally manipulating combinations of the feed port power output values, we quickly came up with schemes with which to implement the feeds

and keep our power division ratios at every junction fairly reasonable. The fractional power routed through each output port, the k values, impedance values and chip resistor values are shown below.

The two elevation feeds employ the same overall power splitting structure; only the impedance values and the meandering runs of modulo 2π equalizing line length differ. The basic half elevation feed structure employed in both the TMM-3 and TMM-6 designs is shown in Figure 2.

It was decided from the start that the characteristic impedance of the system external to the feed and radiating elements would be an assumed 50Ω . The characteristic impedance within the feed/antenna structure could vary from that, however, based on convenience and necessity, which in our cases translated into available space considerations and allowable maximum and minimum values for linewidth based on the $w \leq (\lambda_g / 10)$ assumption and tolerance imposed variations in linewidth as discussed above. Note that Z_0 appears in the equations for Z1-Z4, and by varying Z_0 and monitoring what that does to the width of the lowest impedance line (widest) and the highest impedance line (narrowest) in each power division network (feed), we were able to choose an optimum value of Z_0 in each case.

The half elevation feed etched on Rogers TMM-3 substrate employs a Z_0 of 55Ω in the trunk of the feed, transforming to a Z_0 of 100Ω in the meandering feedline running out to each antenna element. In like fashion, the half elevation feed etched on Rogers TMM-6 substrate employs a Z_0 of 44Ω in the trunk of the feed, and a Z_0 of 100Ω in the meandering feedline running out to each antenna element. The azimuth feed employed a characteristic impedance Z_0 of 50Ω throughout. It was the responsibility of each elevation feed designer to design the matching network from his or her feed to the azimuth feed.

The monitoring of linewidth discussed above was done using Linecalc. Linecalc was also used to determine the width of every line in each power division network after Z_0 for the trunk of each feed was determined (since all the Z1-Z4 values are related to Z_0 through the relations given above) along with their $\pi/2$ (quarter wavelength) electrical lengths.

TMM-3 Half Elevation Feed ($Z_0 = 55\Omega$)

(By mirror symmetry, we can design the other half of the feed.)

Split Number	Power Split	k	R
	0.137849		
1		1.089733	114.9353
	0.122886		
2		1.121763	116.6970
	0.097060		
3		0.682536	92.53947 *
	0.067583		
4		0.905671	104.8119 *
	0.040808		
5		1.206837	121.3761
	0.020632		
6		1.565165	141.0841
	0.008879		
7		2.063444	168.4894
	0.004303		
	—————		
	0.500000		

* Because a k value less than 1.0 was used to calculate these values for R, they are incorrect. They have been recalculated using a value of 1/k in place of k for Split 3 and Split 4.

Split Number	1/k	R (correct)
3	1.465125	135.5819
4	1.104153	115.7284

Split Number	Z1	Z3	Z2	Z4
1	74.54491	53.83103	81.23406	56.19436
2	73.49965	53.44258	82.44920	56.60281
3	95.00594	60.51058	64.84496	49.99126
4	81.78219	56.37935	74.06778	53.65440
5	70.95962	52.47476	85.63672	57.64676
6	62.95066	49.17254	98.52815	61.51807
7	55.91433	45.88963	115.3761	65.91904

TMM-6 Half Elevation Feed ($Z_0 = 44\Omega$)

(By mirror symmetry, we can design the other half of the feed.)

Split Number	Power Split	k	R
	0.137849		
1		1.089733	91.94826
	0.122886		
2		1.121763	93.35758
	0.097060		
3		0.682536	74.03157 *
	0.067583		
4		0.905671	83.84953 *
	0.040808		
5		1.206837	97.10085
	0.020632		
6		1.565165	112.8672
	0.008879		
7		2.063444	134.7915
	0.004303		
	0.500000		

* Because a k value less than 1.0 was used to calculate these values for R, they are incorrect. They have been recalculated using a value of 1/k in place of k for Split 3 and Split 4.

Split Number	1/k	R (correct)
3	1.465125	108.4655
4	1.104153	92.58273

Split Number	Z1	Z3	Z2	Z4
1	59.63593	43.06482	64.98725	44.95549
2	58.79972	42.75406	65.95936	45.28225
3	76.00476	48.40847	51.87596	39.99300
4	65.42575	45.10348	59.25422	42.92352
5	56.76770	41.97981	68.50938	46.11741
6	50.36053	39.33804	78.82252	49.21446
7	44.73147	36.71170	92.30088	52.73523

Next, the power division networks were laid out.

The azimuth feed was done using the layout generator within Academy. The elevation feed designed on TMM-3 was laid out using Autocad, and the elevation feed designed on TMM-6 was laid out in the initial stages in Autosketch, which is a junior version of Autocad put out by the same corporation (Autodesk). The final designs for all the circuits would eventually be assembled together to fit within the real estate extents of standard board sizes using Autocad.

Regarding the elevation feeds, the antenna elements were first sized for each board substrate using the ISI developed microstrip patch design program PATCHANT. PATCHANT is a MathCad sheet that analyzes a microstrip patch of given dimensions (F, W, L, ϵ_r , and ϵ_5) according to the method described in [6]. The patch antenna elements were to have a resonant frequency of 10 Ghz and an input impedance of 100.0 ohms. A drawing of a microstrip patch having an inset feed is shown in Figure 3.

The nominal patch on TMM-3 substrate had a conductor thickness of 1.4 mils, a feed line width $F = 11.00$ mils, a feed insertion depth $\epsilon_3 = 119.0$ mils, a feed isolation gap $\epsilon_5 = 40.0$ mils, a patch resonant length $L = 326.2$ mils, and a patch width $W = 323.2$ mils. The TMM-3 substrate thickness is 20 mils, its relative dielectric constant ϵ_r is 3.2 (as input into PATCHANT by the team), and the dielectric loss tangent δ employed is 0.003. The width W of the patch should be less than $0.99 \cdot L$ (the length of the patch) to avoid producing higher order modes.

The nominal patch on TMM-6 substrate had a conductor thickness of 1.4 mils, a feed line width $F = 6.14$ mils, a feed insertion depth $\epsilon_3 = 103.0$ mils, a feed isolation gap $\epsilon_5 = 50.0$ mils, a patch resonant length $L = 243.1$ mils, and a patch width $W = 241.1$ mils. The TMM-6 substrate thickness is 25 mils, its relative dielectric constant ϵ_r is 6.0, and the dielectric loss tangent δ employed is 0.003. The width W of the patch should be less than $0.99 \cdot L$ (the length of the patch) to avoid producing higher order modes.

Next, a square lattice array of these elements was laid out with an interelement spacing of 0.664 " (664 mils) from element center to element center to ensure that we can safely scan the array out to 45° without fear of grating lobes. With the elements thus laid out, we could envision where the power division network lines would have to be laid. After the initial elevation feed lines had been laid out to connect the driving point of each elevation feed trunk to each antenna element in its respective column, Libra was utilized to check out the electrical performance of the feed. The reader should bear in mind that the driving point of each trunk lies at the output port of an azimuth feed port, of which there are 32. The 32 columns of the array would be implemented by having 32 identical elevation feed trunks with branches arrayed side by side, each one connected to the output of an azimuth feed port.

The next phase of the design process involved electrical performance optimization and modulo 2π line length equalization, causing us to perform very many iterations on each feed to achieve the performance desired. Though we will not discuss the optimization and modulo 2π line length equalization work in this report, the time and effort that it required should not be underestimated by the reader. The optimization and modulo 2π line length equalization were performed using Libra with the implicit assumptions that the

microstrip patches that we designed had $100\ \Omega$ input impedances and didn't electrically disturb conditions around the $100\ \Omega$ feedlines, because the electrical performance of the microstrip patch elements was not taken into account by the Libra design work that we did. Iterative results from Libra would be incorporated into our half elevation feed layouts in Autocad and Autosketch. These results would, in turn, have to be slightly massaged to fit within the available real estate, causing another iteration in Libra using our massaged lengths and bends, etc., until at some point we decided that our designs were acceptable and that we were ready to proceed to the fabrication stage.

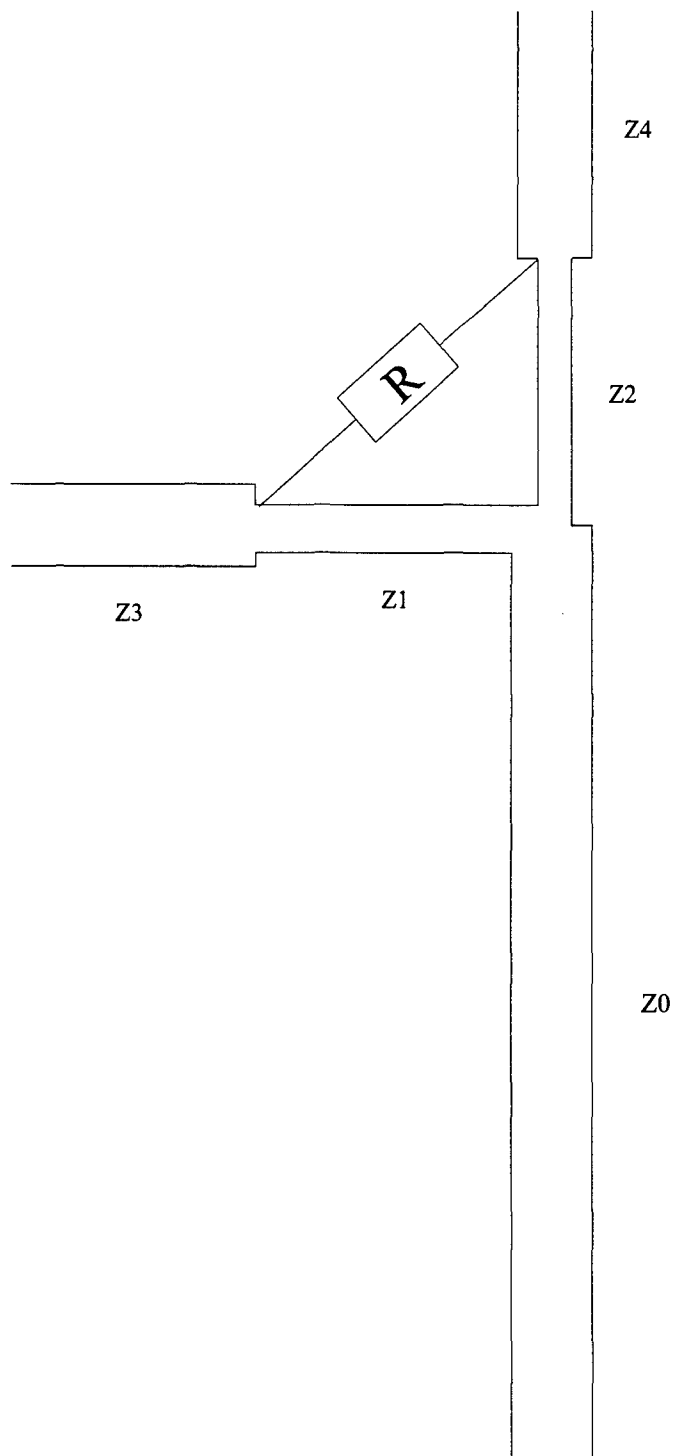


Figure 1. Sketch Of A Single Wilkinson Power Splitter (Divider)

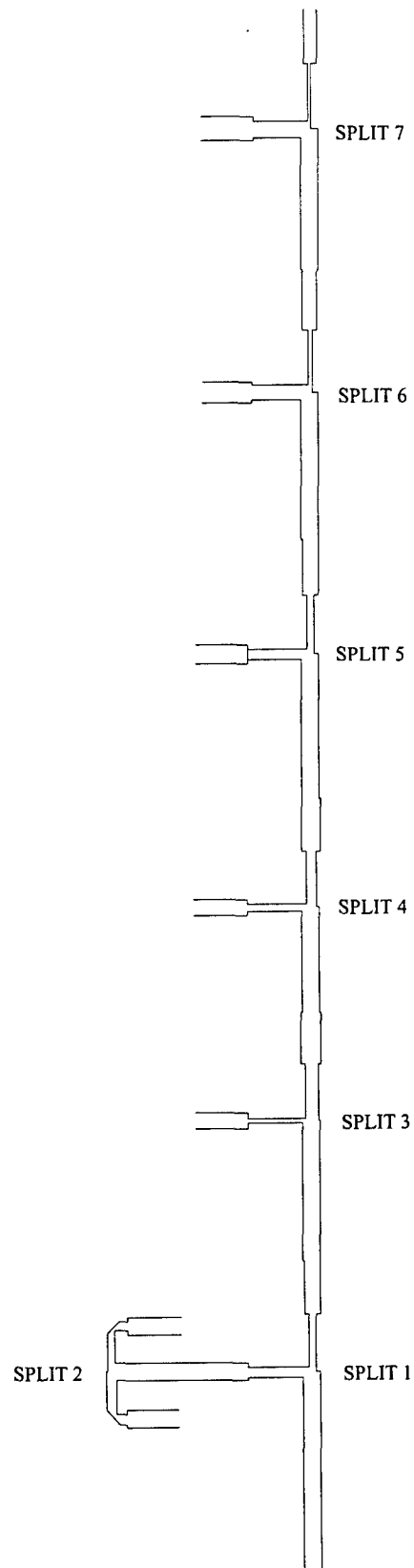


Figure 2. Basic Half Elevation Feed Structure Employed In Both The TMM-3 And TMM-6 Designs

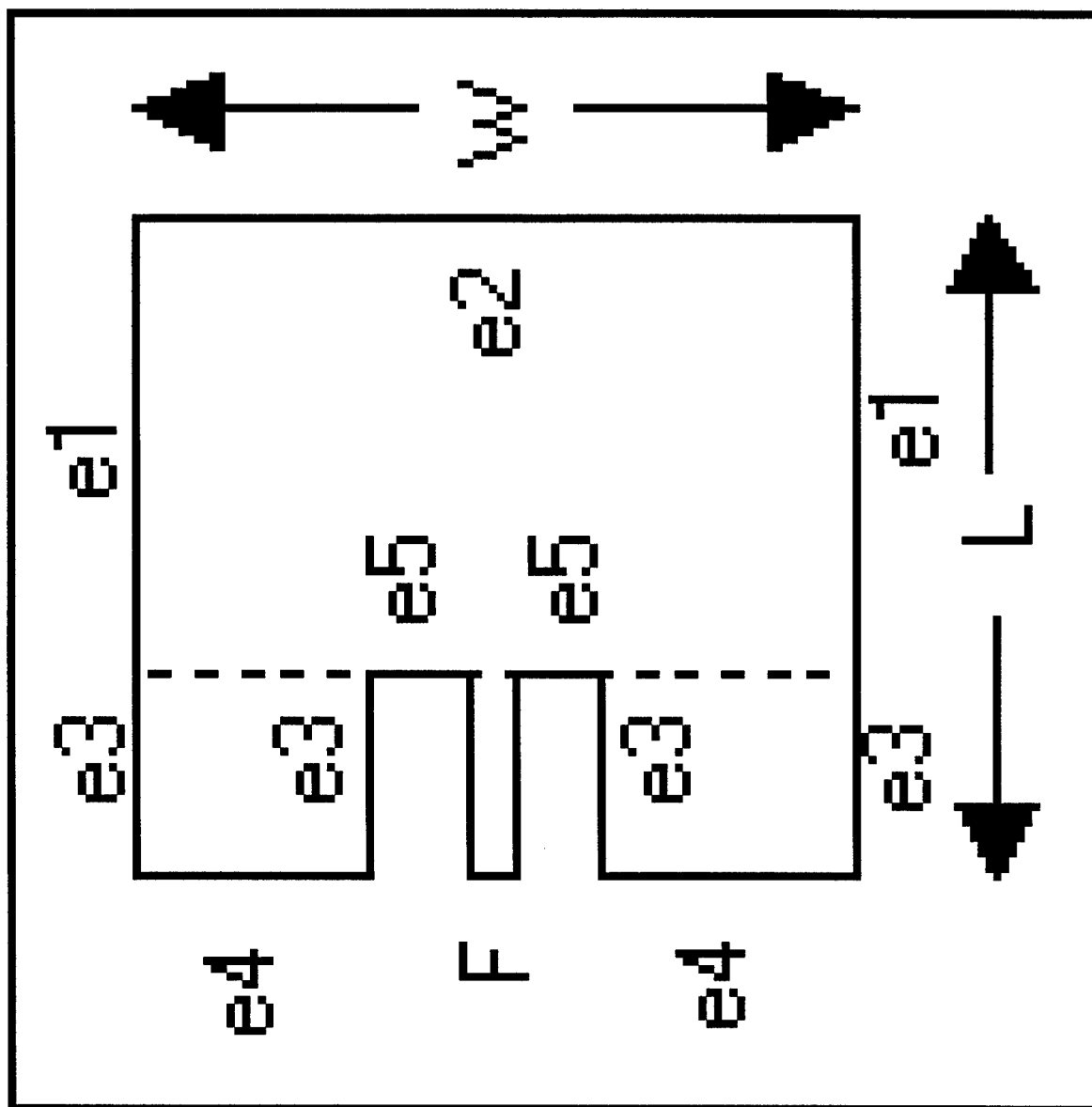


Figure 3. Drawing Of A Microstrip Patch Element Having An Inset Feed

CHAPTER 4 TEST CIRCUIT FABRICATION

At the Army Research Laboratory (ARL) in Fort Monmouth, NJ, we attempted to fabricate the test circuits ourselves.

We created *.DXF files from the layout drawings while at RL and transferred them to ARL using the FTP file transfer protocol. The *.DXF files were made into artwork at ARL though not by us. We did not learn how to operate the photoplotter nor how to develop the artwork produced by it since ARL anticipated that in a few months from our visit we would be able to FTP files to Fort Monmouth and remotely spawn the artwork generation by utilizing some new capability that ARL was going to make available to us over the Internet.

The artwork was made with a 2 mil circular aperture, apparently the smallest one that the photoplotter had, producing a significant amount of granularity which is clearly visible when looking at mitered bends in the masks under a low power microscope.

The substrate board material was cut into smaller pieces on an as needed basis. Each piece was slightly larger than the border of the mask which was to be used on it. The process for each piece was as follows. The piece was dipped in Neutra-Clean for two minutes to remove any fingerprints and dirt, rinsed, then dipped for one minute in a roughly 10% by weight solution of sodium persulfate in water which was heated slightly by means of hotplates to speed up the etching process. This ensured that a clean copper surface was presented. The board was then rinsed, air dried with the aid of pressurized N₂, and placed in an oven for 5 minutes to remove all traces of moisture. Next, the board was dipped in Shipley positive photo resist, pulled out of the resist at one corner with tweezers, held up to drip for a while, then placed in the oven to cure for 45 minutes to 1 hour. The board was then removed from the oven and allowed to cool. After cooling, the board was placed in an ultraviolet "light box" with the mask placed on top of it. The framed glass lid of the box was closed, a vacuum was pulled to clamp the mask firmly on top of the board, and the lid was flipped over to place the mask and board so as to face an ultraviolet light source. The amount of exposure was then set by the operator, and the exposure was turned on. After the exposure was finished, the lid was flipped, the vacuum turned off and the mask and board removed. The board was then placed in a solution of photoresist developer and water to develop away the photoresist on the areas exposed to the ultraviolet light. Cotton swabs were used to aid in removing loosened photoresist. After all the exposed photoresist surrounding the circuit was developed away (except for blobs of photoresist that had accumulated near the bottommost edge of the board when it was curing in the oven) the board was rinsed and placed in the heated sodium persulfate solution to etch. One ounce copper is fairly thick, and it takes a while for the copper to etch away. The possibility of overetching one region of the board and underetching some other region was very great in the process that we were employing, since there was no ready means of stirring or circulating the etchant solution without tearing up the circuit trace on the board or setting up wavefronts in the solution which caused "scalloping" of the circuit trace, where lines of a certain nominal width would etch so as to be narrow in certain spots and wide at others. The amount of undercutting can be significant as well, and it is certainly a greater concern than it would be if we were using half ounce copper metallization. We needed to use one ounce copper because of the power handling requirements that would be placed on the antenna array.

After the etching process was completed, the boards were rinsed off and acetone was used to remove the hardened photoresist from the circuit trace, leaving bare copper. No tin or gold plating was performed to protect the copper from corrosion.

The via holes indicated in the artwork were never drilled and electroplated.

None of the boards that we etched at ARL was usable. Every one had at least minor imperfections. The reasons are manifold.

The process employed at ARL was not suited to our needs, and, in fact, was rather outdated according to modern standards and practice. This is not to say that the facilities and the people at ARL aren't first rate. As a matter of fact, they planned to upgrade their etching facilities in the (then) near future, and the only thing stopping them was lack of money.

We were trying to etch circuits on Rogers TMM-3 and TMM-6 material. The TMM class of substrate material from Rogers maintains relative dielectric constant within tight tolerances across the whole board. The TMM material, however, is very brittle and therefore hard to work with. A number of our circuits were physically large (6" x 12") and it was very difficult to maintain uniformity of etch rate over the whole board, avoiding scalloping and, in some instances, having a section of line trace etched completely away. The relatively thick metallization made the possibility of severe undercutting fairly certain. The granularity introduced in our metallization pattern at the outset because of our masks didn't help, since the pattern on the masks represented the best we would be able to achieve on the substrate. Minor glitches in the artwork that looked as though the pen hadn't fully cleared the transparency sheet and left traces of its passage were present, though none appeared serious. One of the masks had been prematurely exposed to ordinary room lighting by accident, leaving a dark shadow on the artwork. The etchant bath wasn't changed frequently enough, and a few of the circuits, especially the larger ones, are badly pitted in certain areas. It is thought that the buildup of copper sulfate that resulted from not changing the bath is responsible for the pitting action, though we are not certain. Every so often, we would pull boards from the etchant, rinse them off, and check the progress under a microscope. We would check for overetch, using a special pen to touch up weak or etched through areas, and when a line acquired complete definition because all the copper nearby was etched away, we would coat the line with ink from the pen to make certain that no overetching or undercutting would occur on this section of line. It was particularly disheartening to discover pitting on our traces. We tried to cover up already pitted areas with ink, but it just didn't seem to do any good. Sections of groundplane on the back sides of the boards near the edges were etched away, but machining the boards down to the borders of the images on them (so that they would fit snugly into the test fixtures prepared for them) would remove most of this, and the remainder of the etched through ground plane could probably be touched up with conductive paint. It is not known at this time if the unevenness of the cured photoresist layer across the length of the boards was a significant factor in the poor results yielded by the process that we used. It is also not known if the intensity of the ultraviolet light or length of exposure time adversely affected things. The setting on the light box was increased from 150 to 250 in coarse steps as each successive group of boards was exposed. Also, the concentrations of solutes (sodium persulphate for etching, photoresist developer for developing) were gradually increased as the days went by.

A better process would utilize a spinner to apply photoresist uniformly to each board. The ovens would have to be larger, with a means of holding the boards in a horizontal position by gripping them from the corners of the board, well away from where the circuit traces are to be formed. After curing and exposure, the boards would be attached to another spinner, spun, and sprayed with a continual mist of fresh etchant solution. This method works well, and hopefully ARL seriously considered adopting it if/when they upgraded their etch facility.

After getting back to Rome Laboratory, we set about placing our images together in a more formal and better organized fashion. Since our plan was now to send our circuits out to industry for fabrication, the formality and organization was necessary since we ourselves would not be doing the etching, and we could not assume that those who would be doing the etching would have any more knowledge about what we wanted than what we explicitly spelled out for them. Autocad was used to perform this task. Because the PATCHANT program only yielded approximate answers, several patch circuit images were laid out to be etched on the TMM-3 and TMM-6 boards, with insertion depth, length and width varied at two mil increments in the hope that a patch that resonated exactly at 10 Ghz might be produced without the need to cut or paint. Two images of each patch circuit having a particular combination of insertion depth, length and width were laid out for etching on each type of substrate.

A request for quote was prepared and sent out from ISI to a number of microwave printed circuit board etching houses. The requirements were tough to meet, as we well knew from first hand experience. Many of the companies did not bid it because of the tough requirements. Their own adherence to military specifications and the low volume of production meant that the per circuit costs would be higher than we would be willing to pay for test articles. We chose Microwave Printed Circuits (MPC) for their price and their performance for ISI on previous jobs. The substrate material was supplied to them by ISI.

The etched circuits soon were delivered by MPC, and a quick visual inspection was performed before they were accepted.

After acceptance, Jerry Olmstead of ISI mounted the circuit boards in test fixtures especially prepared for them. The Rome Laboratory shop had already built the test fixtures based on sketches and information supplied by us. If a circuit in a test fixture became damaged, it could be removed from the test fixture and replaced with a duplicate circuit.

We were now ready to begin the measurement and testing phase. Prior to testing, a test plan was prepared. The test plan was followed wherever it was practical to do so, and is shown in Appendix C.

CHAPTER 5 S-PARAMETER MEASUREMENT CAMPAIGN RESULTS

Isolated TMM-3 and TMM-6 patch antenna elements mounted in their test fixtures were hooked up to an HP 8510C network analyzer, one at a time, and S11 as a function of frequency was plotted on a Smith chart. Resonance loops were observed that looked something like cardioids. The object was to find the impedance at the inside end of the inner loop of the cardioid and to then alter the insertion depth and the length of the patch to match the input impedance of the inside of the inner loop of the cardioid to $50.0 + j0.0$ ohms at a frequency of 10.000 GHz.

The net result of what we learned was that the insertion depth predicted by the PATCHANT program, supplied to us by ISI, was too deep, in accordance with Chris Wilder's experience. We decreased the insertion depth by painting in part of the notch with silver paint. Trimming the patches is problematic due to the fact that thin strips of copper have to be shaved off the edges of the patch, and it is difficult to do so without accidentally scratching the rest of the antenna element or digging trenches in the dielectric substrate.

For the patches on the TMM-6 substrate, the insertion depth should be on the order of 76 mils, as found from a patch having the nominal dimensions listed in Chapter 3. The length of the patch must be decreased by a small amount from the nominal value, though we don't know exactly what that amount is because we had dug up the dielectric substrate while trimming the copper, and were forced to continue our work with another patch of nominal dimensions. We did not "perfectly" tune any single one of the patches, since we were forced to spread our tuning work over multiple patches due to mishaps like this. The TMM-6 patch circuit with the dug up dielectric substrate is one of those pictured in Appendix E.

The transmission line test fixtures with via hole circuits in them have high S11 values and very low S21 values, which indicates to us that the soldered connection between the two boards in each test fixture might not be good.

The TMM-6 -3dB power divider circuit has a higher S11 value and lower S21 values than hoped for, but these values are probably acceptable.

The TMM-6 H-plane array test circuit was meant to be used in estimating the amount of mutual coupling induced in adjacent elements lying in the H-plane relative to a driven element. However, the test circuit that was examined had a pitted line in it. It appears that an air bubble found its way under the mask during the exposure process, cutting out one side of a 6.14 mil wide line.

Looking at the S11 and S21 parameters for the half elevation feed circuits, it appears that the feed taper and phase match on the TMM-3 substrate is decent and will give about -24 dB shoulders on the antenna pattern. Certainly we had hoped for better performance, though.

There must be a source of great internal reflection in the TMM-6 half elevation feed circuits that we looked at, since we had no real semblance of an amplitude taper or phase match at all. When we looked at the first circuit under a microscope, a pit was noticed on the side of a $100\ \Omega$, 6.14 mil wide feedline, and appears to have been caused by an air bubble trapped under the mask during the exposure process. Nothing else was turned up as being a possible cause for the poor performance of this feed circuit, and it was strongly hoped that its twin didn't suffer the same fate. However, the measurement data from the second TMM-6 half elevation feed circuit was virtually the same as that taken from the first, even though the second TMM-6 half elevation feed circuit had no noticeable pitting. The magnitude and phase data is such that no useful amplitude taper and phase match can be achieved across an aperture using a symmetric arrangement of two of these TMM-6 half elevation feeds. Possible causes for the poor performance of the TMM-6 design might be the following.

The 100 ohm feedlines are very narrow (6.14 mils wide), and the E-fields are not entirely contained under them, fringing out a great deal as a matter of fact. This fringing can cause coupling to adjacent lines. Space considerations precluded an adequate separation of the lines in some cases, where it became necessary to compromise on the minimum recommended interline separation distance by what was hoped would turn out to be only a small amount. The T-shaped part of the feedline run that feeds the inner two ports of the TMM-6 8 port half-elevation feed circuits might be suffering from this coupling problem.

It is thought by some that the mitered bends in the 100 ohm (6.14 mil wide) lines in the TMM-6 half-elevation feed circuits might be causing some of the internal reflections. These line widths were so narrow that we didn't use the optimum mitered bend because it would have constricted the line widths at those bends by a particularly great amount.

The serpentine courses followed by the modulo 2π equalizing line lengths in the TMM-6 half elevation feed versus those in the TMM-3 half elevation feed might also have played a role in causing unwanted coupling among sections of equalizing feedline in the TMM-6 design, causing poor performance.

Based on squaring the linear magnitude S21 terms for the half elevation feed circuits, summing these up and accounting for the input return loss (S11), we seem to be losing 13.5% of our input power to dielectric and copper loss in the TMM-3 half elevation feed (acceptable) and 28% of our input power in the TMM-6 half elevation feed. Some in our group believe that the high value of dielectric and copper loss in the case of the TMM-6 feed structure is mainly due to internal reflections which are causing the microwave energy to bounce back and forth, suffering attenuation. The TMM substrates appear to be very lossy, in addition to their other drawbacks.

The half azimuth feed performed very well. The S21 data was inserted into a file read by the PATT program that ISI (Chris Wilder) had given us to determine design and actual sidelobe levels. Assuming that the -3dB power dividers that we designed perform well, we should see -28 dB sidelobes from the full azimuth feed, with a low input return loss. Most of the feedlines in the half azimuth feed are fairly wide, and the few narrow lines extend only a short distance in length, with plenty of separation between them and adjacent lines. This could in part be responsible for the success of the half azimuth feed. The TMM-3 half elevation feed test circuit had wider feedlines than the TMM-6 half elevation feed test circuit, and had a fairly decent taper across it. These observations are what lead us to believe that E-field fringing around the narrow line width 100 ohm feedlines in the TMM-6 half elevation feed test circuits is the cause of the lack of performance demonstrated by that design.

We reformatted the data files on a PC to create S-parameter tables that Matlab can accept, and plotted the S-parameter response as a function of frequency using Matlab. By comparing the measured data with that predicted by Libra/Touchstone, we can get a feel for how various responses have been shifted in frequency, possibly as a result of coupling between the feedline structures. This process could come in handy if we ever try to deduce in greater detail what went wrong with the TMM-6 elevation feed structure.

CHAPTER 6 FARFIELD ANTENNA PATTERN MEASUREMENT RESULTS

E-plane principal polarization antenna pattern cuts of the farfield patterns for two nominal sized TMM-3 rectangular microstrip antenna patches were taken in a rather crude but creative sense on a network analyzer, for later comparison with antenna pattern cuts that would be taken in an anechoic chamber.

An X-band horn was hooked up to arm #1 of an HP 8510C network analyzer. A TMM-3 isolated patch was connected to arm #2, and S21 was measured over 8.000-12.000 GHz at 5.0 Mhz increments (801 frequency points). Based on the graphical display of S21 vs. frequency, a maximum could clearly be seen around 9.825 or so (plus or minus 5.0 MHz). The value of S21 at 9.825 GHz was recorded manually for different positions of the antenna element relative to the face of the transmit horn, namely, from -90 degrees to +90 degrees at 5 degree increments. This was done for two TMM-3 nominal isolated patches. The patch test fixture was held in place by means of a home-built special jig. An H-plane cross-polarization pattern was also taken, but the test setup must have been limited by background noise at these low S21 values, since the readings often fluctuated by at least one dB, and sometimes by as much as four dB over successive frequency sweeps. We would have then taken data on the nominal sized TMM-6 isolated patch that we had available, but in removing TMM-3 patch #2 we found that its SMA connector had come out of its socket and was lodged in the coaxial cable that we were using to extend the reach of measurement arm #2 of the network analyzer. At a later date, these measurements were repeated for a nominal sized TMM-6 patch. In addition to damage caused by Exacto blades and silver paint, our test circuits also suffered occasional damage when SMA connectors screwed their way out of the test fixtures and pulled tracts of feedline up off the substrate in the process. One of the circuits pictured in Appendix E has suffered this fate.

This was the extent of our having used a network analyzer to measure antenna patterns. From this time forth, we used the indoor anechoic chamber on Tanner Hill, Newport Test Site, to measure farfield antenna patterns.

Two days after the experiment in measuring patterns with the HP 8510C, we measured the antenna patterns of an isolated TMM-3 rectangular microstrip patch element (TMM-3 patch #1) and a linear array of these patches (arrayed in the H-plane) at the Tanner Hill indoor anechoic chamber.

The E-plane principal polarization antenna pattern cut agreed fairly well with the crude ones obtained two days before. The most notable character in all these E-plane patterns was 1) the slight dip (1 dB or so) in the pattern at broadside; 2) the large dip (or "suckout") in the pattern at an angle of about +40 degrees or so that appears to be down about 2 dB or so from the pattern value at -40 degrees; 3) the large hump beyond the suckout; and 4) as the angle off broadside approaches ± 90 degrees the pattern doesn't roll off to about 20 db or so below the peak value (which should have been at broadside) but instead only rolls off by about 8 db from what the peak would have been at broadside if there had been a peak instead of a 1 dB dip. A possible explanation for this odd behavior is the following. The insertion depth of the inset fed patch is too large. We know this to be true because the input impedance of the patch is too low, and in order to raise it such that the patch is matched to its 100 ohm feedline we had to paint over the furthest reaches of the insertion depth with silver paint. Also, the design equations that we used to calculate the initial size of the patch are known to yield insertion depths that are longer than what are needed in practice. Chris Wilder has seen roughly the same behavior in patches he designed using the same equations we used, though the ill effects were much less severe. His patches had a slight pattern dip at broadside and a suckout that occurred much farther from broadside than ours did. We are not certain what kind of pattern rolloff his patches exhibited, but suspect that their E-plane principal polarization pattern cuts did roll off to 20 dB below the values near broadside. We were working with substrates that had higher dielectric constants than those that Chris typically worked with, and he believes that the effects that we see in our TMM-3 patches are brought out more by the fact that the substrate dielectric constant is so high, and are due to the fact that the inset feed by its very nature leads to the formation of two adjacent slots (one on either side of the feedline) that radiate, constructively and destructively, interfering with the pattern of the patch.

The H-plane principal polarization pattern for the isolated TMM-3 patch looked fairly good, although it had a little asymmetry in the pattern and, though it did roll off fairly smoothly, it only rolled off to a little less than about -20 dB or so at the pattern edges relative to the value at broadside, instead of a desired -30 dB or so. We were happy that it at least it rolled off to about 10 dB below the pattern edge value achieved in the E-plane pattern.

The cross-polarization patterns for the TMM-3 isolated patch looked fairly good, with a beautiful null at broadside for the H-plane cross-polarization pattern.

The E-plane principal polarization pattern for the array of TMM-3 patches (two half elevation feeds having radiating elements laid side by side in mirror-like fashion and fed from a common feed point) looked about the same as the E-plane principal polarization pattern for the isolated patch, being fairly broad with a slight dip at broadside. There was a suckout to either side of the center, and a hump on the far side of each suckout. The H-plane principal polarization pattern resembled an array pattern, since the elements were, after all, arrayed in the H-plane, but really didn't have much desirable character. Chris Wilder described it as a "formless blob of energy", and attributed its shape to the fact that the elements weren't matched to the feedlines, and that the resulting mismatches destroyed all semblance of a pattern that we would expect to see from an array with antenna elements which were well matched to their feedlines.

Other pattern measurements were taken at the indoor anechoic chamber at a later date.

CHAPTER 7 SUMMARY

Though the objectives of this project weren't met, the team members feel that if the work had been continued through another design iteration, much better results could have been achieved. There are grains of wisdom that were uncovered in the course of this effort that anyone could profit from in future antenna array design work. The author believes that these grains are presented clearly in the text. It is hoped that the readers of this document will benefit from our experiences and be able to produce quality antenna designs without having to travel the same design path that we did.

The Rogers TMM-3 and TMM-6 substrates are difficult to work with. This has been attested to by etching houses as well as by our own experiences. The narrowness of some of the elevation feedlines (leading to possibly excessive fringing effects and susceptibility to pitting) and the necessity to pack the meandering lines (to achieve modulo 2π line length equalization) into very cramped quarters in all likelihood lead to coupling which adversely impacted our tapers, especially in the case of the TMM-6 half elevation feed. Certain rules of thumb that we tried to adhere to had to be put aside in some instances while designing the TMM-6 half elevation feed because there was not enough board real estate available. The presence of the feedlines on the same board as the radiating elements might have negatively impacted our array patterns, though it is difficult to say with any degree of certainty what caused the "formless" patterns that we measured, since we weren't able to achieve the clean tapers that we had hoped for from the half elevation feeds, had difficulty matching the radiating elements to the feedlines, and had difficulty producing good radiation patterns from the individual patch elements. All these factors probably played a role in producing the "formless" farfield patterns. Tuning of the patches required patience and plenty of spare patches etched in a wide variety of dimensions about the nominal values to minimize the amount of manual tuning that had to be done. Extra circuit boards were also necessary so that replacements were available should an SMA connector screw out of a test fixture and pull part of the feedline off the substrate, or so that a circuit with a pitted feedline could be replaced with an equivalent circuit having no pitting.

Finally, there is a strong possibility that more than one mode was being excited in the patches. The patches were very nearly square (ignoring the inset), and the predicted resonant frequency for the (1,0) mode was very close indeed to that predicted for the (0,1) mode. The kink in the resonance loop plot for an isolated, unmodified patch shown in the third figure in Appendix H is apparently indicative of an element with two nearly degenerate modes (two modes whose resonant bands overlap). According to Reference 12, pages 10-28 and 10-29, whenever an isolated, unloaded patch exhibits the behavior illustrated in the third figure in Appendix H, one could expect that multiple modes are present.

REFERENCES

1. ISI Briefing Charts, 1992-1993, prepared by Christofer Wilder and Ronald Gauss for presentation to the Rome Laboratory team members.
2. Sonnet Software Reveals Tangential Electric Fields, Wavelengths, Volume 9, Number 1, March 1993, page 12, published by Eesof Incorporated.
3. Eesof Element Catalog, Version 3.5, published by Eesof Incorporated.
4. Full-Wave Spectral-Domain Analysis of Compensation of Microstrip Discontinuities Using Triangular Subdomain Functions, by Tzyy-Sheng Horng, William E. McKinzie and Nicolaos G. Alexopoulos, IEEE Transactions on Microwave Theory and Techniques, Volume 40, Number 12, December 1992.
5. Design Considerations for Low Sidelobe Microstrip Arrays, by David M. Pozar and Barry Kaufman, IEEE Transactions on Antennas and Propagation, Volume 38, Number 8, August 1990.
6. Simple Model for the Input Impedance of a Coax-Fed Rectangular Microstrip Patch Antenna for CAD, by F. Abboud, J.P. Damiana & A. Papiernik in the IEE (not IEEE) Journal, Part H, October 1988, page 323.
7. Computer-Aided Design of Microstrip Couplers With Accurate Discontinuity Models, by E. Hammerstad, KLAB, N 7034 Trondheim-NTH, Norway, IEEE Microwave Theory and Techniques Symposium, 1981.
8. Experimental Study of Symmetric Microstrip Bends and Their Compensation, by R.J.P. Douville and D.S. James, IEEE Transactions on Microwave Theory and Techniques, MTT26, March 1978.
9. Equivalent Capacitances for Microstrip Gaps and Steps, by P. Silvester and P. Benedek, IEEE Transactions on Microwave Theory and Techniques, MTT-20, November 1972.
10. Equivalent Capacitances of Microstrip Open Circuits, by P. Silvester and P. Benedek, IEEE Transactions on Microwave Theory and Techniques, MTT-20, August 1972.
11. The Equivalent Circuit of Some Microstrip Discontinuities, by B. Easter, IEEE Transactions on Microwave Theory and Techniques, MTT-23, August 1975.
12. Antenna Handbook - Theory, Applications and Design, edited by Y.T. Lo and S.W. Lee, Van Reinhold, 1988, pages 10-10, 10-11, 10-28, 10-29.

APPENDIX A COMMONLY ENCOUNTERED DISCONTINUITIES IN MICROSTRIP LINES - THEIR USES, PHYSICAL AND ELECTRICAL IMPACT ON CIRCUITS, AND LUMPED ELEMENT EQUIVALENT CIRCUITS

Discontinuities in microstrip lines produce disturbances to the electric and magnetic fields in the vicinity of each discontinuity.

A disturbance to the electric field manifests itself as a capacitance, producing a buildup of excess charge. A disturbance to the magnetic field manifests itself as an inductance, producing current flow disturbances.

Knowledge of discontinuity behavior can be gainfully employed by the circuit designer. Bear in mind that a straight microstrip line of uniform width is nothing more than a transmission line. For more interesting and desirable effects, discontinuities of some sort have to be present.

Commonly encountered discontinuities in microstrip include the following:

- a) mitered bends;
- b) T-junctions;
- c) steps;
- d) open circuits;
- e) short circuits;
- f) series gaps;
- g) crossovers;
- h) narrow transverse slits;
- i) via holes to ground.

MITERED BENDS

By mitering a bend, you have [3,8]

- a) eliminated a high tangential E-field air dielectric breakdown (arcing) point;
- b) eliminated a "pocket" where excess charge tends to build up, resulting in parasitic capacitance, leading to an unwanted reactance term, which causes return loss at the bend and shifts resonant frequency;
- c) not disturbed the current flow by much compared to the unmitered case.

Refer to Figure 4.

The optimal miter, expressed as a fractional quantity, is given by the following expression [3,8]:

$$\frac{X}{D} = 0.52 + 0.65e^{-1.35(W/H)} \quad (1)$$

where $\frac{W}{H} \geq 0.25$, $\epsilon_r \leq 25$ and H is the substrate height

and, by geometry, the reference plane shift S is given by:

$$S = W\left(\frac{2X}{D} - 1\right) \quad (2)$$

where S is the amount that n1 and n2 are shifted back away from the bend. Reference planes n1 and n2 mark the boundaries within which the disturbed fields at the bend are contained.

It is possible to overcompensate by mitering. The optimal miter is such that the capacitance term is reduced to the point where it could actually become inductive.

Figure 5 shows the usual current distribution on a meander line, where red is high current and blue is low current, with the spectral colors representing intermediate values. Three important aspects of this distribution are shown. First, note the high current (red) on the edge of the microstrip line. This is the well-known "edge singularity" present in all planar circuits. Second, the standing wave is also visible. This is a non-50Ω line terminated in 50Ω. Third, note that in going around the bend, nearly all current takes the inside edge.

Figure 6 [2] displays the tangential electric field distribution over a meander line. There is strong tangential electric field at the low current points and a weak electric field at the high current points, as expected. Unexpectedly, however, there is a strong electric field on the outside edge of the bend. While the total current through the line is high at the bend, because the current all flows on the inside edge, it leaves the outside edge with high voltage. During operation, this point could break down, especially if one of the standing waves had a voltage peak here.

Figure 7 [4] illustrates a top view of a right angle bend and shows a miter that will be applied, with the microstrip line broken up into triangular subdomains. It also presents an equivalent circuit for the mitered bend and a longitudinal view of the microstrip line on the substrate. Figure 8 [4] illustrates the magnitude of the edge singularity of the electric surface currents as they exist at and near a mitered bend discontinuity.

T-JUNCTIONS

Let port 1 in Figure 9 [4] be the input port. Energy coupled into port 1 would "rather" go through port 2 than port 3. This effect becomes more noticeable as frequency is increased, and is definitely evident at X-band. Full wave analysis predicts this. Static analysis as performed in Libra does not. If further analysis of the results obtained from our test circuits indicates that power distribution in the feed structures is being adversely affected by this effect, our redesign could make use of compensated T-junctions, similar to the mitered one shown in Figure 10 [4]. Other compensated T-junctions appear in the literature as well, where the line joining port 1 and port 2 is slightly constricted in width, and the section of line in the immediate vicinity of port 3 is widened. A way to remember this is to note that we are trying to reduce current flow to port 2 and increase current flow to port 3 such that the current split ratio that is achieved is the one that we want. Therefore we constrict the connecting section of line from port 1 to port 2 to reduce current flow to port 2, and widen the line at port 3 to "catch" more current flow from port 1 and route it to port 3.

In Figure 9 [4], the dashed lines (reference planes) do not completely contain the disturbed fields. The resulting parasitic capacitance and inductance values causing charge buildup and reference plane shifts that are associated with the T-junction may be negative. For moderate to high impedance branch lines (port 3 in the above figure) the junction capacitance becomes reduced below that of either the port 1 or port 2 microstrip line capacitance per unit length. Thus, capacitance is taken out of the junction and the equivalent circuit capacitance for the junction is negative. If the parasitic capacitance for the junction is positive, the strip lengths must be shortened. If the parasitic capacitance calculated for the T-junction is negative, the strip lengths must be increased.

Figure 11 [4] depicts current flow through a mitered T-junction, where the incident current comes out of port 3 and flows into port 1 and port 2. Note that the current flow in Figure 11 is coming from port 3, not port 1 as is assumed in Figures 9 and 10.

STEPS

Note the pockets of excess charge in Figure 12. There will be an effective line extension to the wider line (of width $W1$) due to the buildup of excess charge.

OPEN CIRCUITS

Open circuits can be used as matching stubs. One example which springs readily to mind involves using an open circuited line to compensate for mismatch due to a plated through via hole encountered when transitioning from one substrate board to another one possessing a different relative permittivity.

There is an effective line extension of the open circuited line due to the excess charge buildup. We compensate for this effective increase by decreasing the physical length of the open circuited stub by an amount equal to the effective increase to null out its effect, leaving us with an effective $\lambda/2$ stub.

An unmitered open circuited line is depicted in Figure 13, and is intended to show the buildup of charge at the end of the physical line.

The geometry of an unmitered and a mitered open circuited line (open-end discontinuity) is shown in Figure 14 [4]. Mitering is applied to reduce the amount of stored charge at the end of the line, hence reducing the capacitance that the line terminates in. The magnitude of electric surface currents on a mitered open-end discontinuity (open circuit stub) are shown in Figure 15 [4].

SHORT CIRCUITS

We will not discuss these here. A short circuit stub is physically implemented as an open-end discontinuity much like an open circuit would be. The difference is that a short circuit stub is $\lambda/4$ in length, as opposed to $\lambda/2$ (the length of an open circuit stub).

SERIES GAPS

Series gaps are used to couple energy to edge-coupled filters, ring resonators, square loop resonators, and so forth.

CROSSOVERS

Crossovers are useful for creating low impedance stubs.

NARROW TRANSVERSE SLITS

Narrow transverse slits contribute series inductance (edge current is disturbed).

PLATED THROUGH VIA HOLE TO GROUND

Plated through via holes to ground are used in rectangular quarter wave microstrip patch antennas to force an E-field null at the far end of the patch i.e. on the side of the patch opposite the side where the feedline connects to the patch.

Plated through via holes which do not connect to ground are used as conducting lines to route current from one board to another in a multiboard microstrip circuit

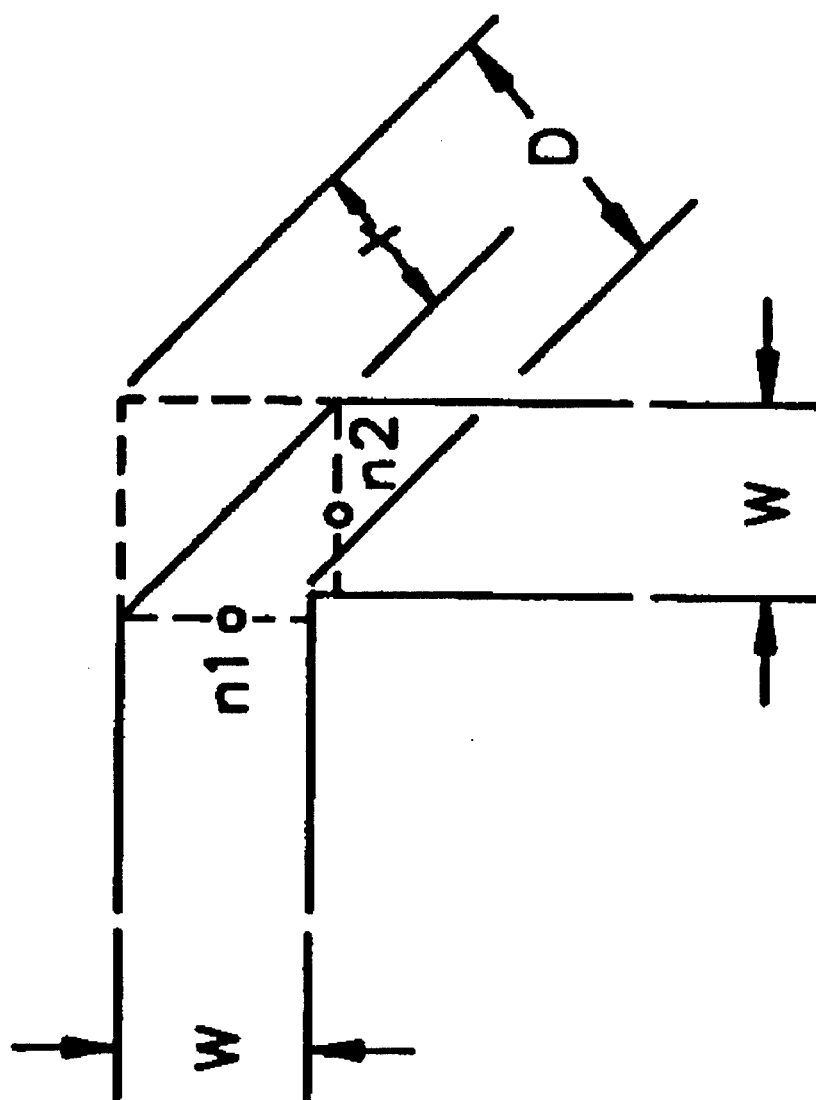


Figure 4. Sketch Of A Mitered Bend With Important Dimensions Indicated

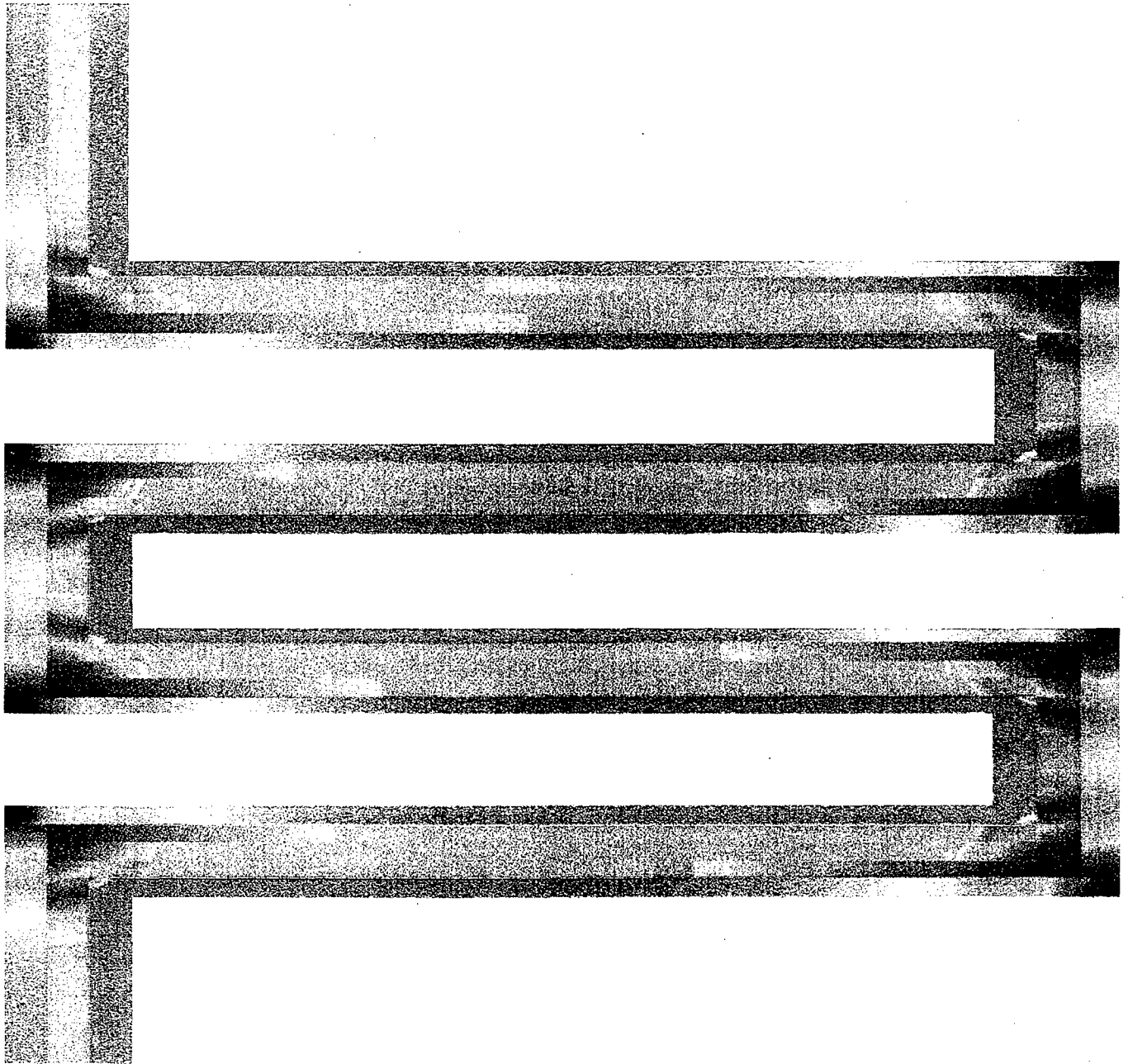


Figure 5. Current Distribution On A Microstrip Meander Line

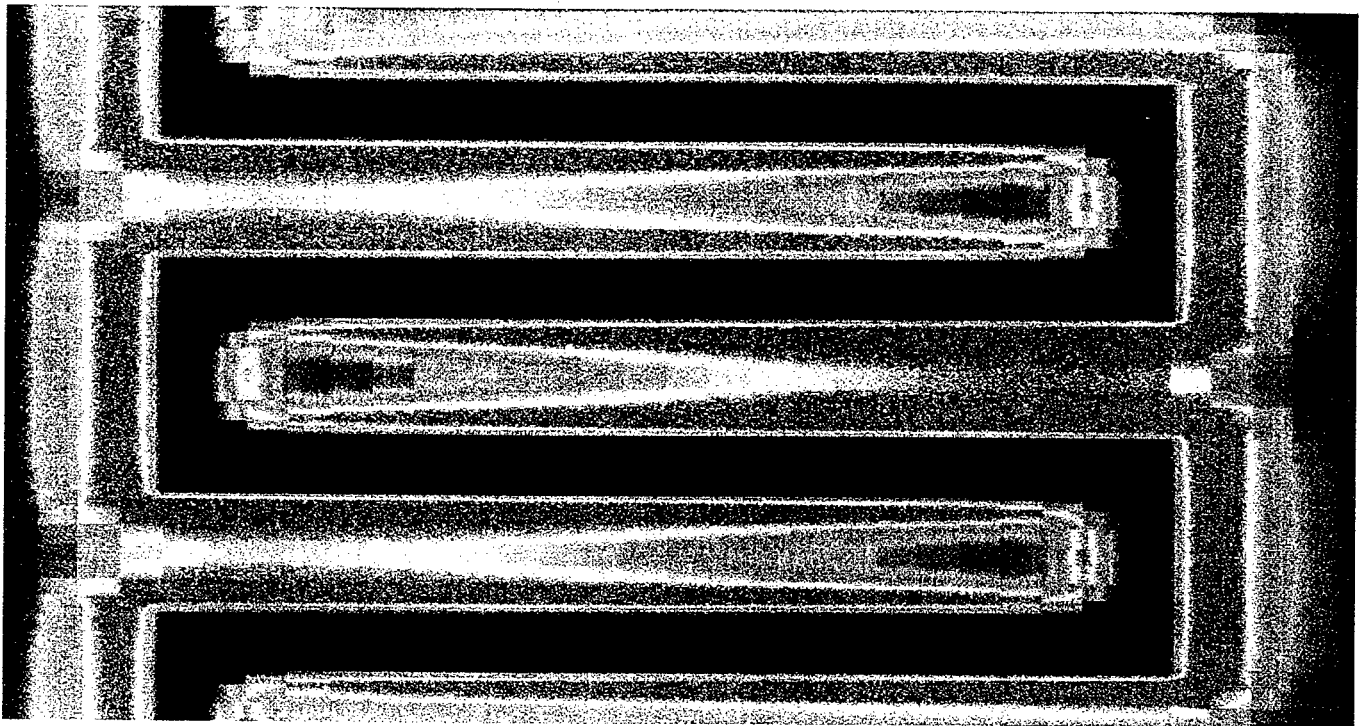


Figure 6. Tangential Electric Field Distribution Over A Microstrip Meander Line

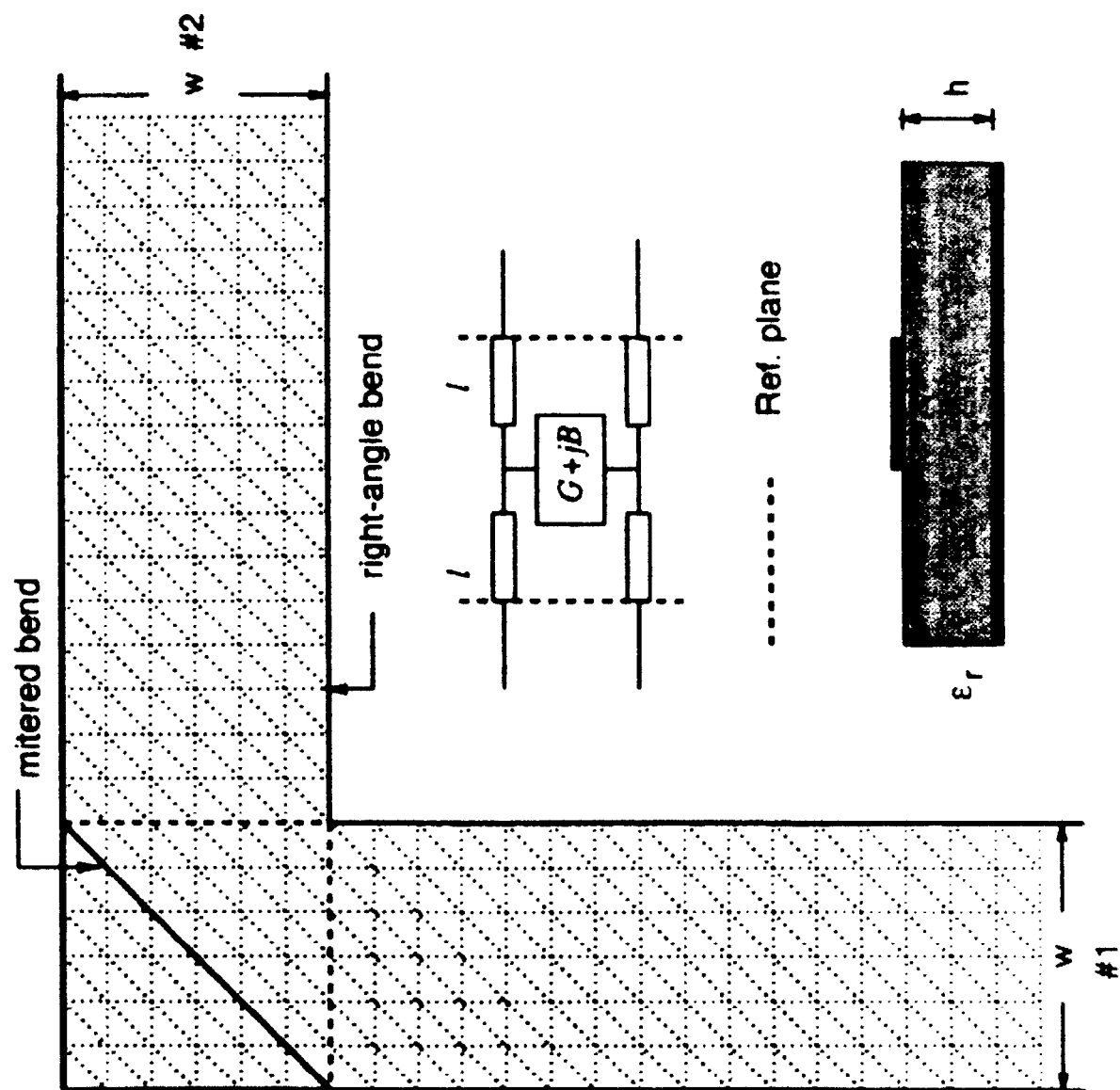


Figure 7. The Geometry Of Right Angle And Mitered Bend Discontinuities As Utilized In Figure 8 For A Mitered Bend

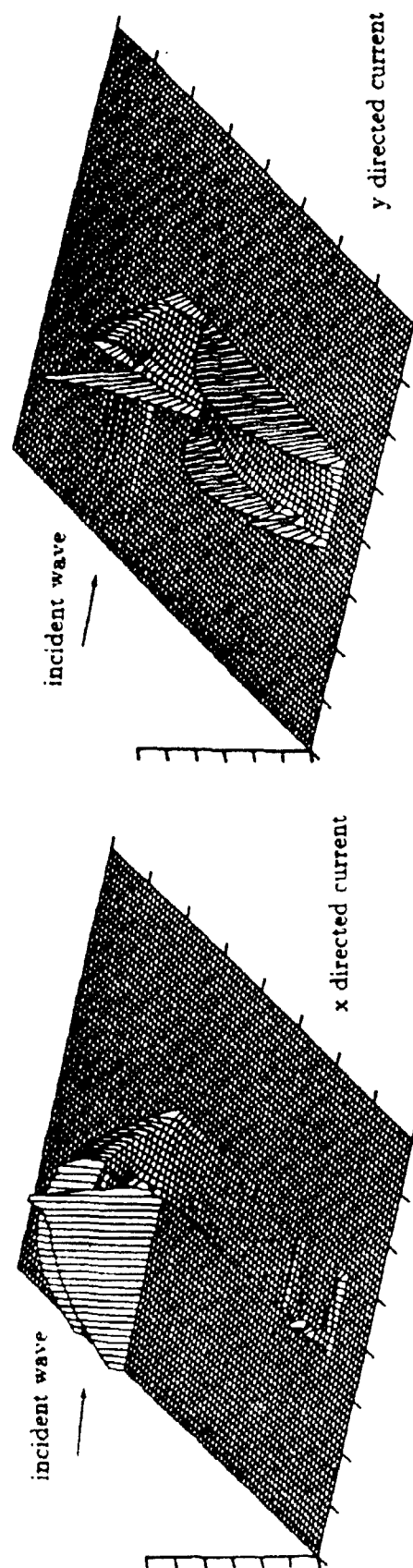


Figure 8. Magnitude Of Electric Surface Currents At A Mitered Bend

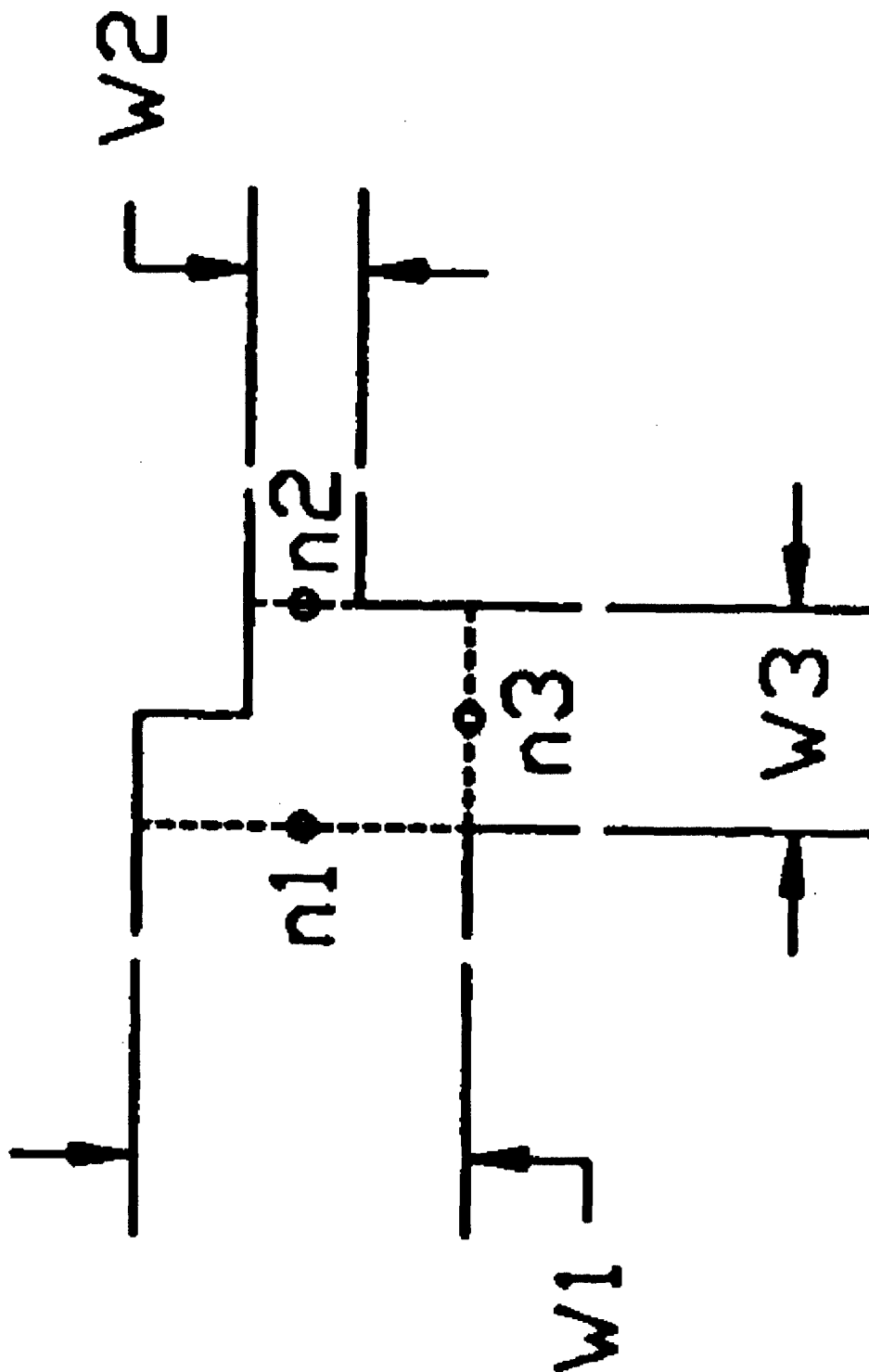


Figure 9. Sketch Of A Microstrip T-Junction With Important Dimensions Indicated

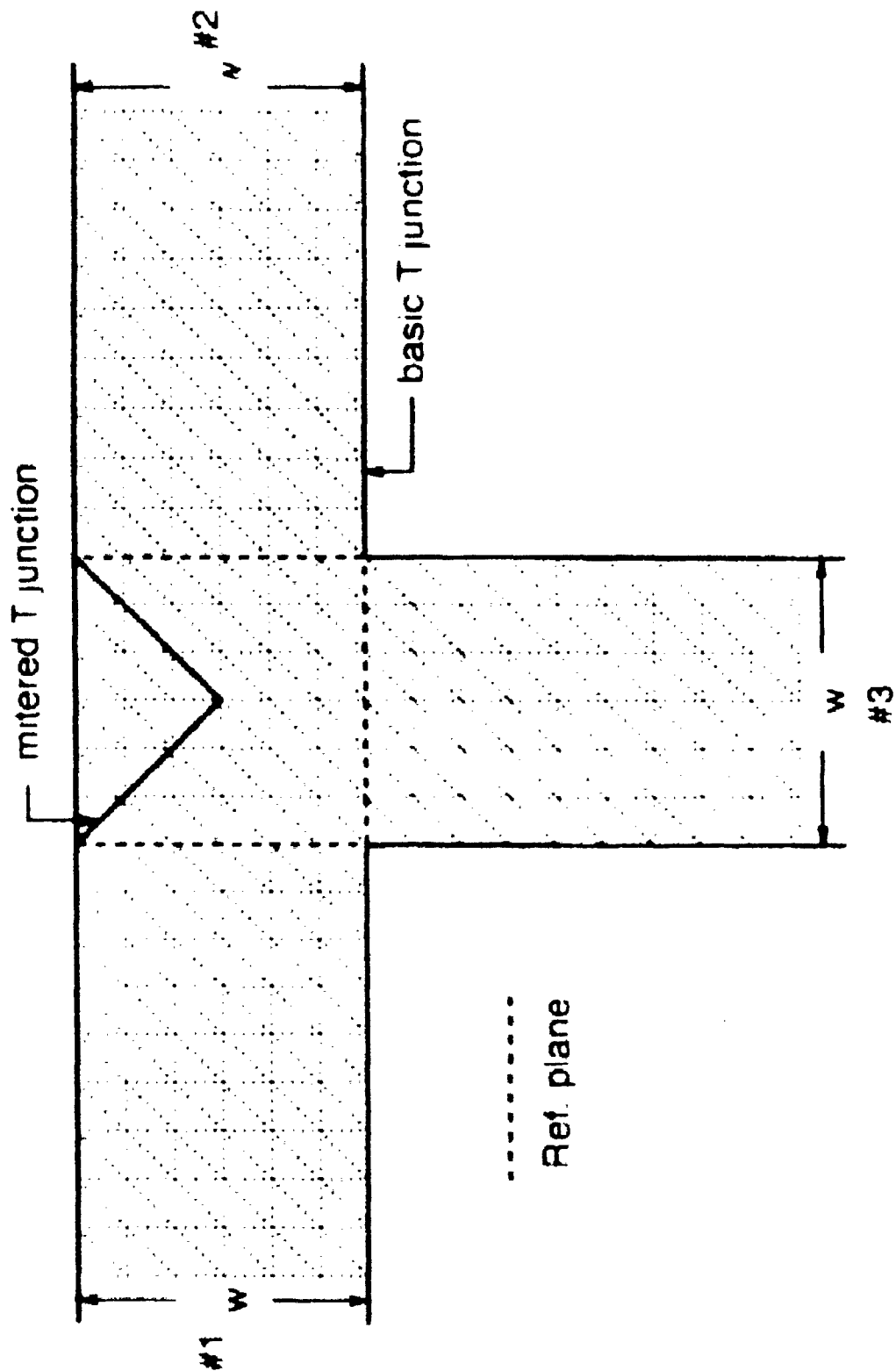


Figure 10. The Geometry Of A Mitered T-Junction As Utilized In Figure 11

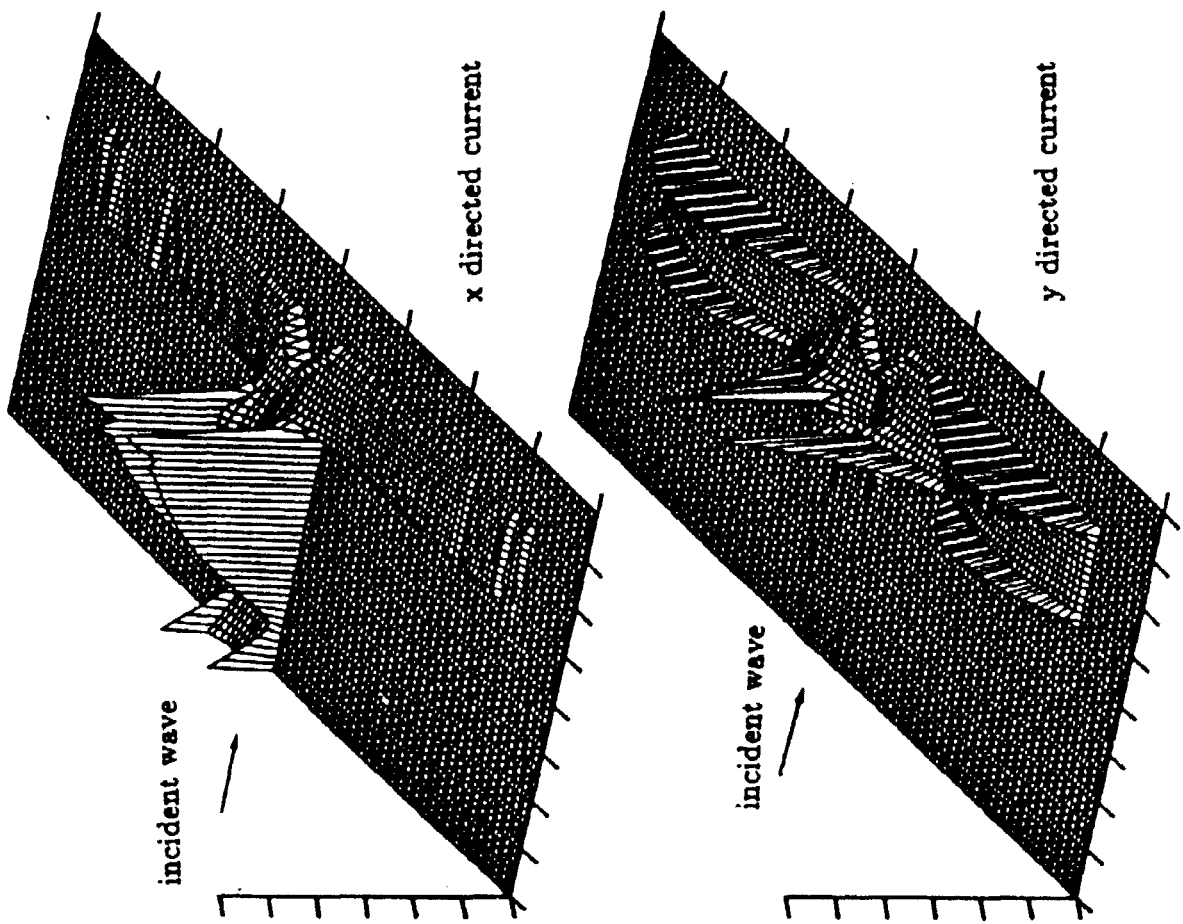


Figure 11. Magnitude Of Electric Surface Currents On A Mitered T-Junction

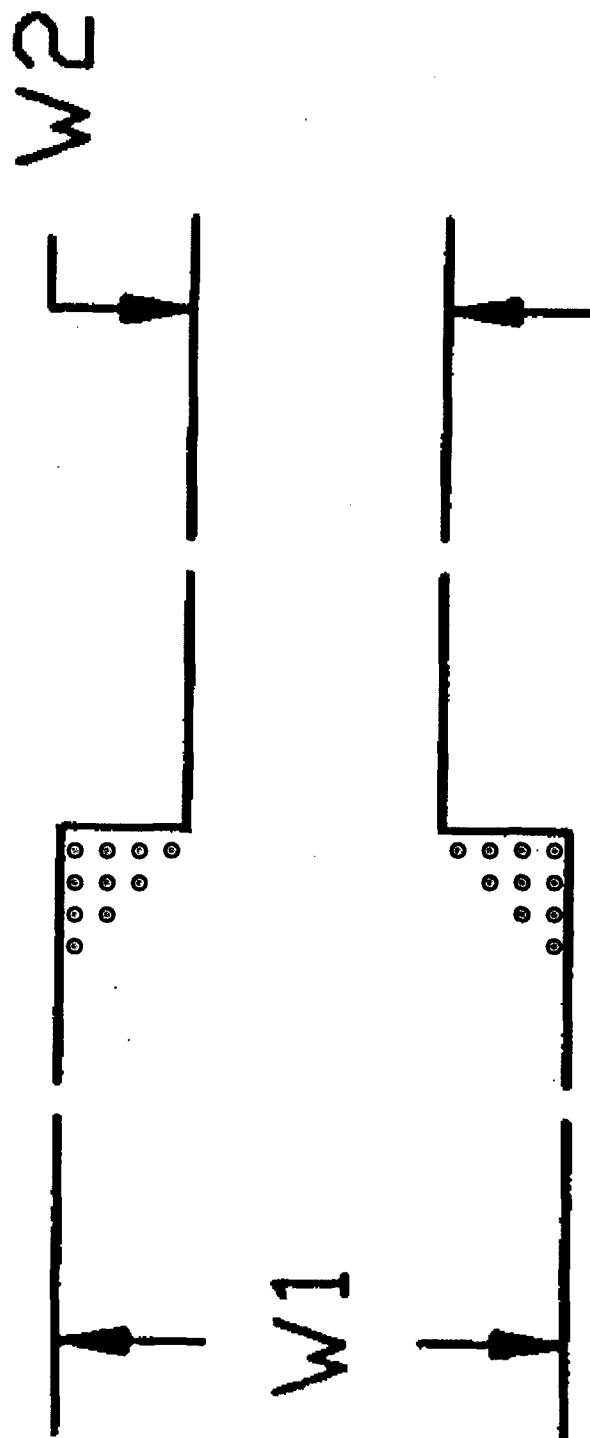


Figure 12. A Step In Line Width For A Microstrip Line With Charge Buildup Indicated By Dots In The Corners



Figure 13. An Open End Discontinuity, With Charge Buildup At The End Shown As Dots, Forming An Open Circuit Matching Stub Much Like The Ones Used In The Plated Through Via Hole Test Circuits

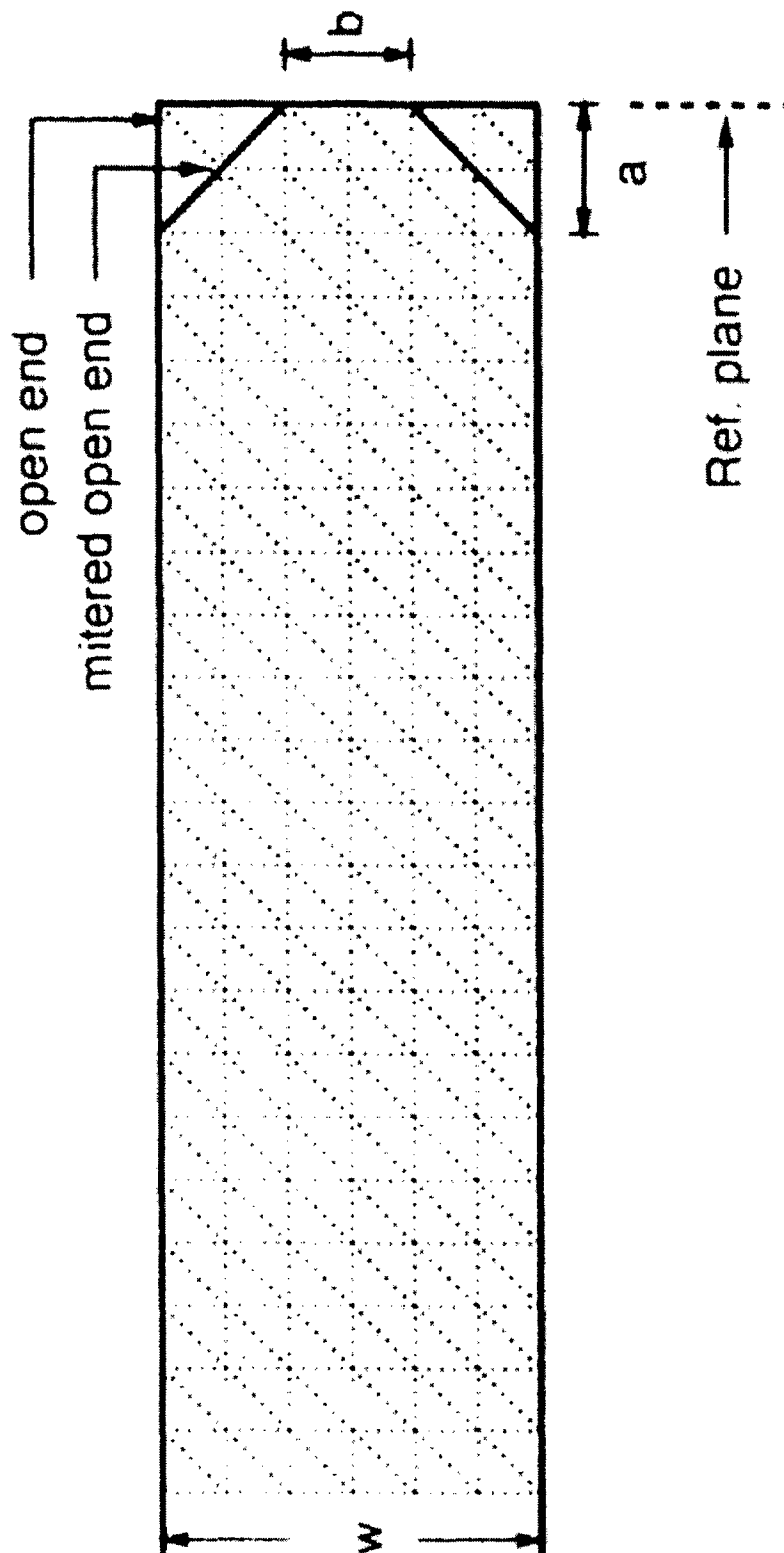


Figure 14. Geometry Of Unmitered And Mitered Open End Discontinuities As Utilized In Figure 15 For The Mitered Open End Discontinuity

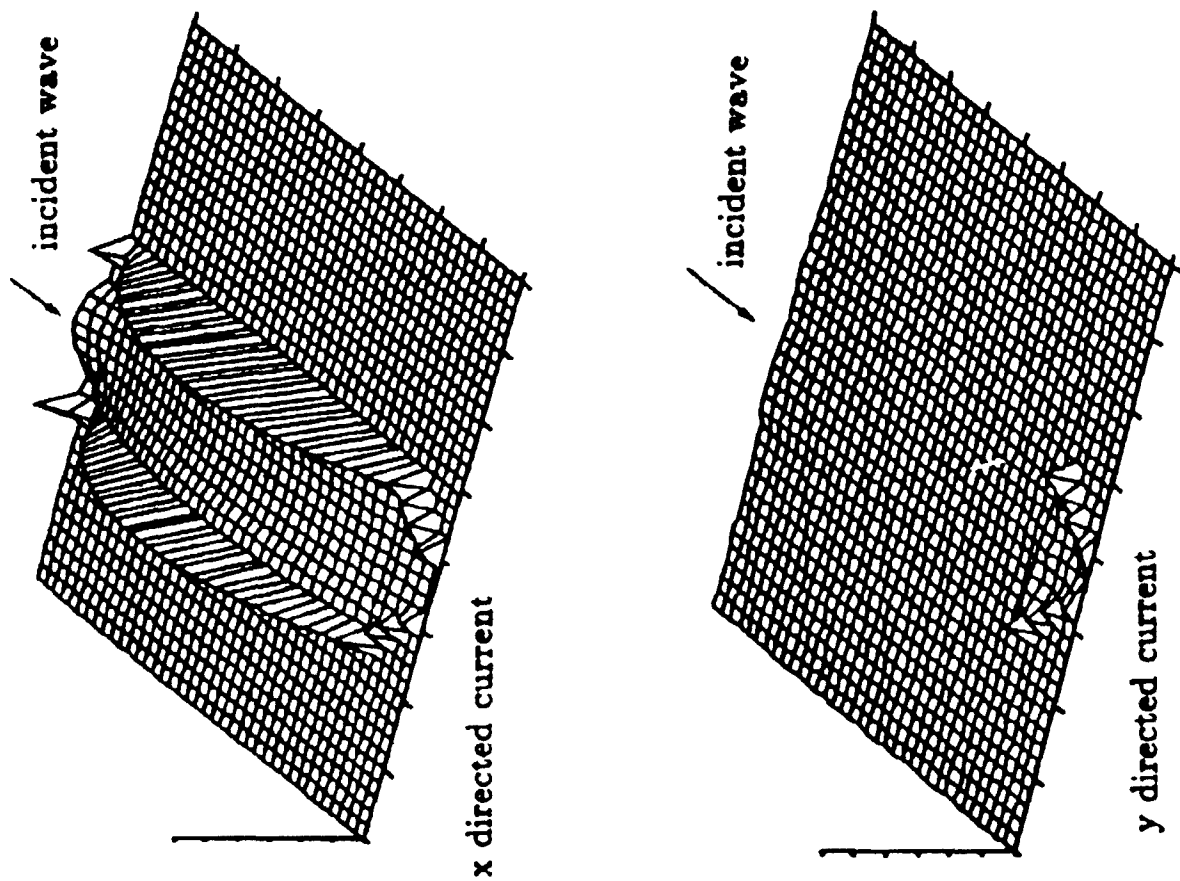


Figure 15. Magnitude Of Electric Surface Currents On A Mitered Open End Discontinuity

APPENDIX B CAVITY MODEL FOR A MICROSTRIP PATCH ANTENNA¹²

Refer to Figures 16 and 17 for graphical details.

When current is injected into a microstrip element, a charge distribution is established between the surface of the ground plane and the upper and lower surfaces of the patch. Two tendencies manifest themselves.

- 1) There is an attractive tendency between opposing charges on the lower surface of the patch and on the upper surface of the ground plane. The attraction tends to keep patch charge concentrated at the bottom of the patch.
- 2) There is also a repulsive tendency between like charges at the bottom of the patch. This tends to push some of the charge around the edge of the patch onto its top surface.

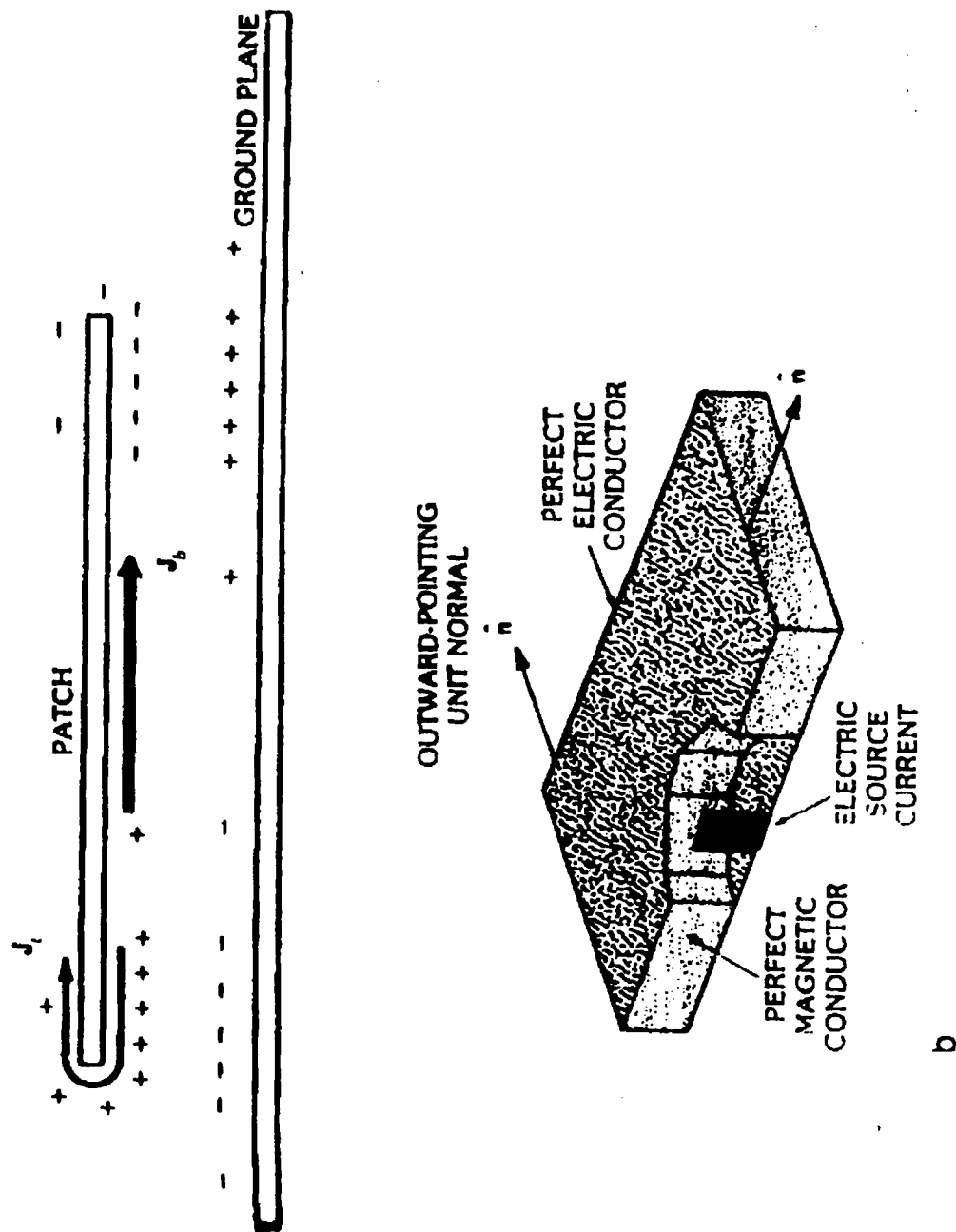
When the patch is very thin the first tendency dominates and most of the charge on the patch resides at its bottom side. Only a small amount of current flows around the edge onto its upper surface. The component of magnetic field tangential to the patch edge is small but non-zero.

One could introduce a perfect magnetic conductor in the plane between the patch edge and the ground plane without affecting the fields under the patch. To find the shape of the magnetic field distribution under the patch, one can replace the antenna by an ideal cavity as in Figure 16. From the magnetic field distribution the shape of the electric field can also be found. However, the amplitude of the field under the patch can not be found by just analyzing the cavity model alone. For example, if dielectric constant within the cavity was assumed to be lossless, then this model would yield a purely reactive input impedance.

Of course, the input impedance of the antenna is not purely reactive. The impedance function for an ideal cavity has only real poles. The actual antenna impedance has complex poles. The real part of the ideal cavity model poles and the real part of the antenna poles are almost identical and they are based on the shape of the antenna.

The imaginary parts of the poles account for power loss by radiation, dielectric losses and conduction losses. To make the cavity model more resemble the antenna, one can add losses to the cavity dielectric.

The objective then becomes to find how much loss to add to the cavity model so that the imaginary part of its poles near the frequency of interest matches that of the imaginary part of the antenna impedance poles.



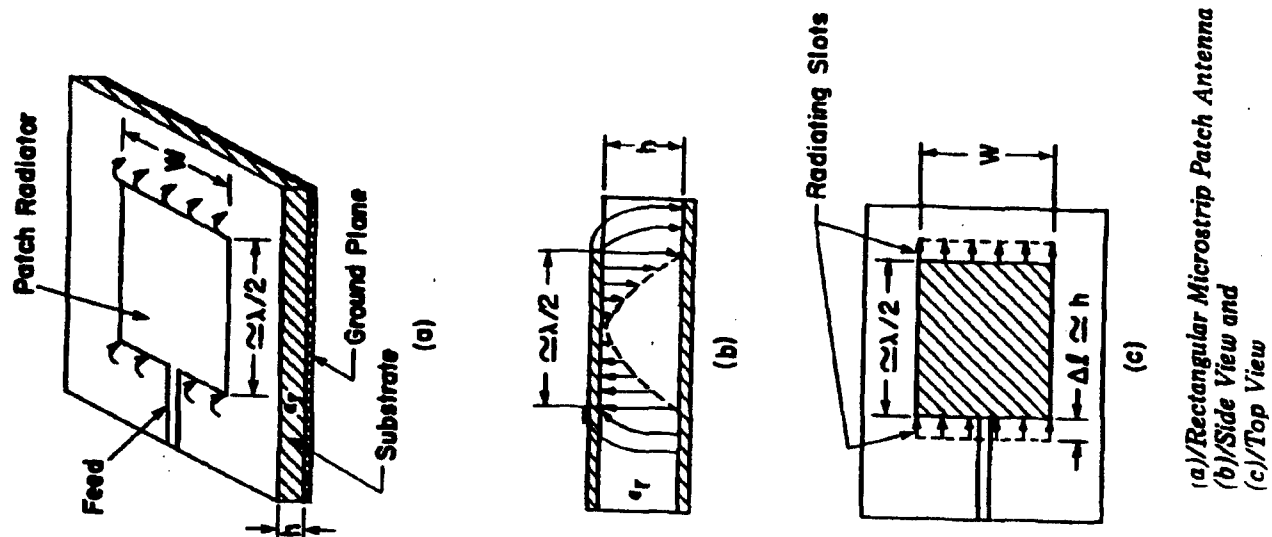


Figure 17. Rectangular Microstrip Patch Antenna (No Inset Feed)

APPENDIX C TEST PLAN

OBJECTIVE: The objective of this test plan is to provide the measurement team with rudimentary guidance on what measurements to take during the S-parameter and antenna pattern measurement runs to be made under this program.

S-PARAMETER MEASUREMENTS ON THE HP 8510 VECTOR NETWORK ANALYZER (VNA):

CALIBRATION OF THE HP 8510 EQUIPMENT:

- 1) The HP 8510 shall be precalibrated, recalibrated and postcalibrated in such a manner as to bracket groups of measurements and at a reasonable time interval to ensure that the equipment settings don't drift appreciably. Guidance shall be obtained from personnel who are familiar with the equipment.
- 2) Calibration shall be performed in accordance with the established practices and procedures employed in the measurement facility, using the various open circuit, short circuit and standard impedance loads available in the facility for use during such calibrations.
- 3) Calibrations shall be stored on the 8510 and on floppy disk for subsequent use and for the record until such time as they are deemed unnecessary.
- 4) Manuals shall be consulted whenever personnel in the measurement facility are unable to provide guidance.

MEASUREMENTS: The following measurements shall be made on every test circuit with respect to category. The measurements shall be organized according to substrate type (TMM-3 or TMM-6) and name and description of each circuit. In the case of multiple copies of each circuit, measured results shall be tabulated for each for subsequent comparison. Both tabular/numerical and graphical output will be produced and saved.

RECTANGULAR MICROSTRIP ISOLATED PATCH ANTENNA ELEMENTS:

Over a frequency sweep of 9.0 to 11.0 GHz, S11 (input return loss) shall be measured and used to determine the input impedance of the antenna element. A resonance loop on a Smith chart shall be obtained for subsequent use in tuning the antenna elements.

E-PLANE ARRAYS:

Over a frequency sweep of 9.0 to 11.0 GHz, S11 (input return loss) shall be measured and used to determine the input impedance of the central arrayed antenna element. A resonance loop on a Smith chart shall be obtained for subsequent use in tuning the arrayed antenna elements. The signals coupled to the adjacent (outer) antenna element feedlines as a result of mutual coupling between the antenna elements in the array shall be measured in order to quantify mutual coupling effects in the E-plane.

H-PLANE ARRAYS:

Over a frequency sweep of 9.0 to 11.0 GHz, S11 (input return loss) shall be measured and used to determine the input impedance of the central arrayed antenna element. A resonance loop on a Smith chart shall be obtained for subsequent use in tuning the arrayed antenna elements. The signals coupled to the (outer) antenna element feedlines as a result of mutual coupling between the antenna elements in the array shall be measured in order to quantify mutual coupling effects in the H-plane.

3-DB POWER DIVIDERS:

Over a frequency sweep of 9.0 to 11.0 GHz, S11 (input return loss), S21 and S31 shall be measured.

TRANSMISSION LINE TEST CIRCUIT:

Over a frequency sweep of 9.0 to 11.0 GHz, S11 (input return loss) and S21 shall be measured.

ONE HALF AZIMUTH FEED:

Over a frequency sweep of 9.0 to 11.0 GHz, S11 (input return loss) shall be measured, along with Sk1; k=2:17.

ONE HALF ELEVATION FEED:

Over a frequency sweep of 9.0 to 11.0 GHz, S11 (input return loss) shall be measured, along with Sk1; k=2:9.

ELEVATION COLUMN ARRAY:

Over a frequency sweep of 9.0 to 11.0 GHz, S11 (input return loss) shall be measured.

ANTENNA ELEMENT TUNING:

Based on the resonance loops that we get from the various patches, we will have a fair idea of which patch(es) to trim with an Exacto knife. The trimming shall be performed under a microscope, a mil at a time, until the resonance loop swings around far enough that we achieve a good resonance at a center frequency of 10 GHz. Both insertion depth and length/width must be modified by trimming. An optimum combination exists such that the patch will resonate at 10 GHz, but we don't know how to achieve this optimum other than by cut and try. We don't really have a step by step procedure other than repeatedly trimming the patches.

ANTENNA PATTERN MEASUREMENT AT THE NEWPORT ANECHOIC CHAMBER:

CALIBRATION:

- 1) The test setup shall be precalibrated, recalibrated and postcalibrated in such a manner as to bracket groups of measurements and at a reasonable time interval to ensure that the equipment settings don't drift appreciably. Guidance shall be obtained from personnel who are familiar with the equipment.
- 2) Calibration shall be performed in accordance with the established practices and procedures employed in the anechoic chamber, using the various calibration equipment available in the chamber for use during such calibrations.
- 3) Calibrations shall be stored, if possible, in the equipment's memory and on floppy disk for subsequent use and for the record until such time as they are deemed unnecessary.
- 4) Manuals shall be consulted whenever personnel at the facility are unable to provide guidance.

ANTENNA PATTERN MEASUREMENT:

Both copolar and crosspolar farfield antenna patterns shall be measured along the cardinal axes of the antenna elements and subarrays over a range of frequencies, spanning 9.975 to 10.025 GHz, at 25 MHz increments, with 10.000 GHz being the nominal resonant frequency of the radiators.

APPENDIX D DETAILED DRAWINGS OF THE IMAGES SENT TO MPC FOR ETCHING ON THE TMM-3 AND TMM-6 SUBSTRATE BOARDS

Figure 18 is a picture of the “blueprints” or circuit images in one of two .DXF files that we sent to Microwave Printed Circuits that contained the information for an 18” by 24” Rogers TMM-3 substrate board that was to be etched for us.

Figure 19 is a zoomed in version of Figure 18 in which we focus in on the half azimuth feed circuit to be etched on Rogers TMM-3 substrate.

Figure 20 is a zoomed in version of Figure 18 in which we focus in on the full elevation feed circuit with radiating elements to be etched on Rogers TMM-3 substrate.

Figure 21 is a picture of the “blueprints” or circuit images in the second of two .DXF files that we sent to Microwave Printed Circuits that contained the information for an 18” by 24” Rogers TMM-3 substrate board that was to be etched for us. Not all our TMM-3 circuit images would fit on one board, so what didn’t fit within the board dimensions allowed for (18 by 24 inches) in the file shown in Figure 18 was placed in this file.

Figure 22 is a picture of the “blueprints” or circuit images in the .DXF file that we sent to Microwave Printed Circuits that contained the information for an 18” by 24” Rogers TMM-6 substrate board that was to be etched for us. The narrow portion of the feedline that leads directly into each one of the inset fed rectangular patches is 6.14 mils (0.00614 inches) wide.

Figure 23 is a zoomed in version of Figure 22 in which we focus in on the full elevation feed circuit with radiating elements to be etched on Rogers TMM-6 substrate. We tried to achieve a -35 dB taper across this feed, in the hope that we would end up with a -30 dB taper or better, but the results were much poorer than anticipated. The weighting and subsequent power division ratios were originally devised with this in mind, so the taper that we designed for in both the TMM-6 and TMM-3 cases was one that, if achieved, would yield -35 dB sidelobe levels.

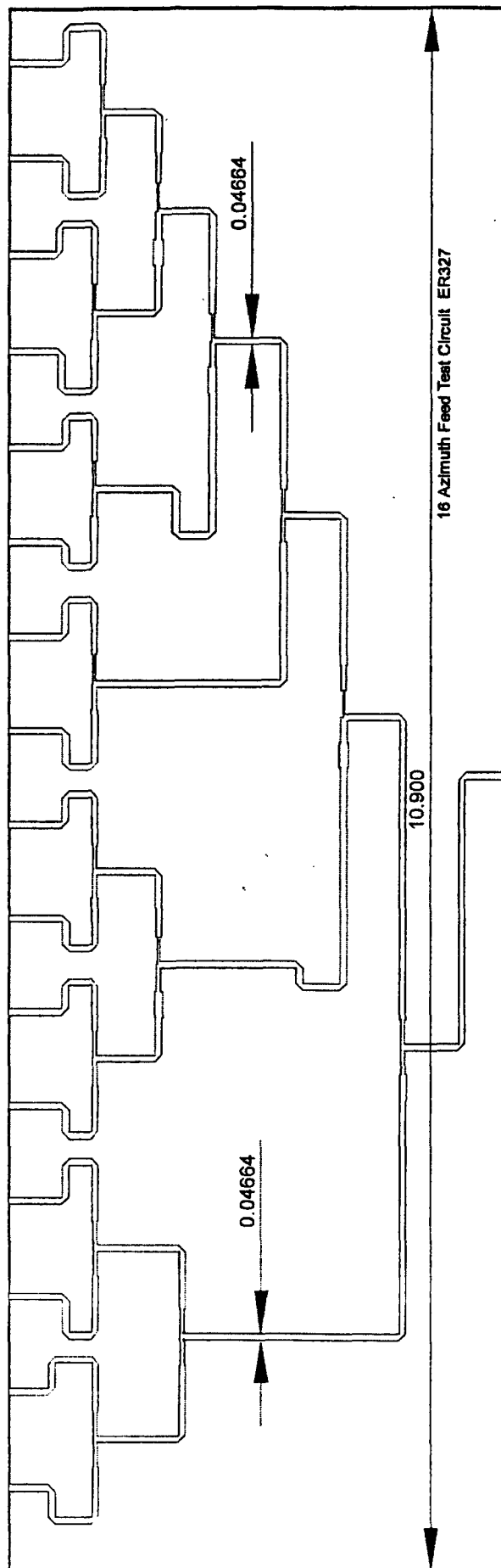


Figure 19. TMM-3 Board 1 - Half Azimuth Feed

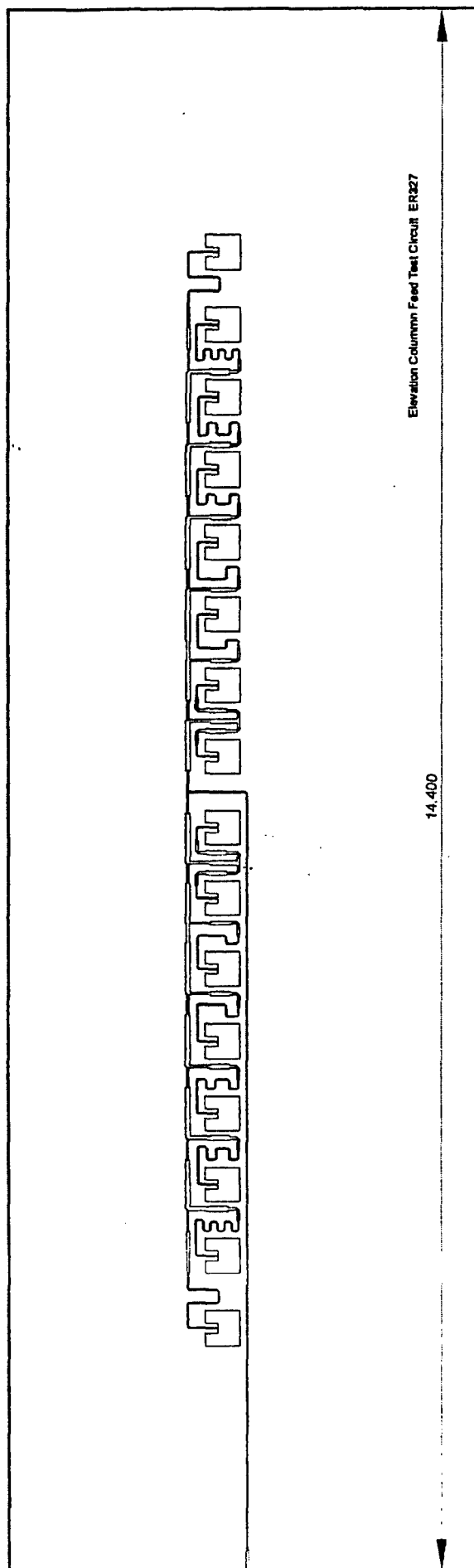


Figure 20. TMM-3 Board 1 - Full Elevation Feed and Microstrip Patches

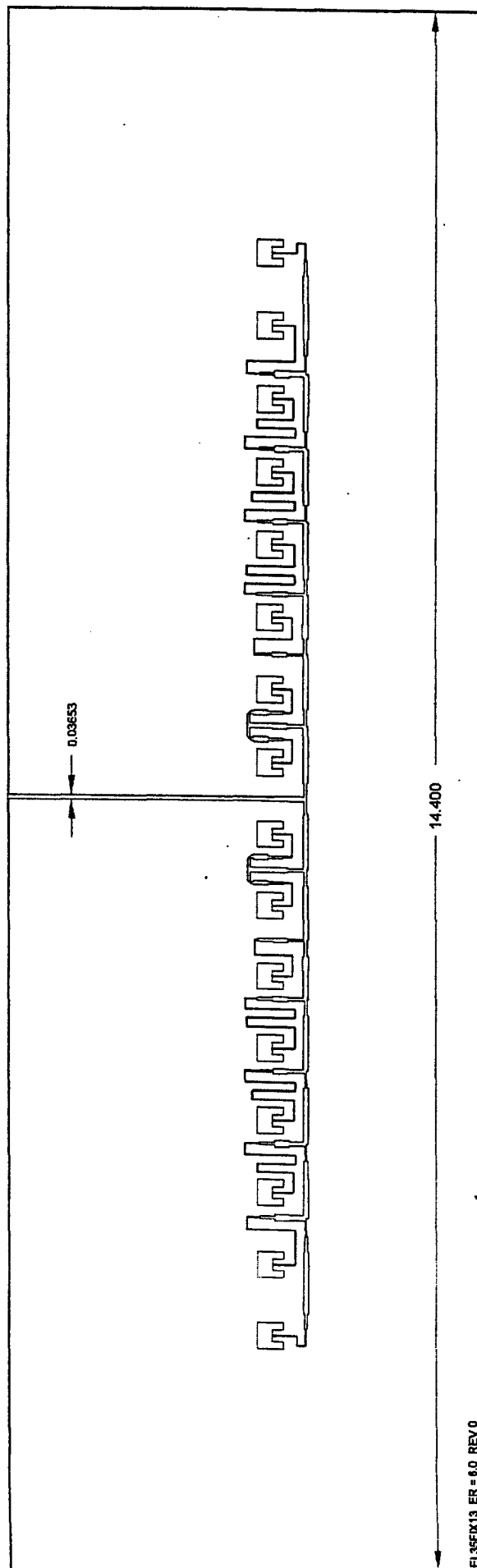


Figure 23. TMM-6 Board - Full Elevation Feed and Microstrip Patches

APPENDIX E COLOR COPIED PHOTOGRAPHS OF SELECTED TEST CIRCUITS AS THEY LOOKED AFTER THE TESTING AND TUNING PHASE WAS COMPLETED

Figure 24 shows four isolated patch circuits in their test fixtures after the testing and tuning phase was completed. What looks like tape holding the circuits to the test fixtures is in fact just that. Sometimes the adhesive under the circuit just wasn't enough to keep the substrate board from curling up around the edges and pulling loose from the fixture. The patches and feedlines fabricated on TMM-6 substrate (shown on the left) were smaller than those fabricated on TMM-3 substrate (shown on the right) due to the higher relative dielectric constant of TMM-6 material versus that for TMM-3 material. The TMM-6 nominal patch shown at lower left is the one mentioned earlier in the text when patch tuning is discussed and we mention that one of our best TMM-6 patch circuits was damaged when a deep trough was cut into the substrate during the removal of copper from the patch (trimming). The incision is clearly visible on the side of the patch furthest from the feedline. The whitish substance on 3 of the 4 patches shown is silver paint used in tuning the patches. The TMM-3 patch circuit at lower right appears much as it looked when first mounted in its test fixture.

Figure 25 depicts a fully tuned full elevation array consisting of two half elevation arrays in mirror image and fed from a common point. The elevation array is fabricated on TMM-3 substrate material. The whitish substance on the patches is silver paint that is meant to make the inset feed point on each patch not quite so inset. Remember that the PATCHANT MathCad worksheet predicted that the inset for the feed points had to be much deeper than what was actually needed.

Figure 26 depicts some of our lesser known test circuits mounted in their test fixtures. Three dB power dividers are shown on the left, while plated through via holes are shown on the right. The plated through via hole test fixture for the TMM-6 via and the plated through via hole test fixture for the TMM-3 via are shown such that both sides of the test fixture used to hold the vias are visible. Each plated through via hole test fixture holds two board pieces – a TMM-3 piece and a TMM-6 piece. The 3 dB power divider test circuit shown at upper left suffered damage when one of the SMA connectors (the one at the top) twisted out of its socket, tearing up the feedline as it did so.

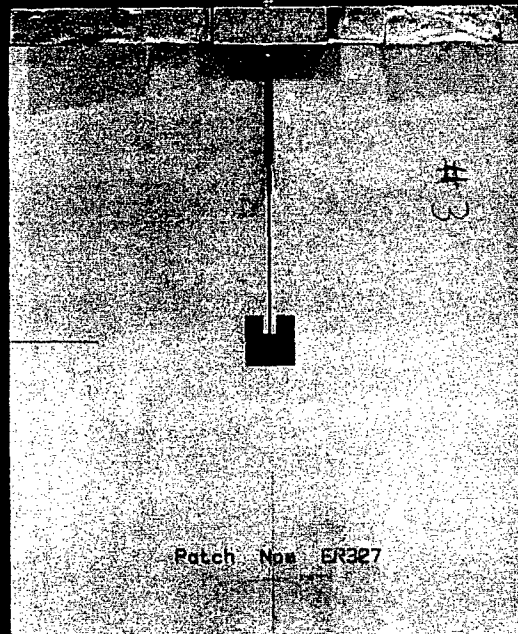
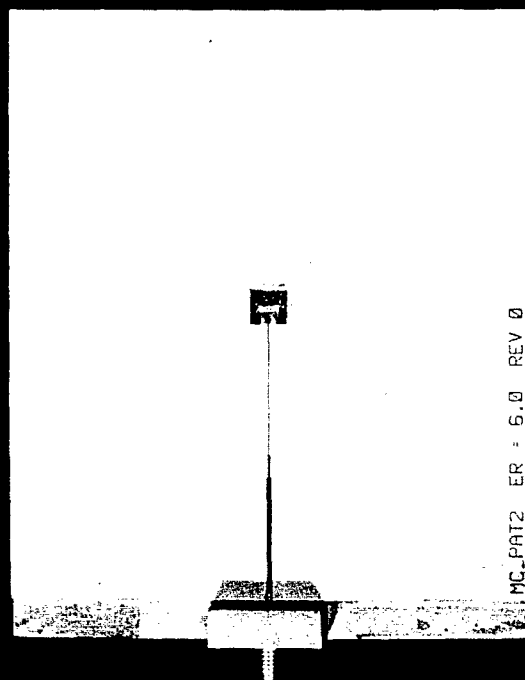
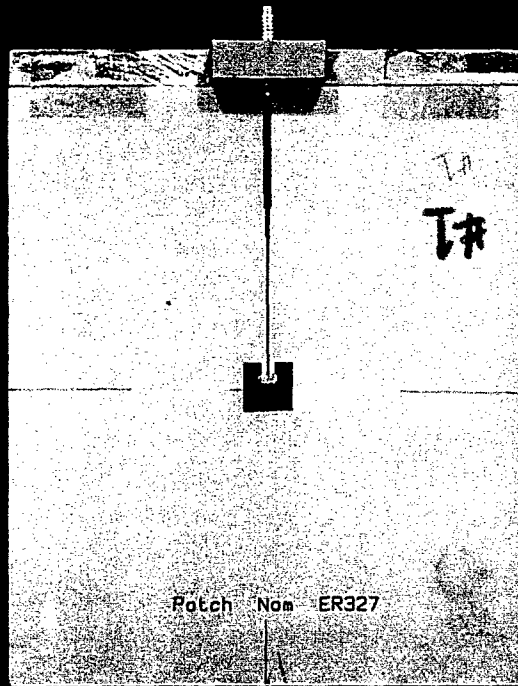
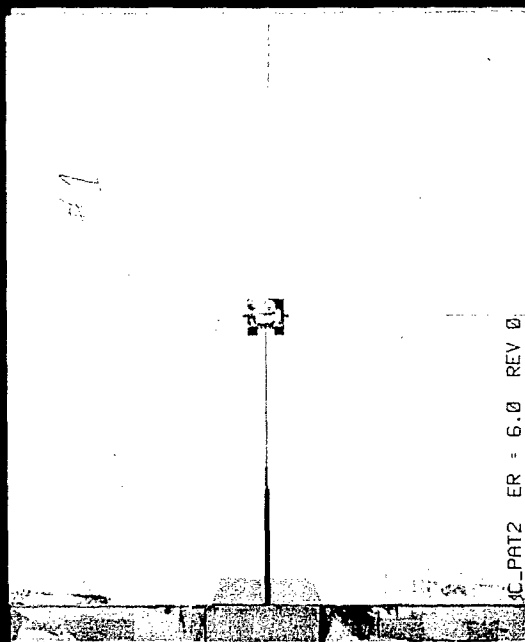
Figure 27 shows some of our elevation feedline-only test circuits.

Figure 28 shows some of our E-plane patch array test circuits.

Figure 29 shows some of our H-plane patch array test circuits.

Figure 30 shows a half azimuth feed test circuit mounted on TMM-3 substrate material.

Figure 31 shows a full elevation array consisting of two half elevation arrays in mirror image and fed from a common feedpoint. The elevation array is fabricated on TMM-6 substrate material.



1 2 3 4 5 6 7 8 9 10 11

Figure 24. Four Isolated Patch Circuits In Their Test Fixtures

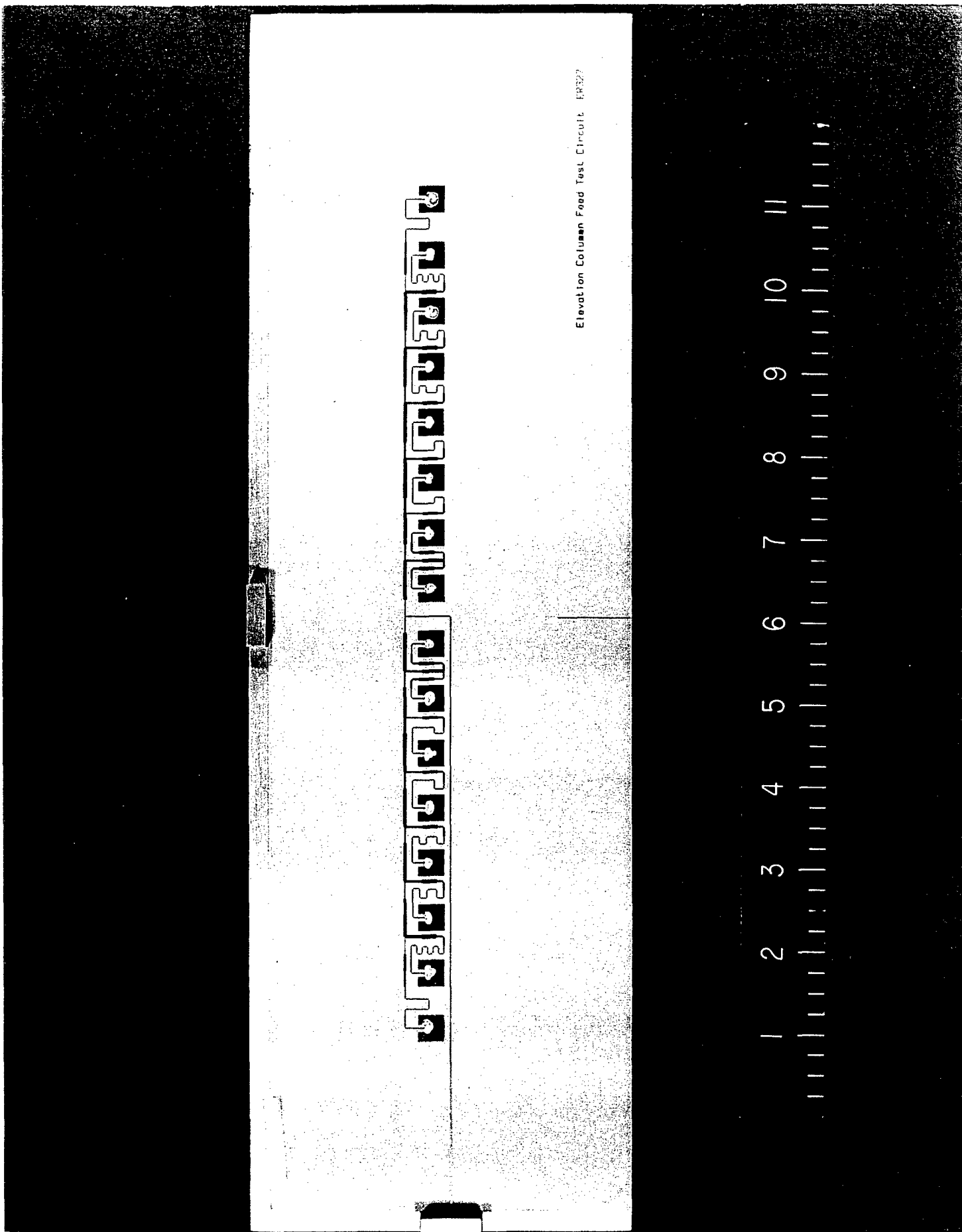
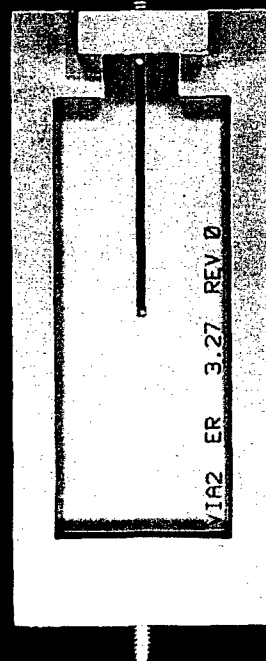
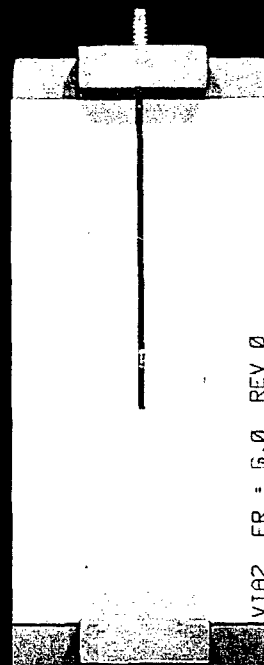
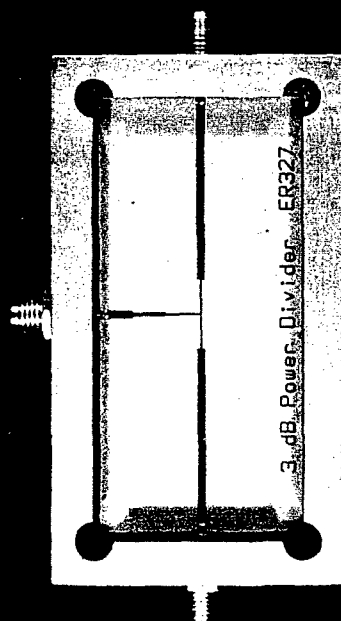
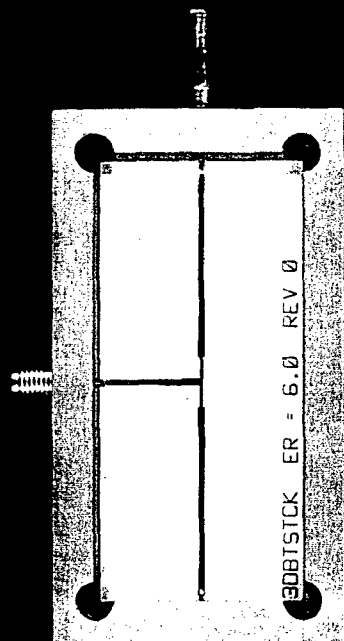
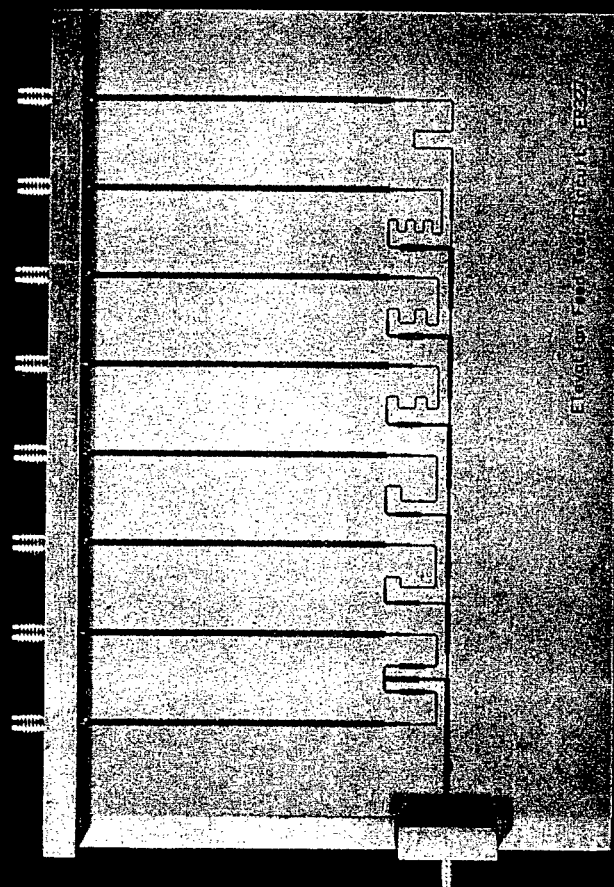
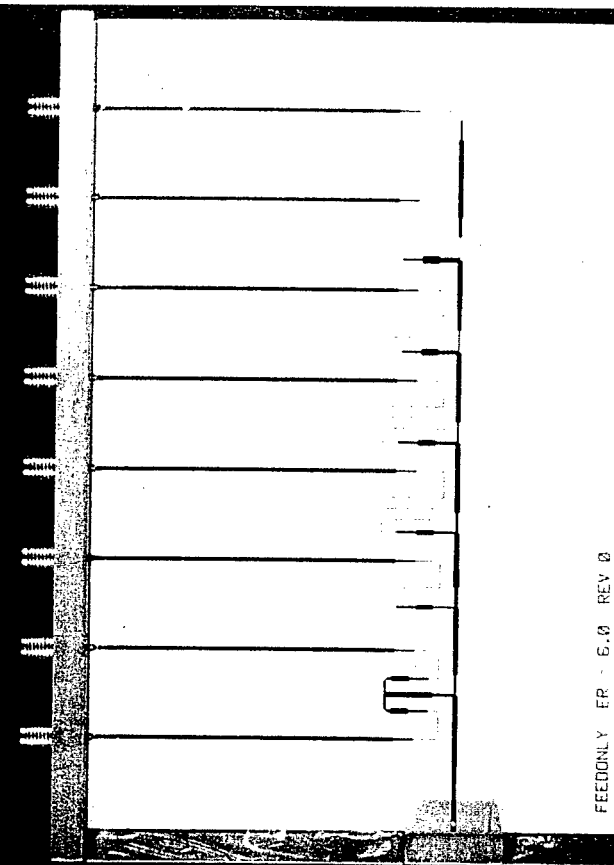


Figure 25. Tuned TMM-3 Full Elevation Array



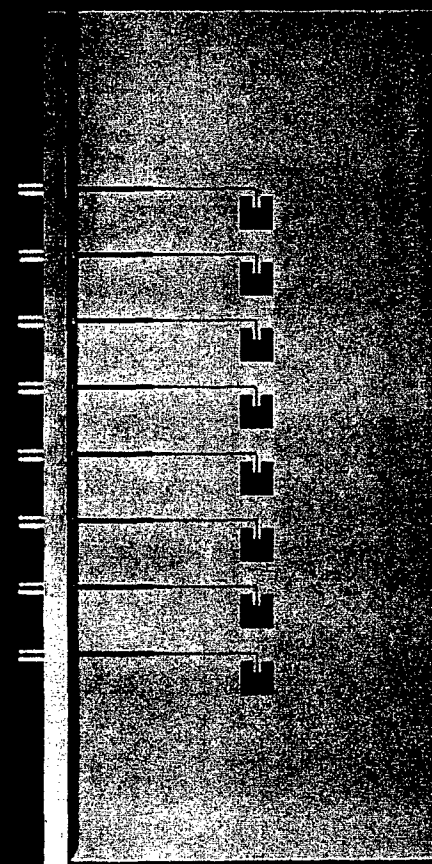
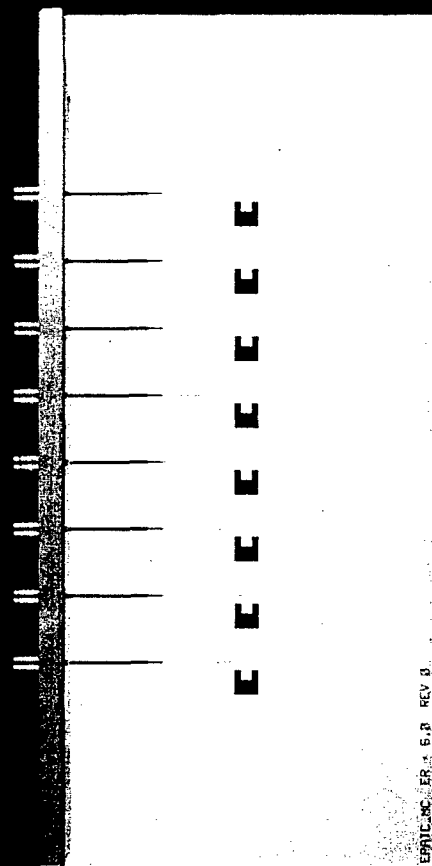
1 2 3 4 5 6 7 8 9 10 11

Figure 26. 3 dB Power Divider And Plated Through Via Hole Circuits



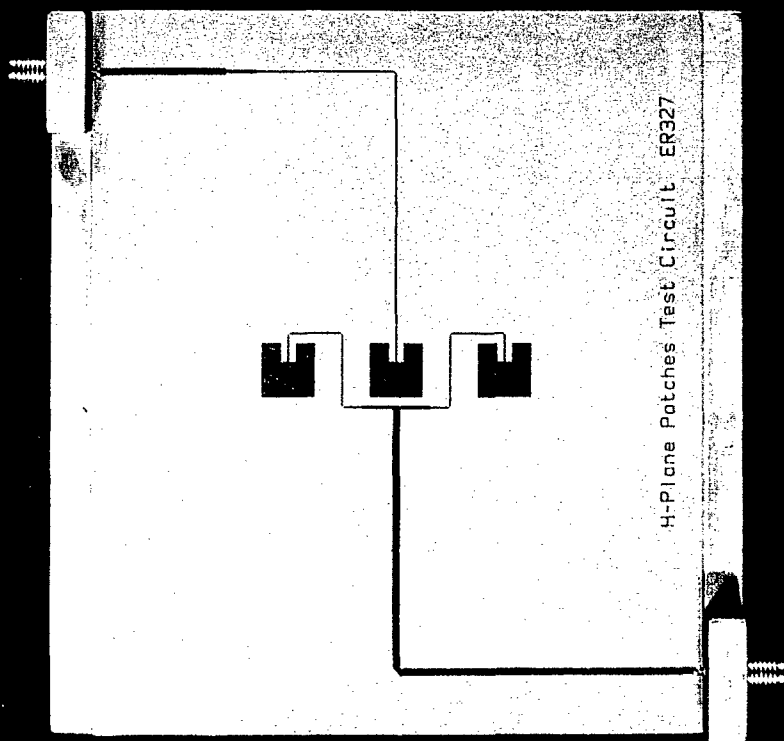
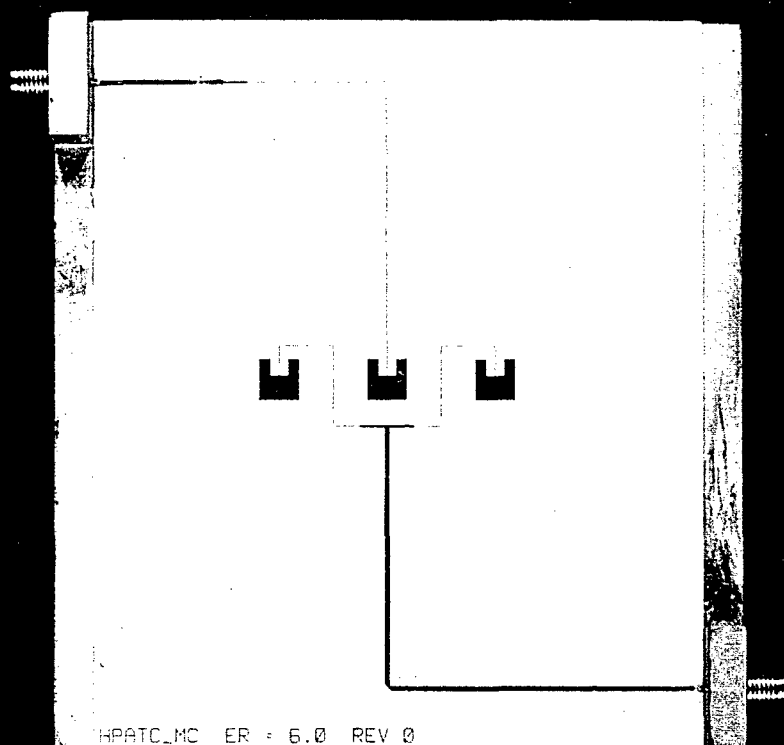
2 3 4 5 6 7 8 9 10

Figure 27. Elevation Feedline-Only Test Circuits



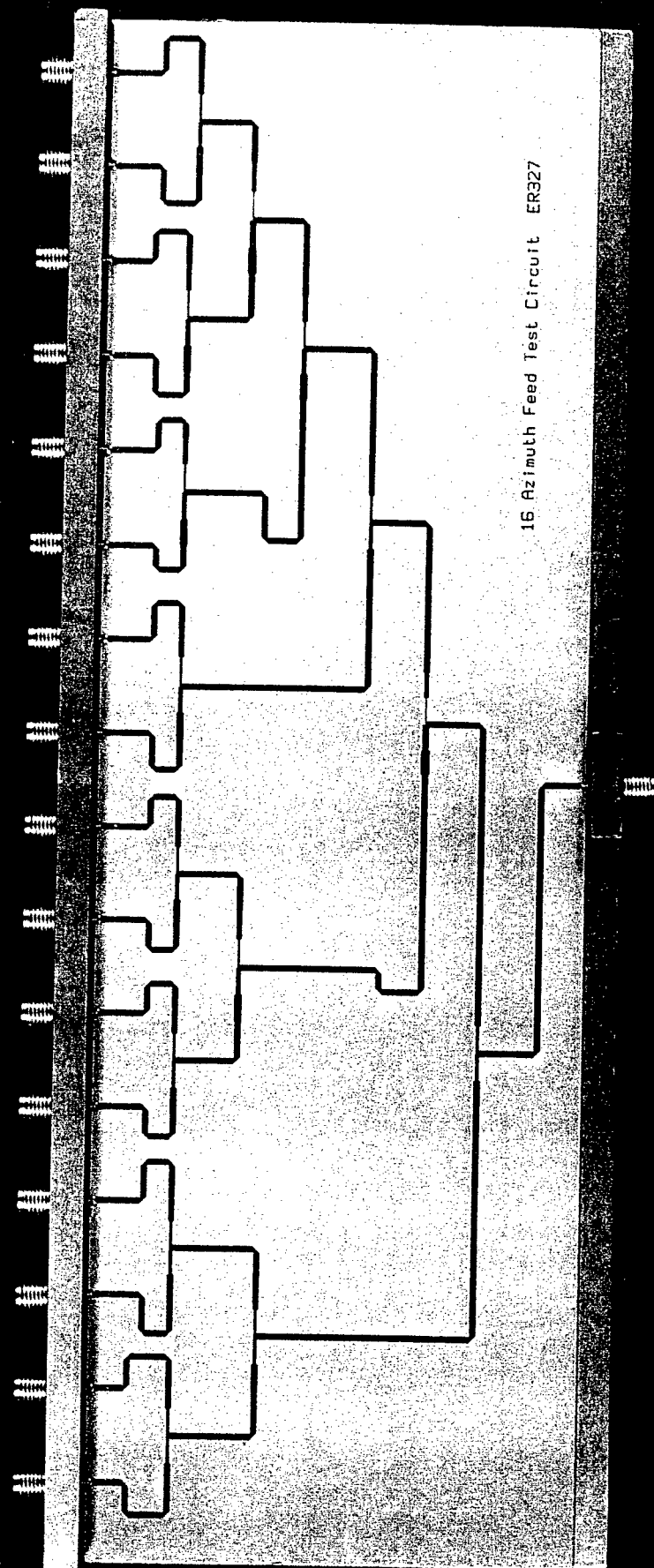
2 3 4 5 6 7 8 9 10 11

Figure 28. E-Plane Patch Array Test Circuits



2 3 4 5 6 7 8 9 10 11

Figure 29. H-Plane Patch Array Test Circuits



2 3 4 5 6 7 8 9 10 11

Figure 30. TMM-3 Half Azimuth Feed

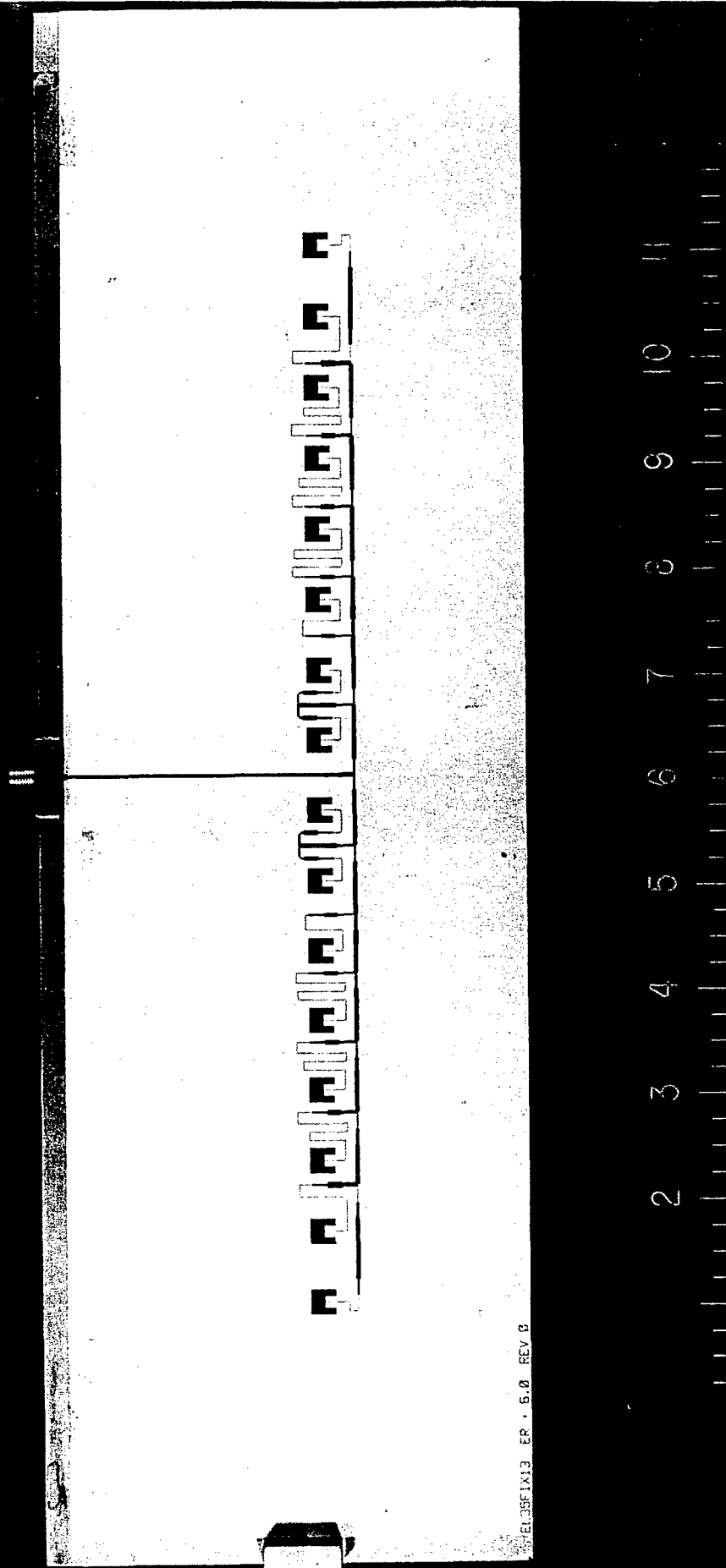


Figure 31. TMM-6 Full Elevation Array

APPENDIX F PLOTS ILLUSTRATING THE MEASURED AND SIMULATED S21 DATA COMPILED FOR THE HALF AZIMUTH AND HALF ELEVATION FEED OUTPUT PORTS VERSUS FREQUENCY

In general for the following plots, as port number increases, magnitude decreases. However, in instances where the plot traces cross each other like strands of spaghetti, remember the order of colors given for the plot under consideration and the general decrease in magnitude with increasing port number, and decoding which S21 magnitude trace corresponds to what output port becomes trivial.

Figure 32: The magnitudes are plotted in color for ports 1-16 in the following order of colors.

Port 1: red	Port 5: red	Port 9: red	Port 13: red
Port 2: green	Port 6: green	Port 10: green	Port 14: green
Port 3: blue	Port 7: blue	Port 11: blue	Port 15: blue
Port 4: black	Port 8: black	Port 12: black	Port 16: black

Figures 33, 34 and 35: The magnitudes are plotted in color for ports 1-8 in the following order of colors.

Port 1: red	Port 5: red
Port 2: green	Port 6: green
Port 3: blue	Port 7: blue
Port 4: black	Port 8: black

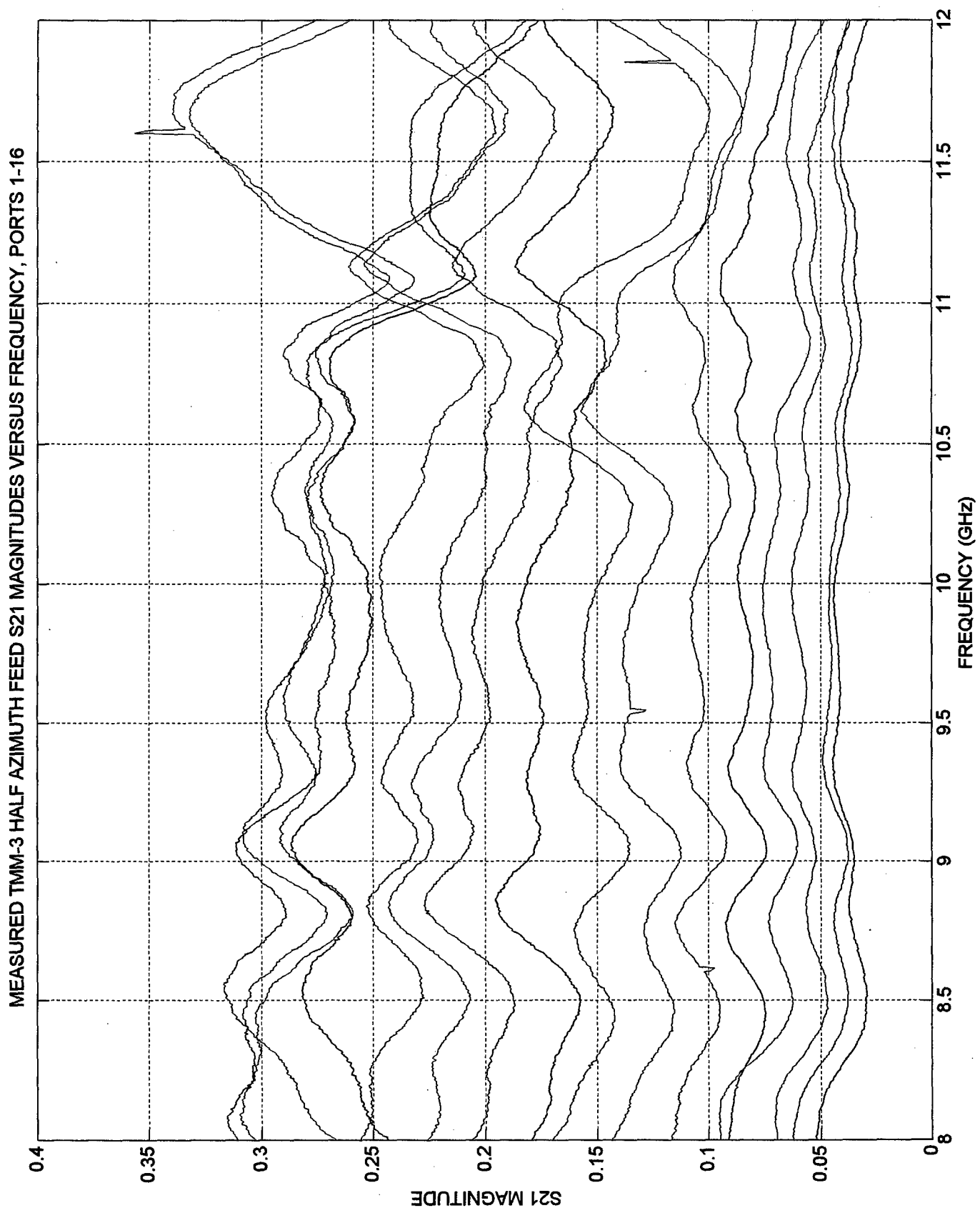


Figure 32. Measured TMM-3 Half Azimuth Feed S21 Magnitudes Versus Frequency, Ports 1-16

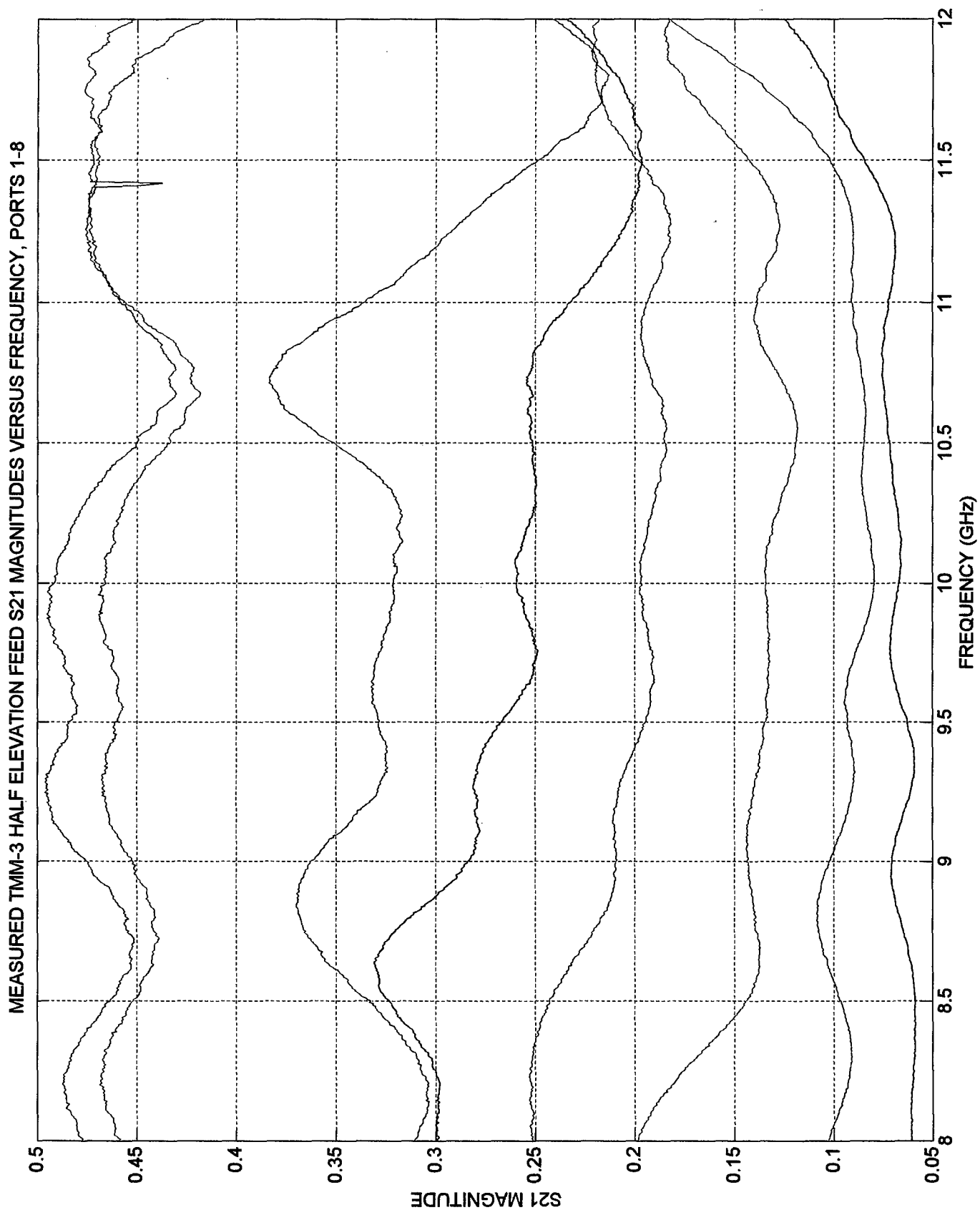


Figure 33. Measured TMM-3 Half Elevation Feed S21 Magnitudes Versus Frequency, Ports 1-8

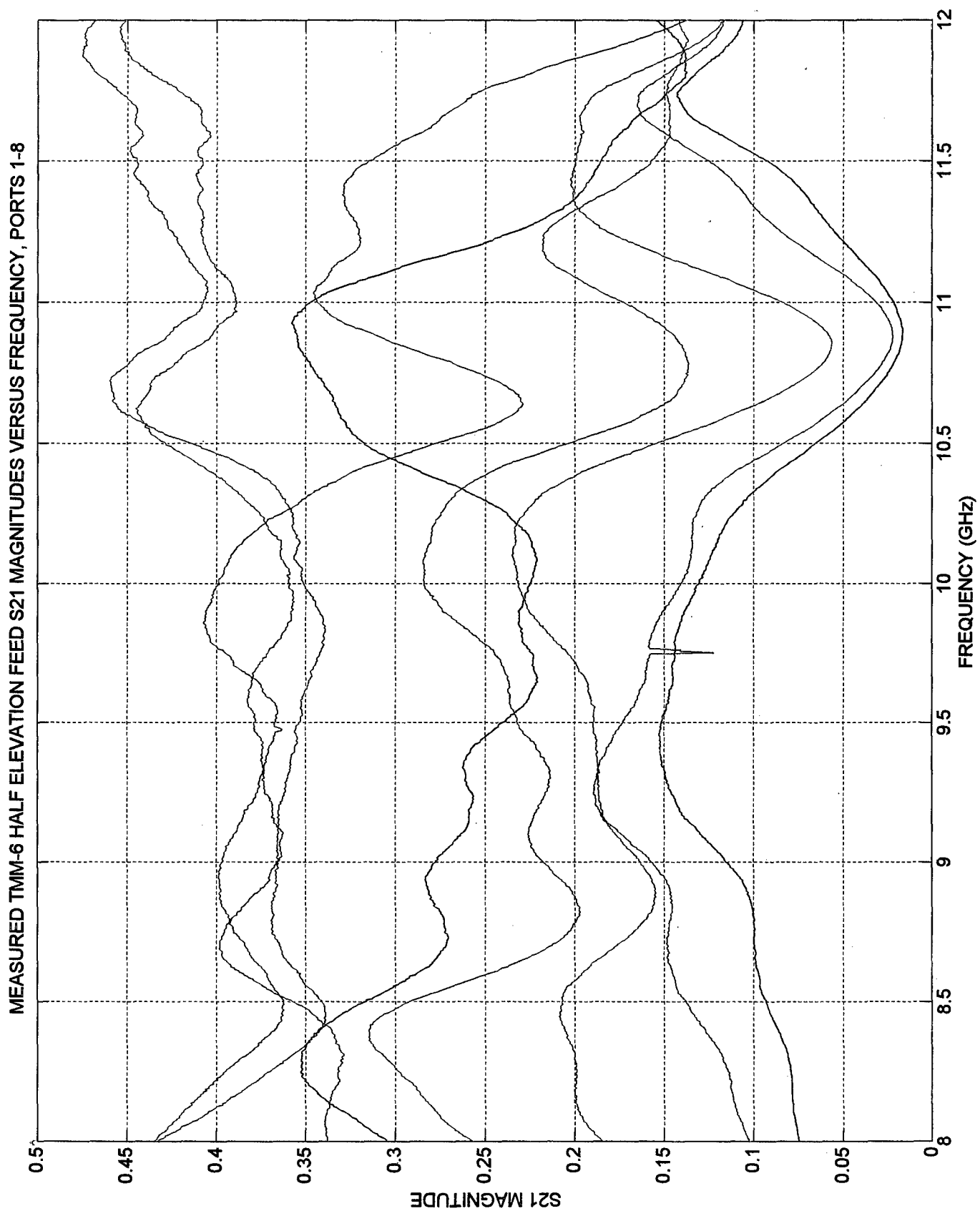


Figure 34. Measured TMM-6 Half Elevation Feed S21 Magnitudes Versus Frequency, Ports 1-8

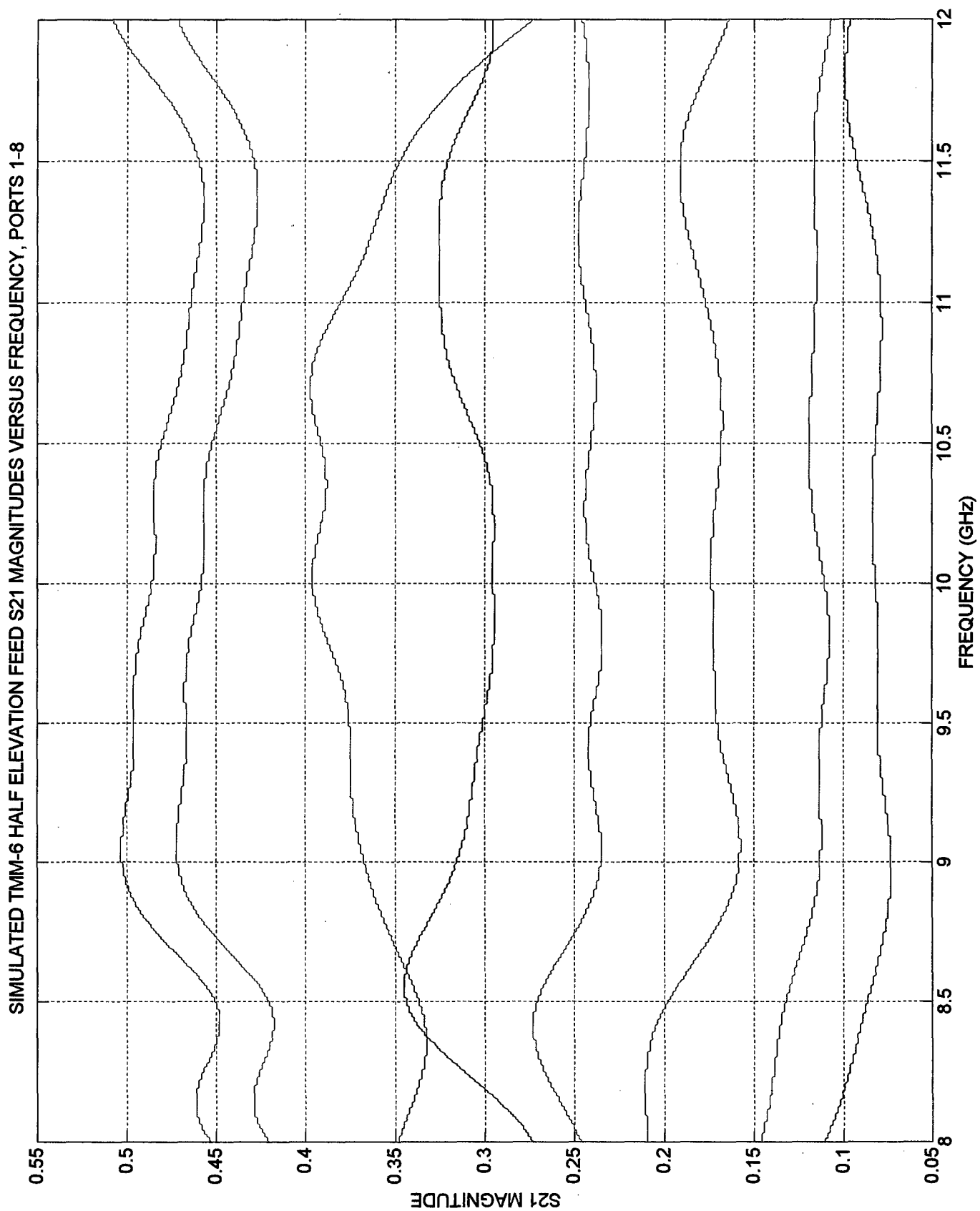


Figure 35. Simulated TMM-6 Half Elevation Feed S21 Magnitudes Versus Frequency, Ports 1-8

**APPENDIX G PLOTS ILLUSTRATING THE MEASURED S21 DATA
COMPILED FOR THE HALF ELEVATION FEEDS AT BAND CENTER AND
AT THE BAND EDGES, ALONG WITH SIMULATED AND THEORETICAL
S21 DATA AT BAND CENTER**

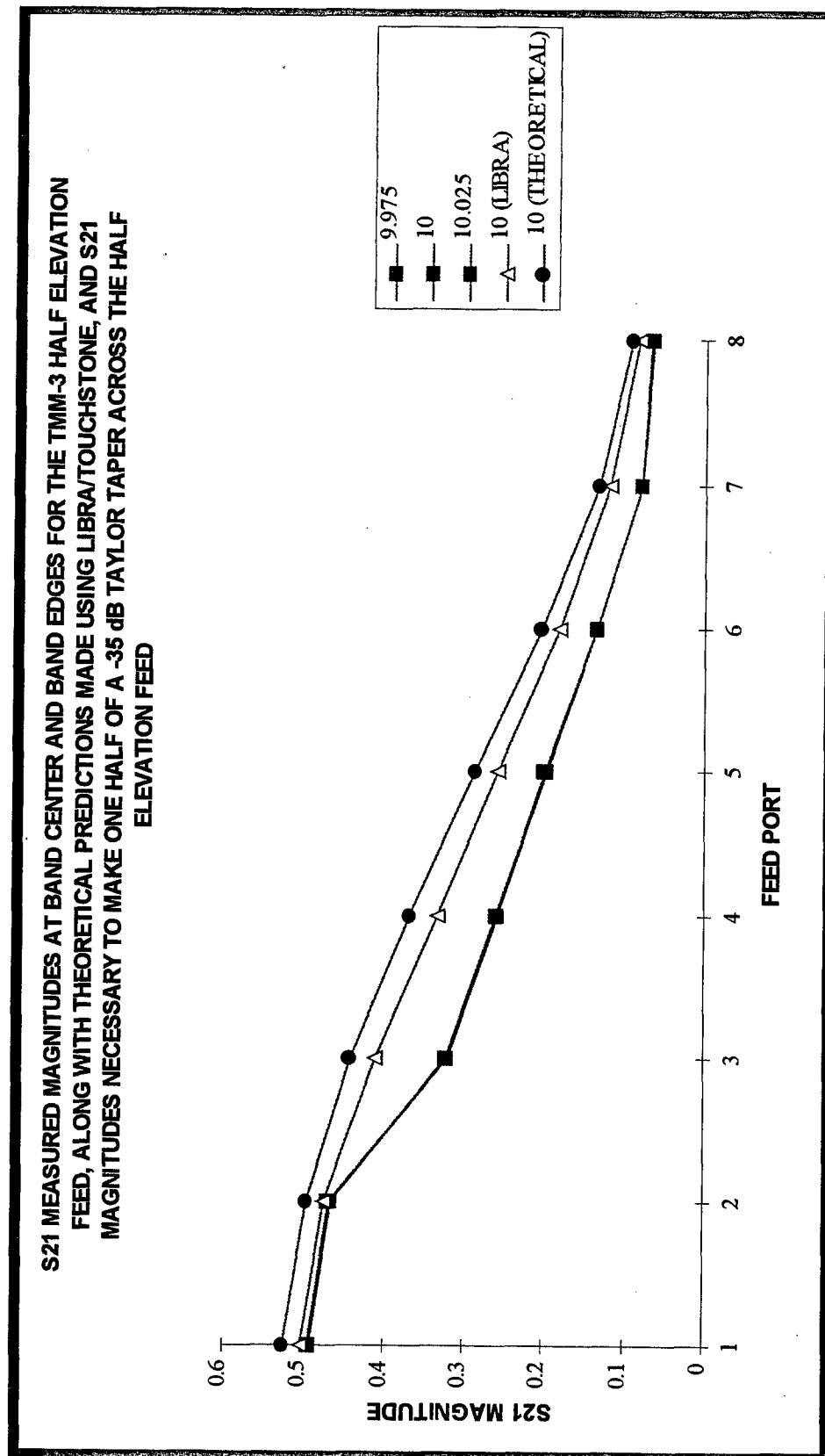


Figure 36. S21 Magnitudes Versus Port Number For The TMM-3 Half Elevation Feed

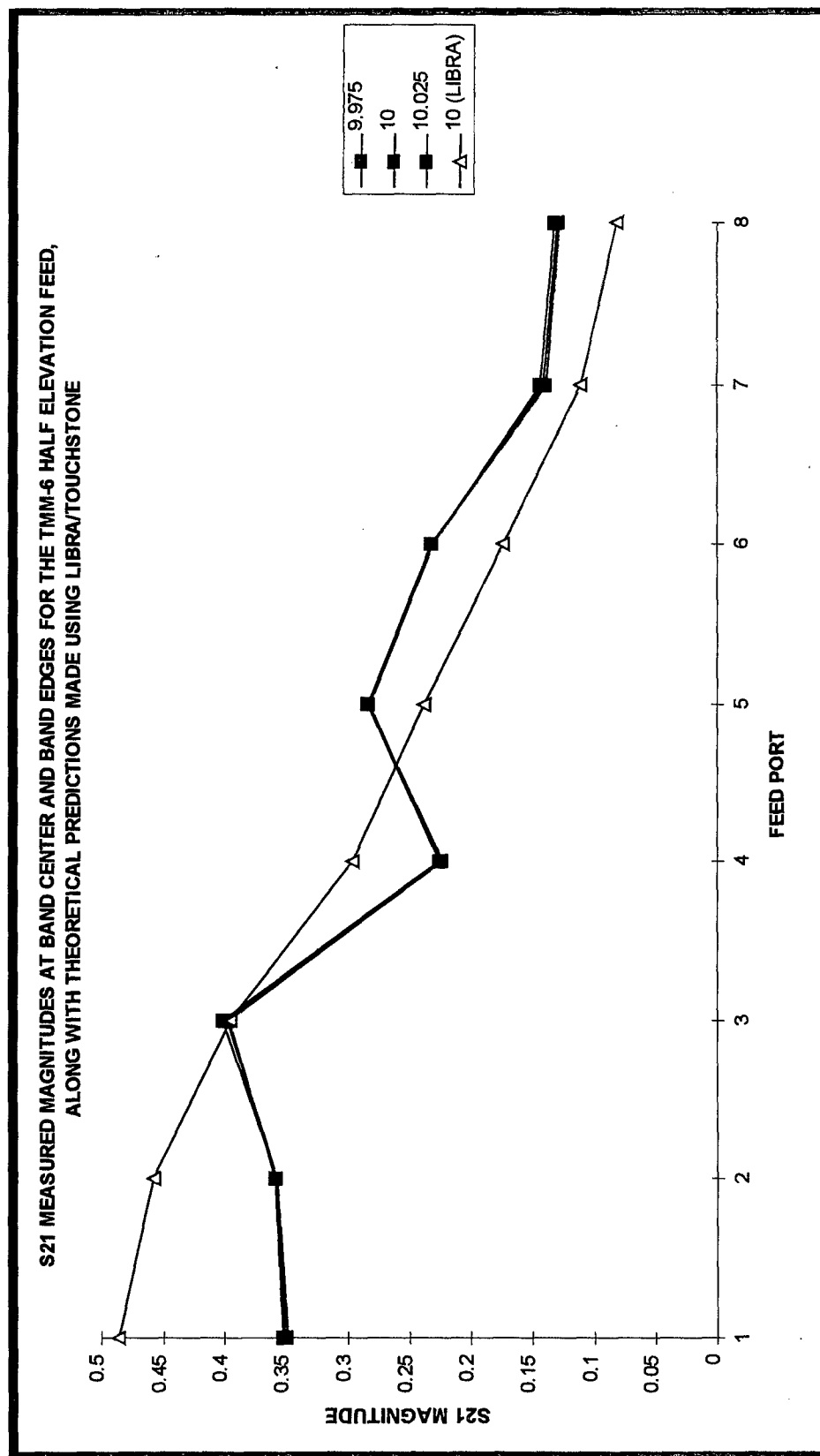


Figure 37. S21 Magnitudes Versus Port Number For The TMM-6 Half Elevation Feed

**APPENDIX H SELECTED SMITH CHARTS SHOWING RESONANCE LOOPS
FOR ISOLATED MICROSTRIP PATCH ELEMENTS MEASURED WITH AN
HP 8510C NETWORK ANALYZER**

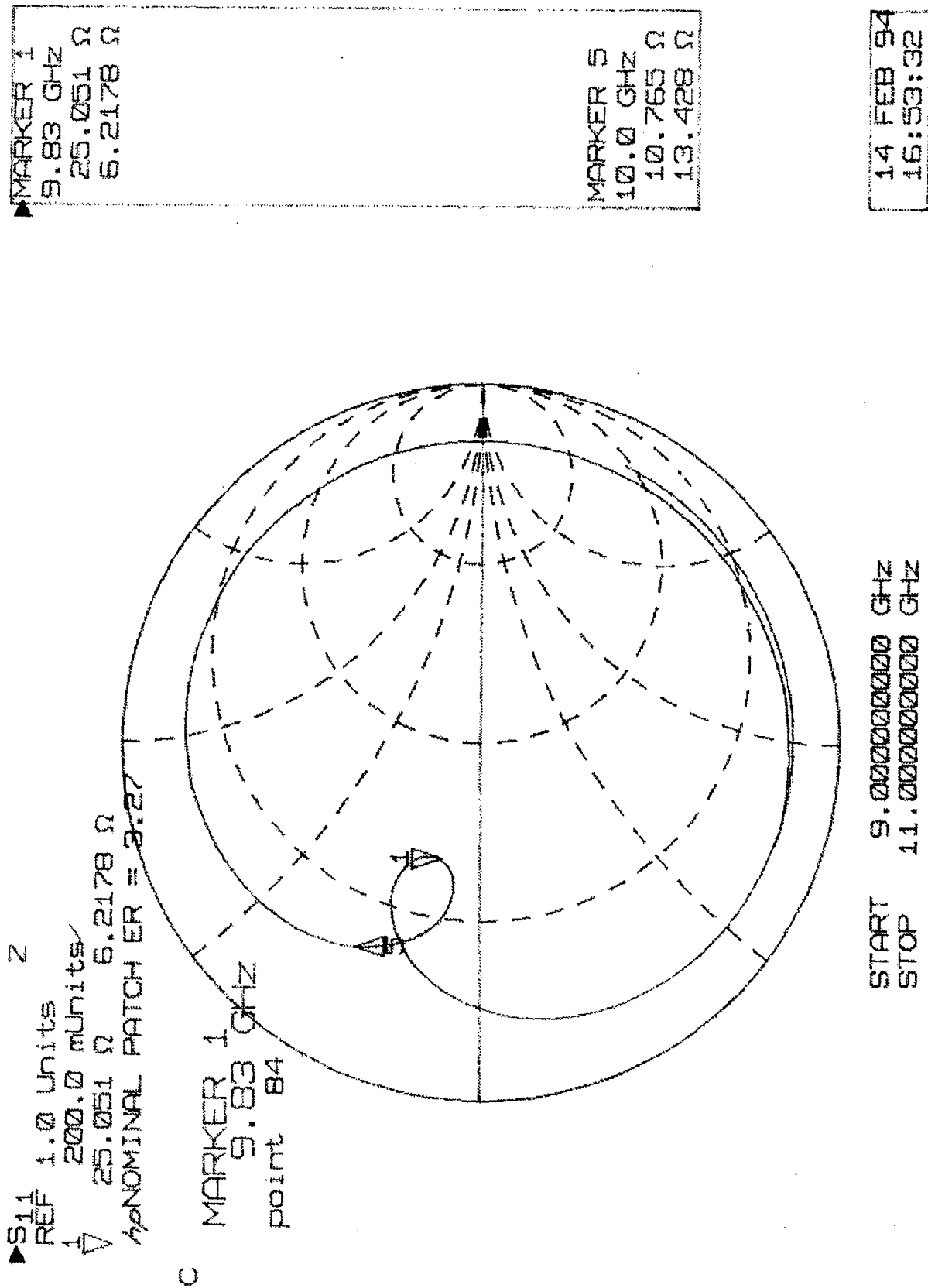


Figure 38. Resonance Loop For An Isolated, Nominal, Unmodified TMM-3 Patch Circuit As A Function Of Frequency, Plotted In Smith Chart Form

MARKER 1
 9.82 GHz
 34.545 Ω
 22.709 Ω
 MARKER 2
 9.92 GHz
 46.846 Ω
 2.5938 Ω
 MARKER 3
 10.03 GHz
 26.394 Ω
 -3.0166 Ω

07 FEB 94
 11:48:52

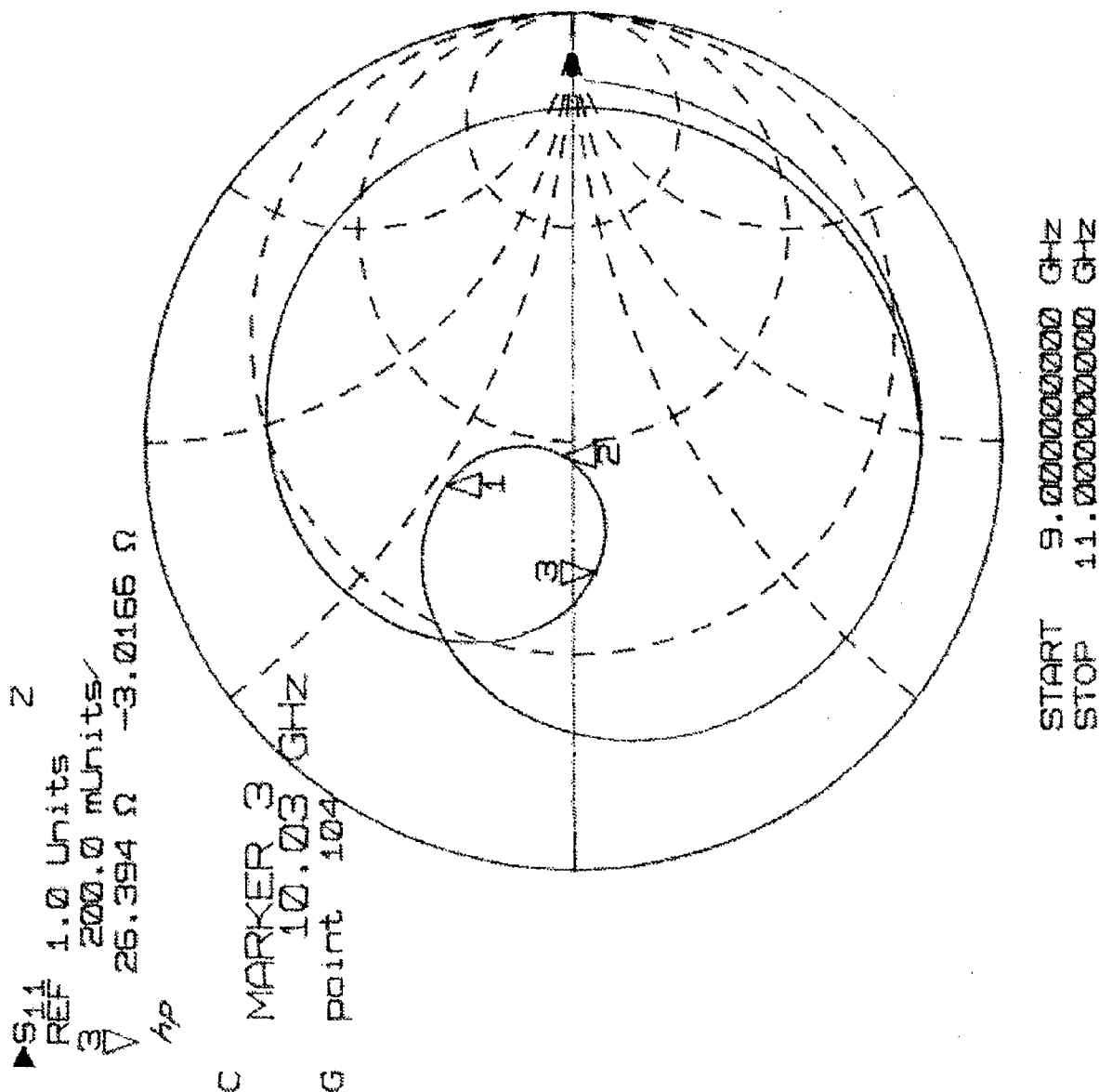


Figure 39. Resonance Loop For An Isolated, Nominal, Painted TMM-3 Patch Circuit As A Function Of Frequency, Plotted In Smith Chart Form

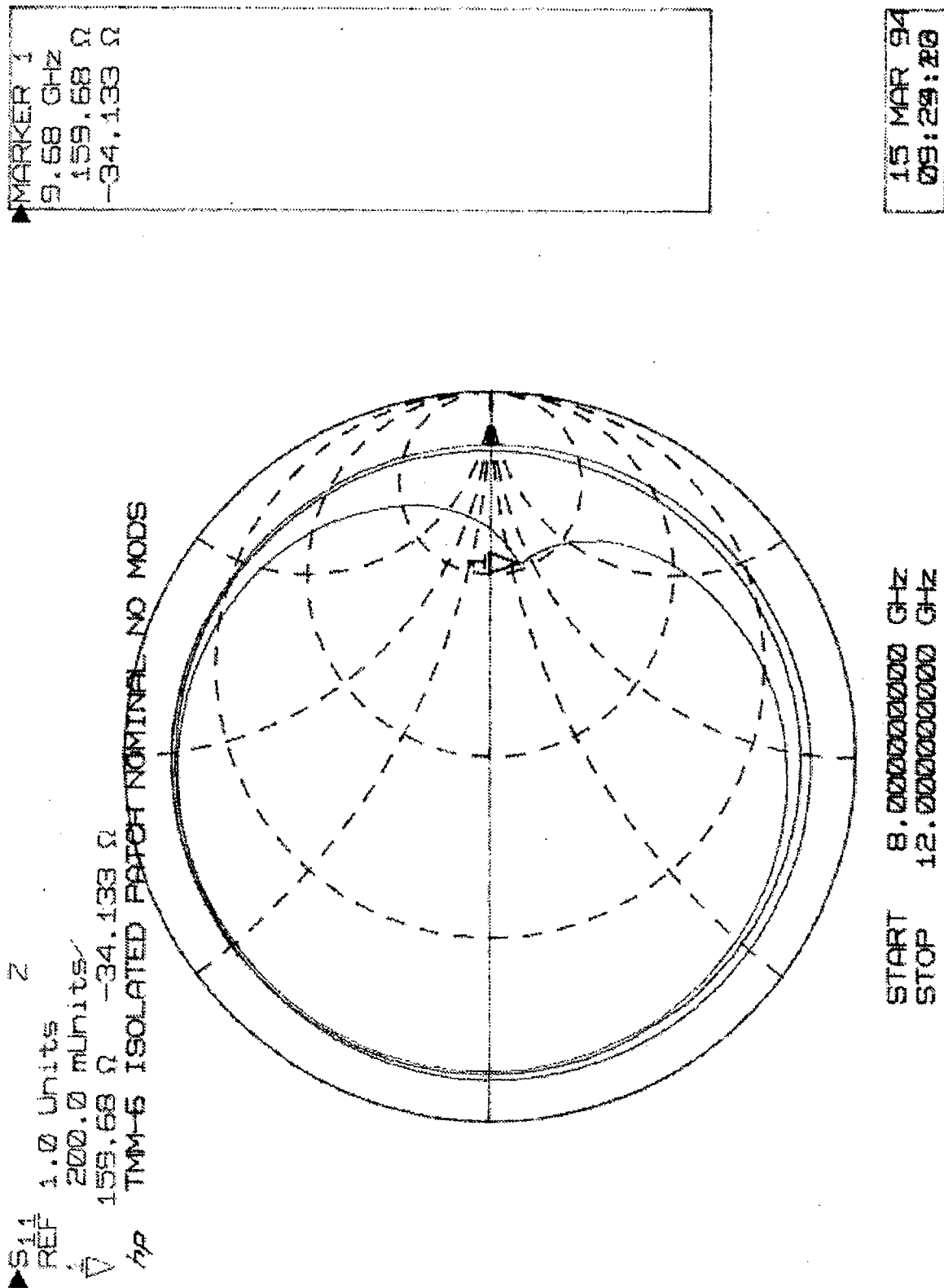


Figure 40. Resonance Loop For An Isolated, Nominal, Unmodified TMM-6 Patch Circuit As A Function Of Frequency, Plotted In Smith Chart Form

MARKER 1
 9.985 GHz
 85.84 Ω
 -55.937 Ω
 MARKER 2
 10.135 GHz
 48.107 Ω
 -0.3418 Ω

08 APR 54
 15:12:58

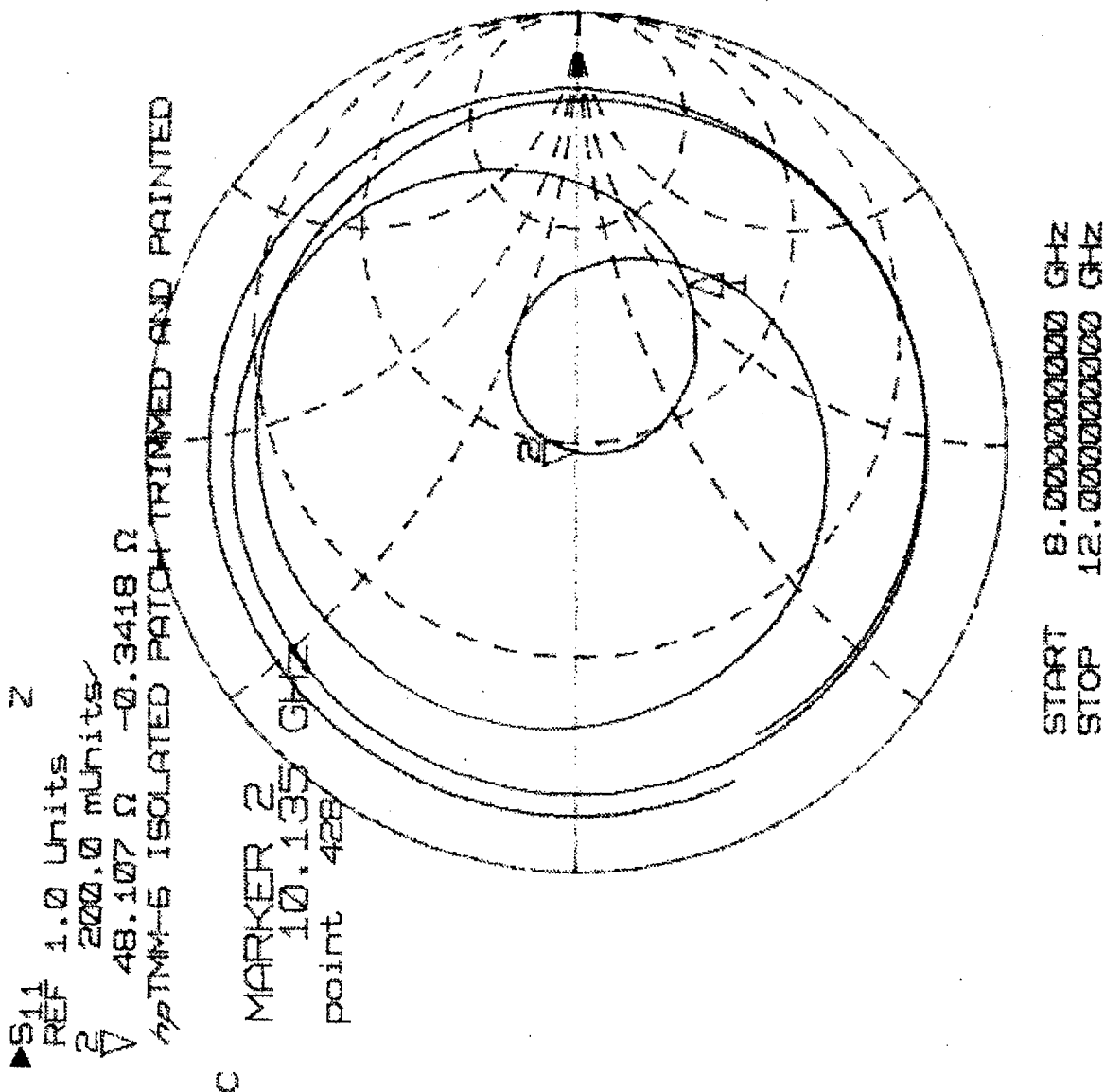


Figure 41. Resonance Loop For An Isolated, Nominal, Trimmed And Painted TMM-6 Patch Circuit As A Function Of Frequency, Plotted In Smith Chart Form

**APPENDIX I SELECTED PLOTS SHOWING S11 VERSUS FREQUENCY FOR
THE TMM-3 ELEVATION ARRAY AND FOR AN ISOLATED TMM-6
MICROSTRIP PATCH MEASURED ON THE HP 8510C NETWORK
ANALYZER**

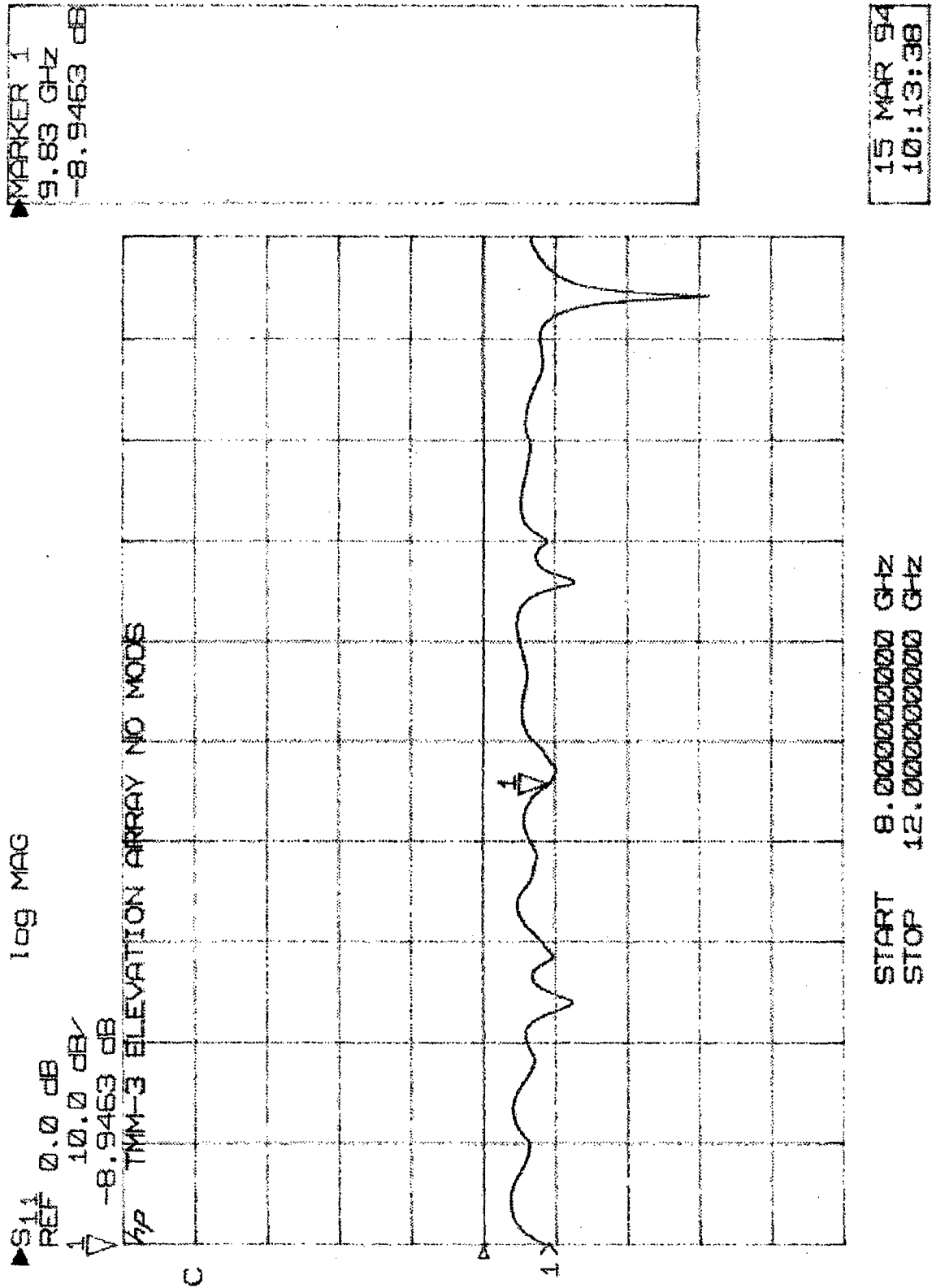


Figure 42. S11 Versus Frequency For The Unmodified TMM-3 Elevation Array

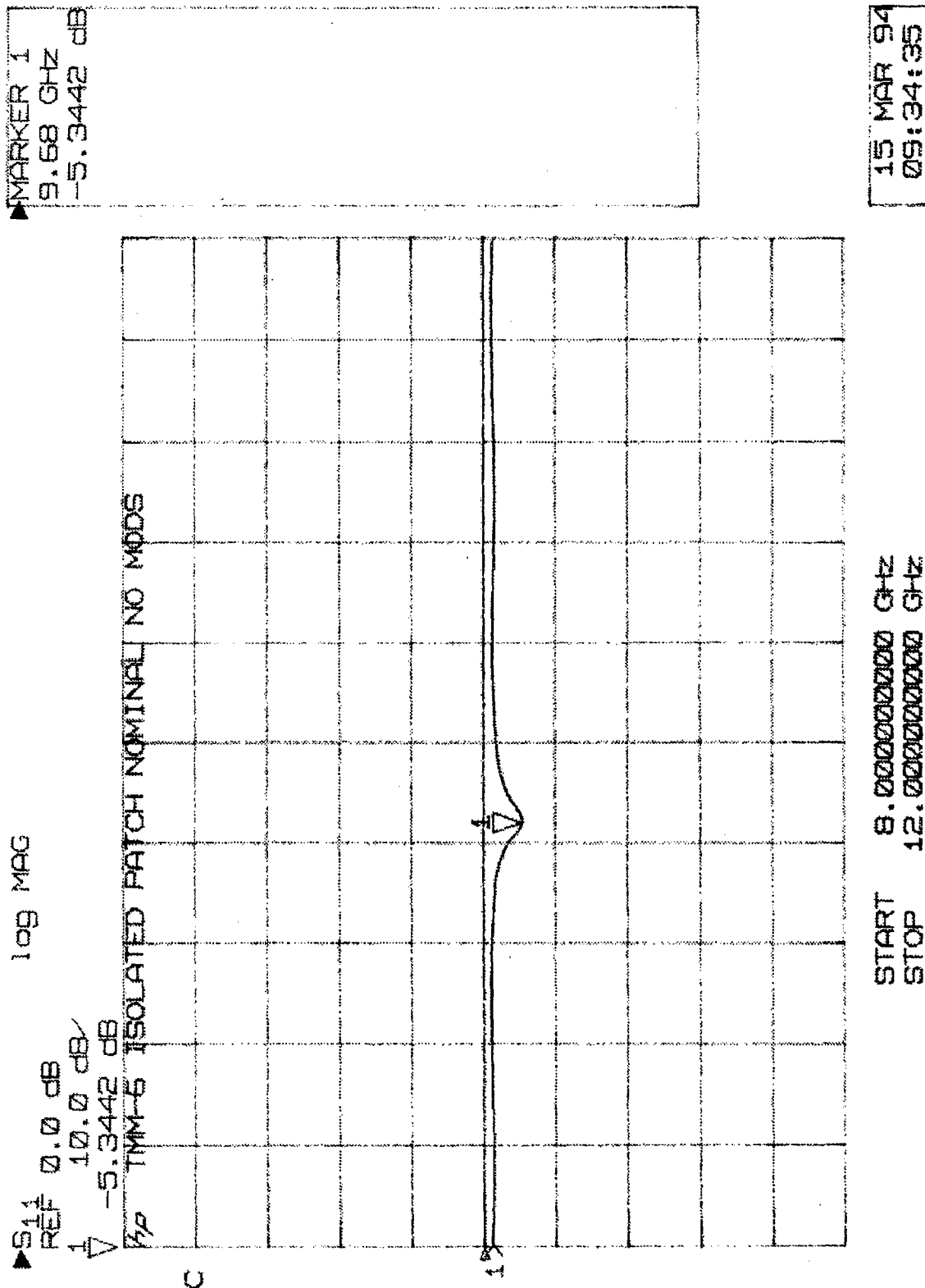


Figure 43. S11 Versus Frequency For An Isolated, Nominal, Unmodified TMM-6 Patch Circuit

**APPENDIX J ISOLATED MICROSTRIP PATCH FARFIELD ANTENNA
PATTERNS MEASURED WITH AN HP 8510C NETWORK ANALYZER**

MEASURED E-PLANE PRINCIPAL POLARIZATION PATTERN CUTS FOR TWO ISOLATED TMM-3 RECTANGULAR MICROSTRIP PATCHES, 9.825 GHz

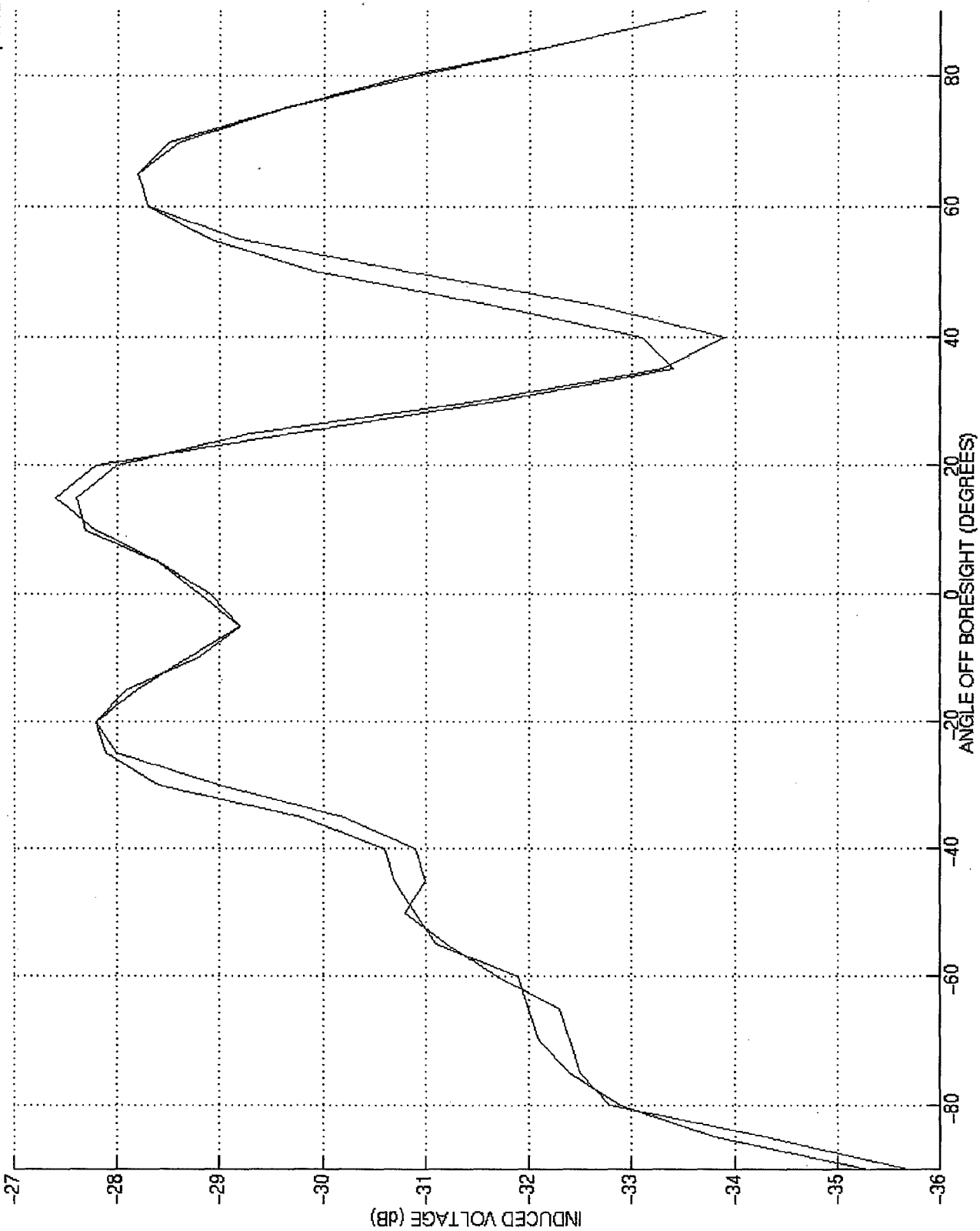


Figure 44. E-Plane Principal Polarization Antenna Pattern Cuts For Two Isolated TMM-3 Rectangular Microstrip Patch Elements With Inset Feeds, Frequency = 9.825 GHz, Measured Using An HP 8510C

MEASURED E-PLANE PRINCIPAL POLARIZATION PATTERN CUT FOR A TRIMMED, PAINTED, ISOLATED TMM-6 RECTANGULAR MICROSTRIP PATCH, 9.985 GHz

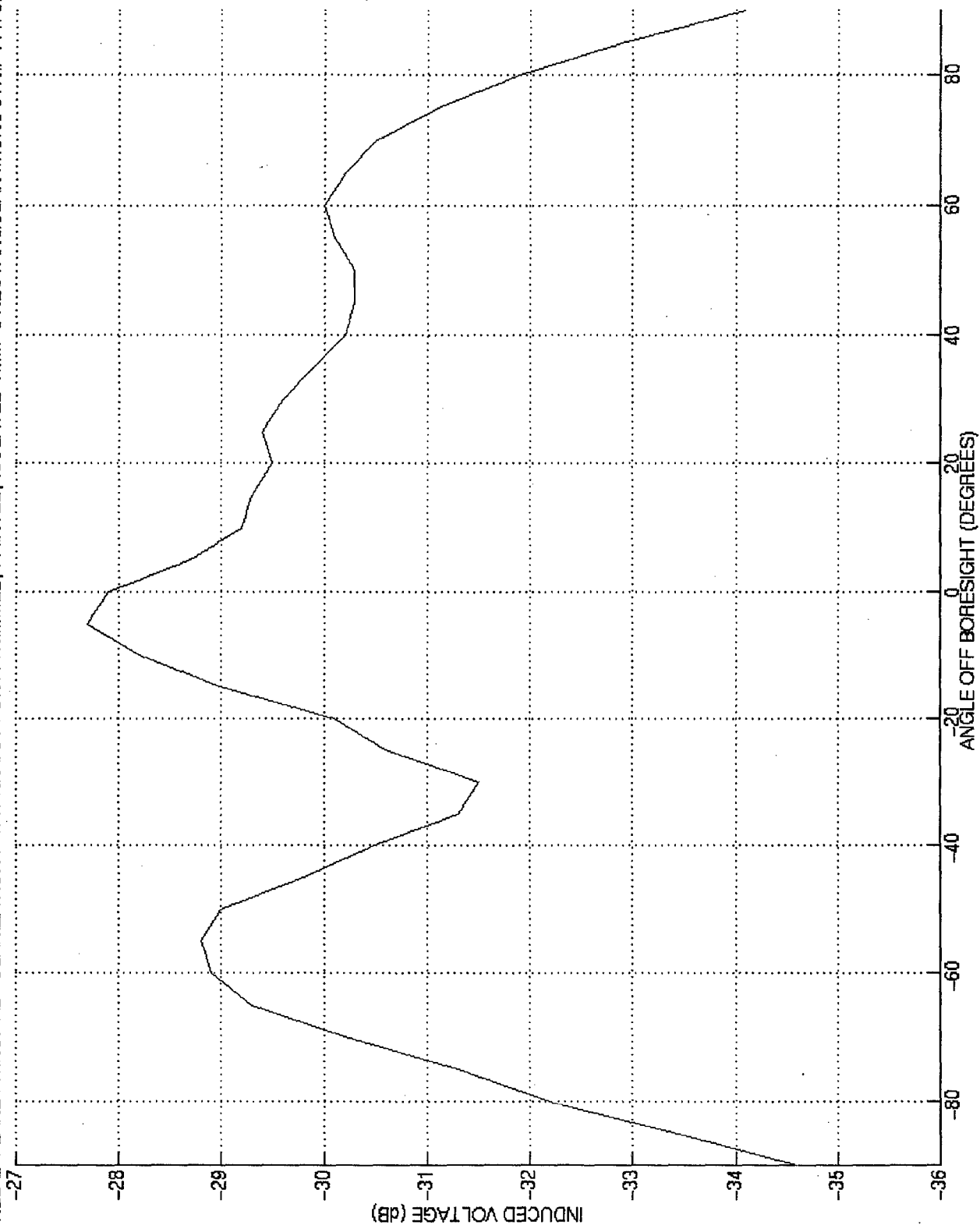


Figure 45. E-Plane Principal Polarization Antenna Pattern Cut For An Isolated, Trimmed And Painted TMM-6 Rectangular Microstrip Patch Element With An Inset Feed, Frequency = 9.985 GHz, Measured Using An HP 8510C

**APPENDIX K FARFIELD ANTENNA PATTERNS MEASURED IN THE
ANECHOIC CHAMBER AT TANNER HILL**

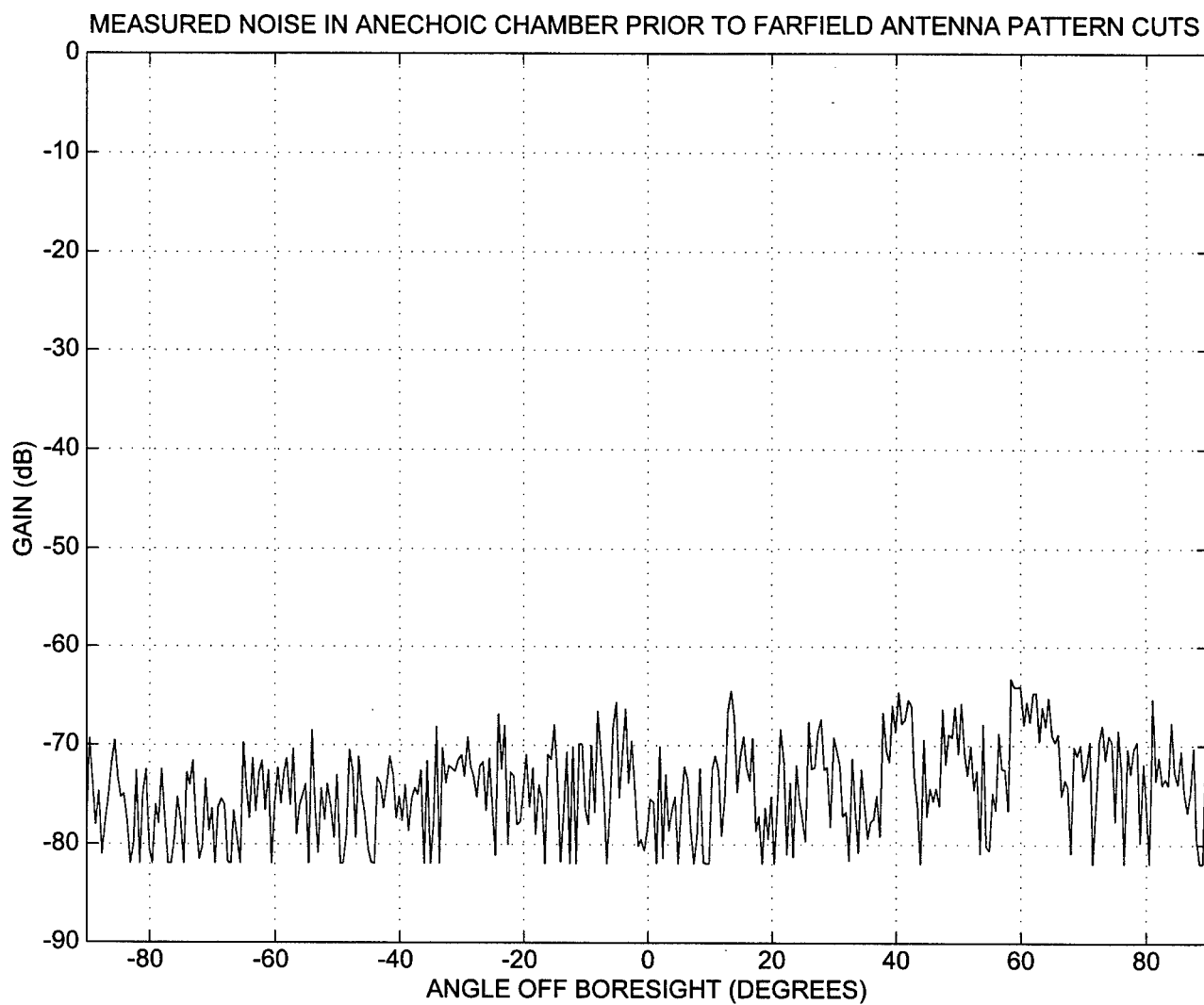


Figure 46. Measured Noise In The Newport Anechoic Chamber Prior To Farfield Antenna Pattern Cut Measurements, Frequency = 9.830 GHz

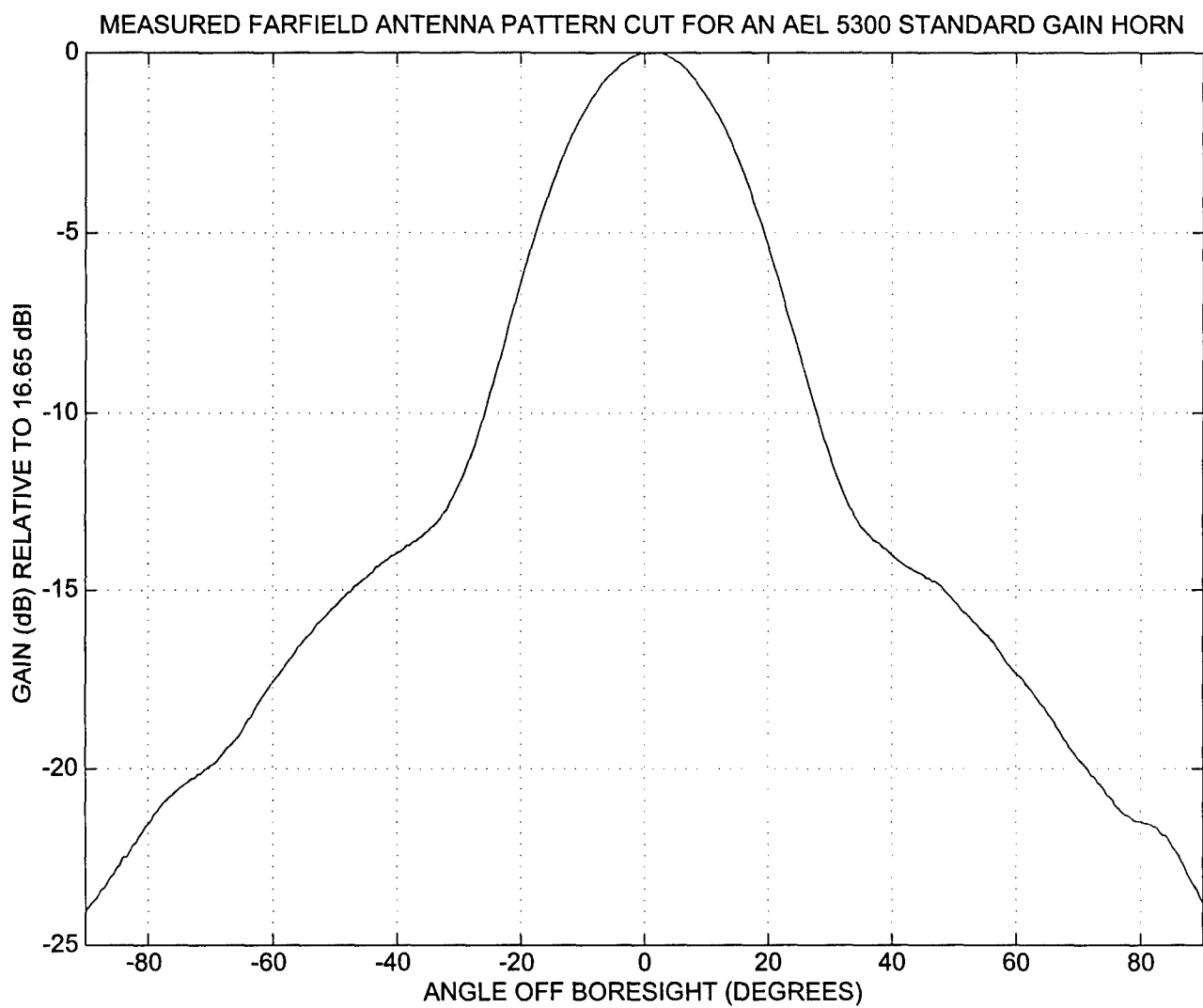


Figure 47. Measured Farfield Antenna Pattern Cut For An AEL 5300 Standard Gain Horn, Frequency = 9.830 GHz

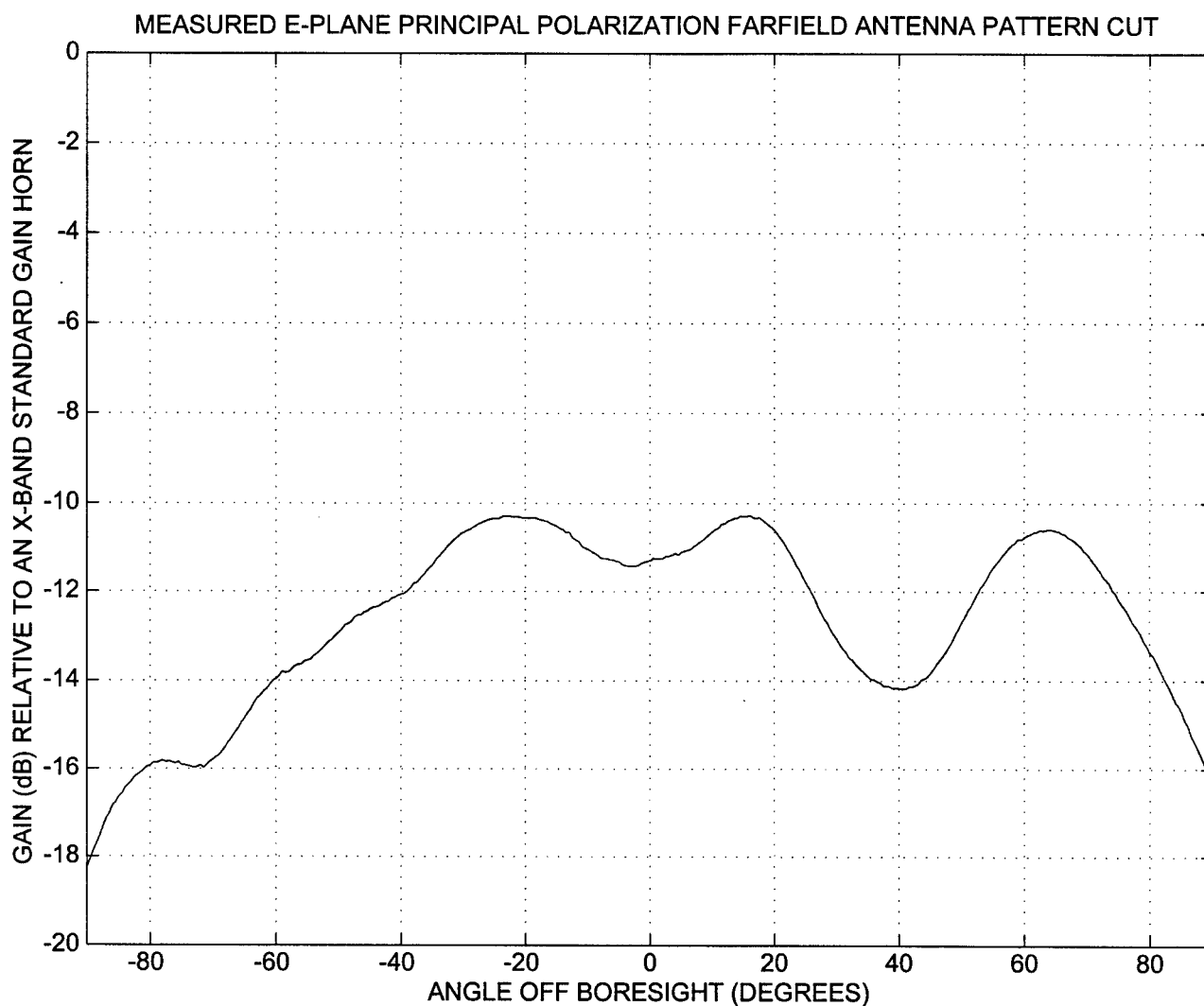


Figure 48. Measured E-Plane Principal Polarization Farfield Antenna Pattern Cut For An Isolated TMM-3 Rectangular Microstrip Patch Element With An Inset Feed, Frequency = 9.830 GHz

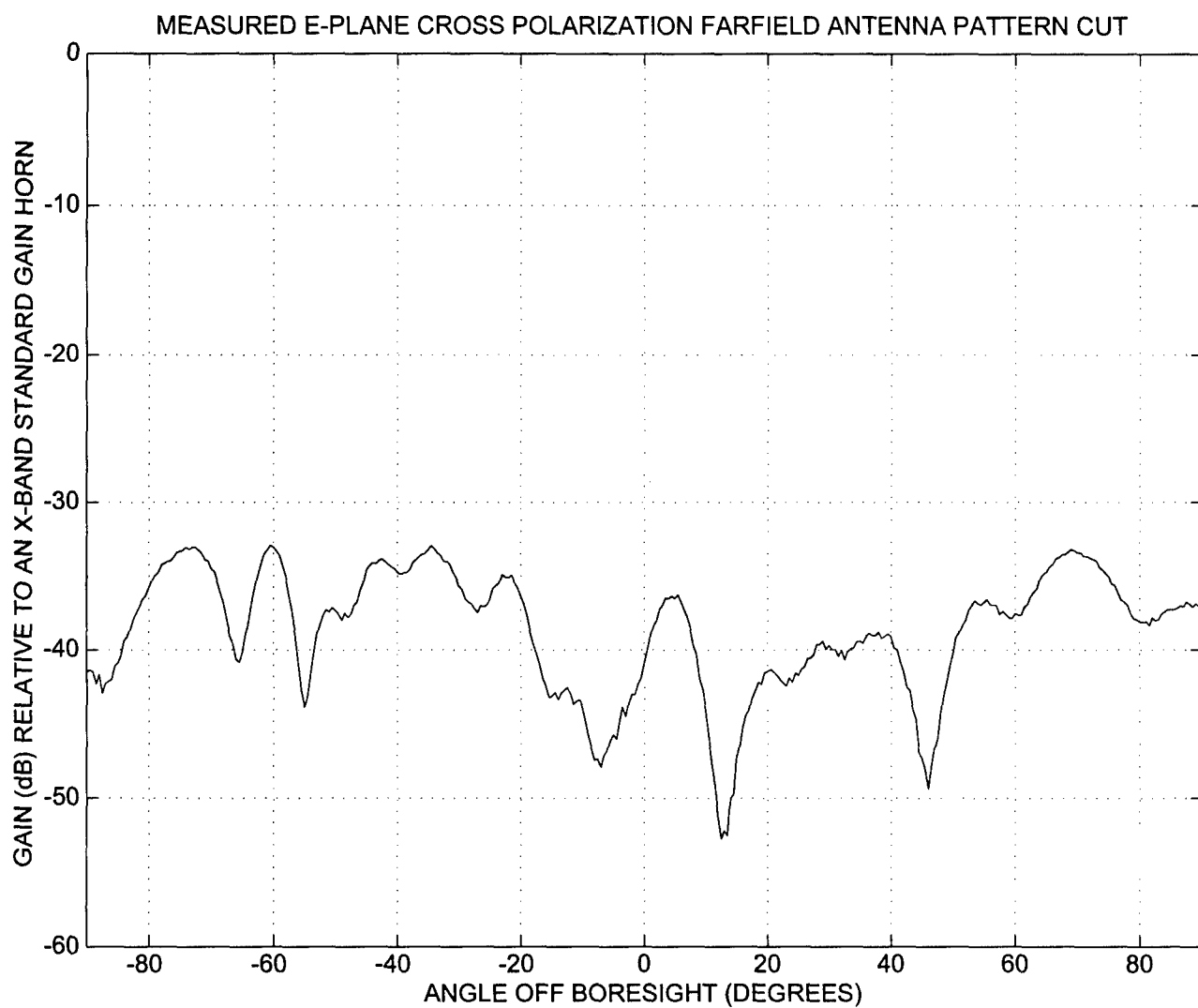


Figure 49. Measured E-Plane Cross Polarization Farfield Antenna Pattern Cut For An Isolated TMM-3 Rectangular Microstrip Patch Element With An Inset Feed, Frequency = 9.830 GHz

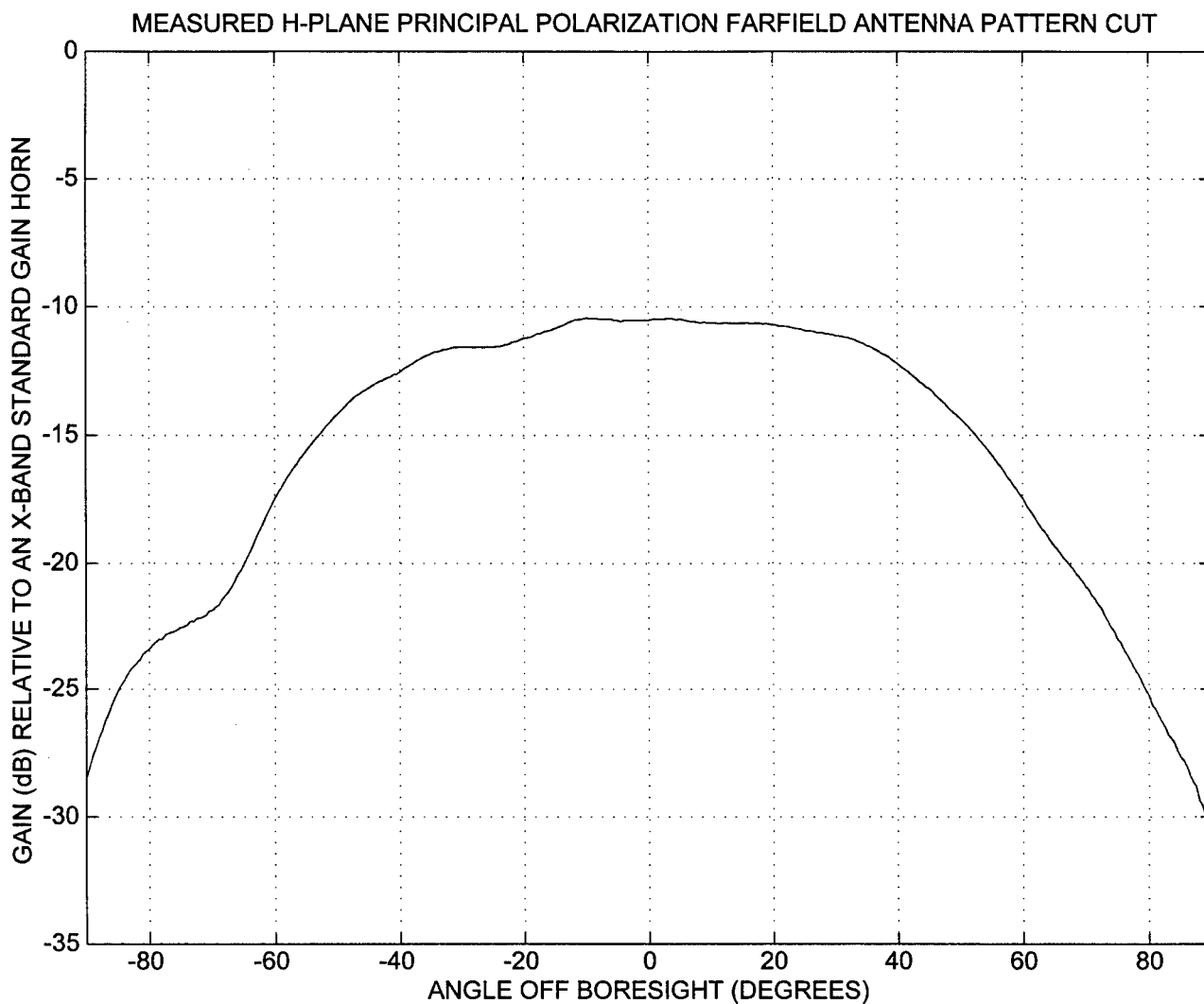


Figure 50. Measured H-Plane Principal Polarization Farfield Antenna Pattern Cut For An Isolated TMM-3 Rectangular Microstrip Patch Element With An Inset Feed, Frequency = 9.830 GHz

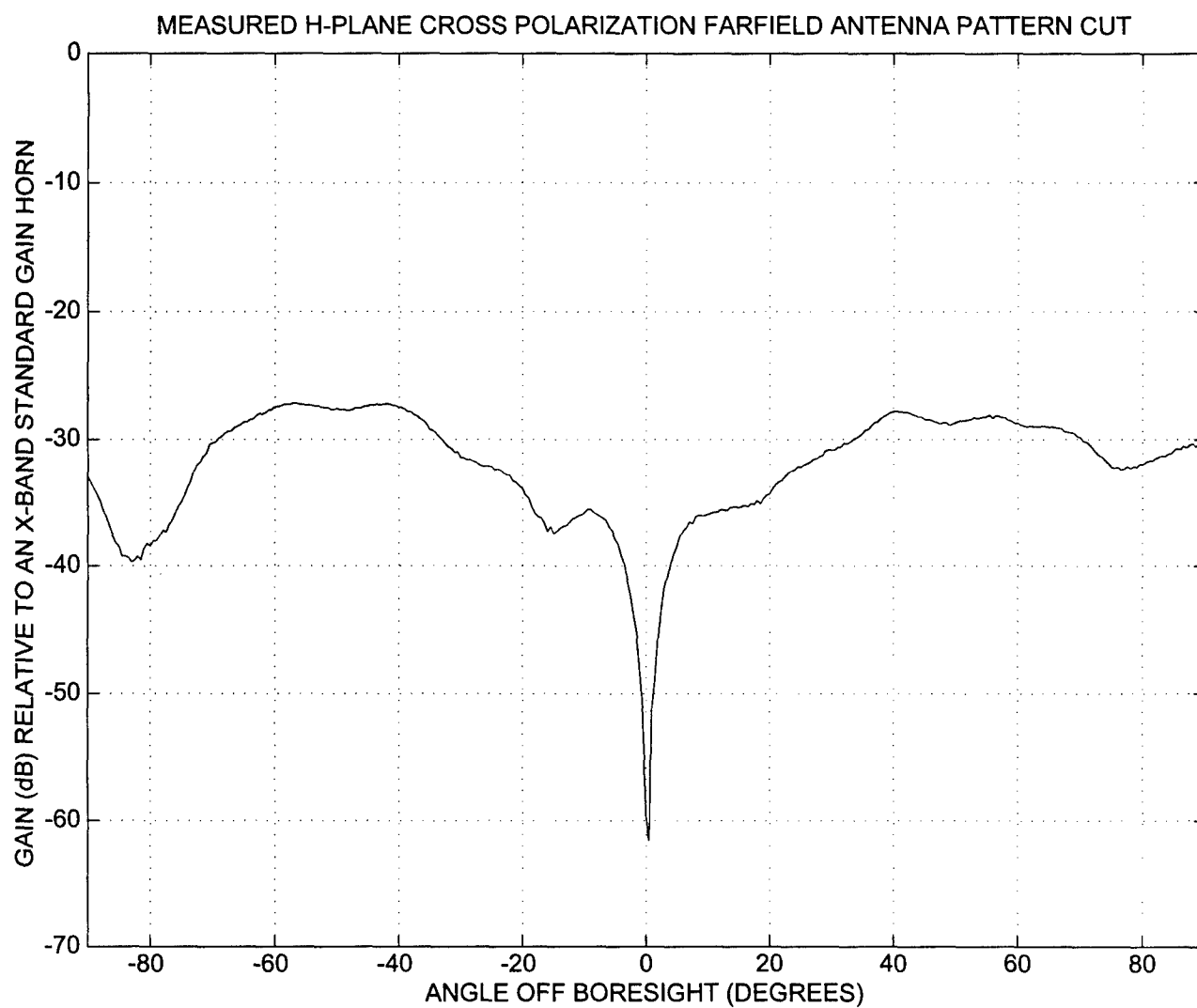


Figure 51. Measured H-Plane Cross Polarization Farfield Antenna Pattern Cut For An Isolated TMM-3 Rectangular Microstrip Patch Element With An Inset Feed, Frequency = 9.830 GHz

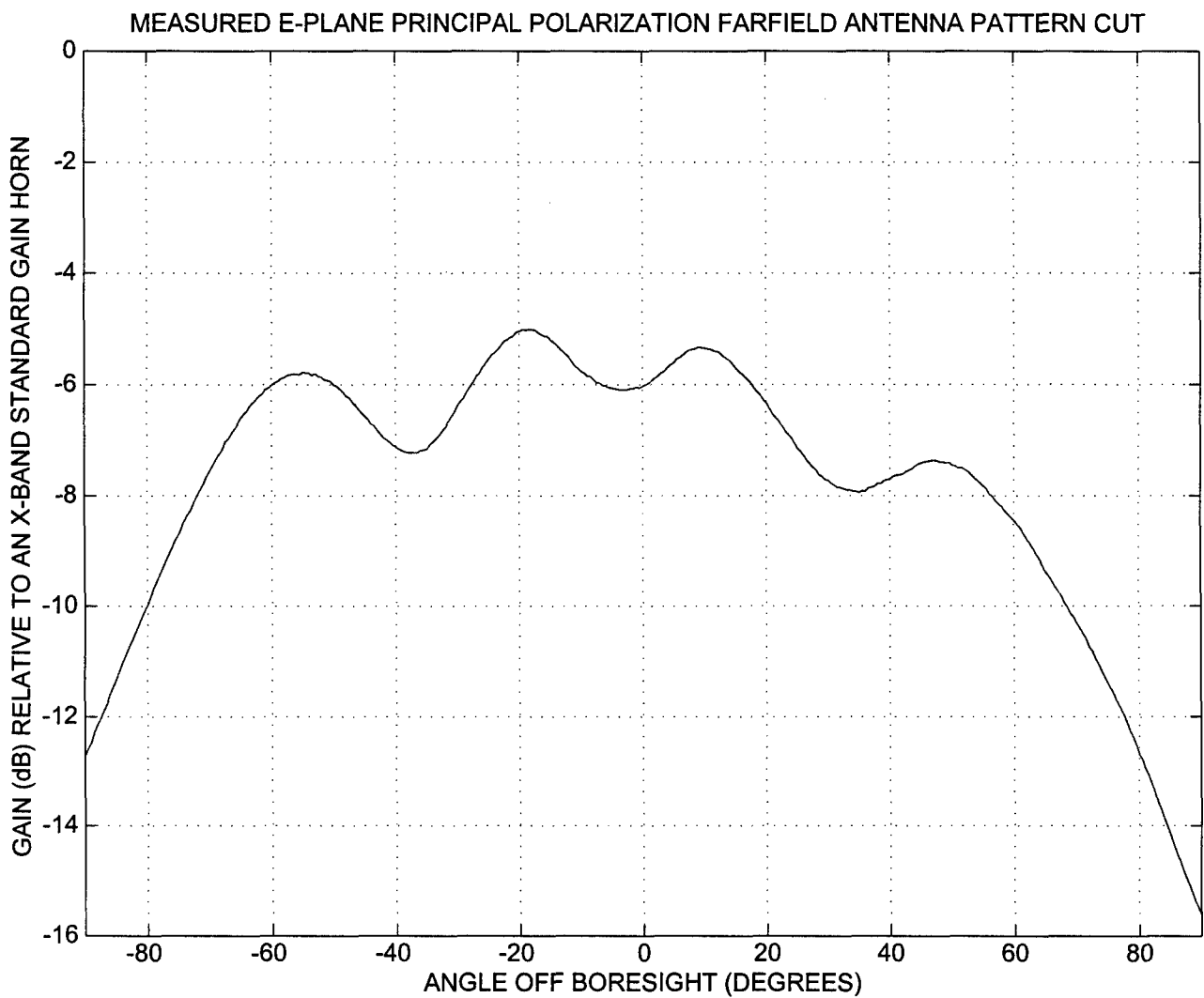


Figure 52. Measured E-Plane Principal Polarization Farfield Antenna Pattern Cut For An Array Of TMM-3 Rectangular Microstrip Patch Elements With Inset Feeds Arrayed In The H-Plane, Frequency = 9.830 GHz

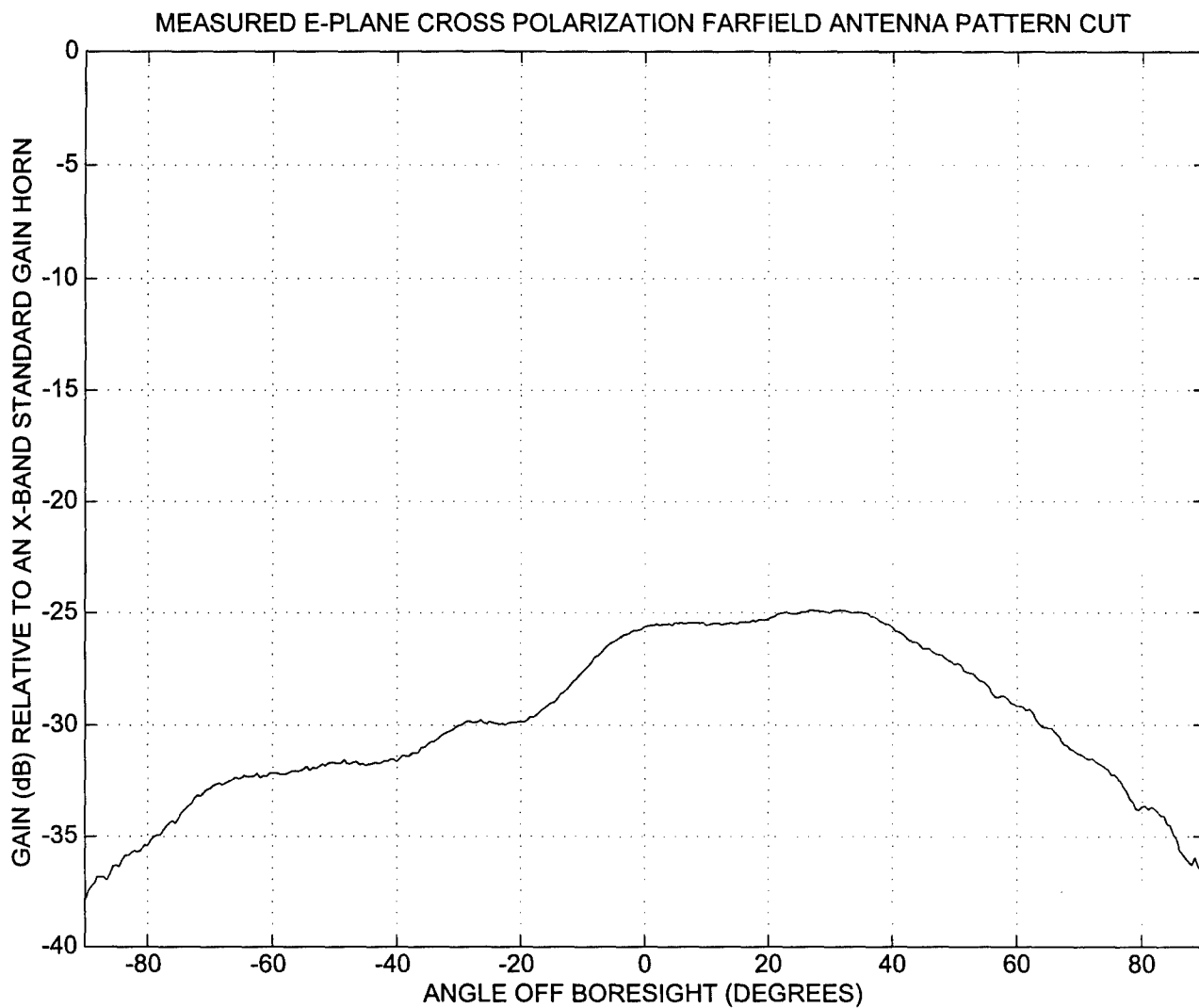


Figure 53. Measured E-Plane Cross Polarization Farfield Antenna Pattern Cut For An Array Of TMM-3 Rectangular Microstrip Patch Elements With Inset Feeds Arrayed In The H-Plane, Frequency = 9.830 GHz

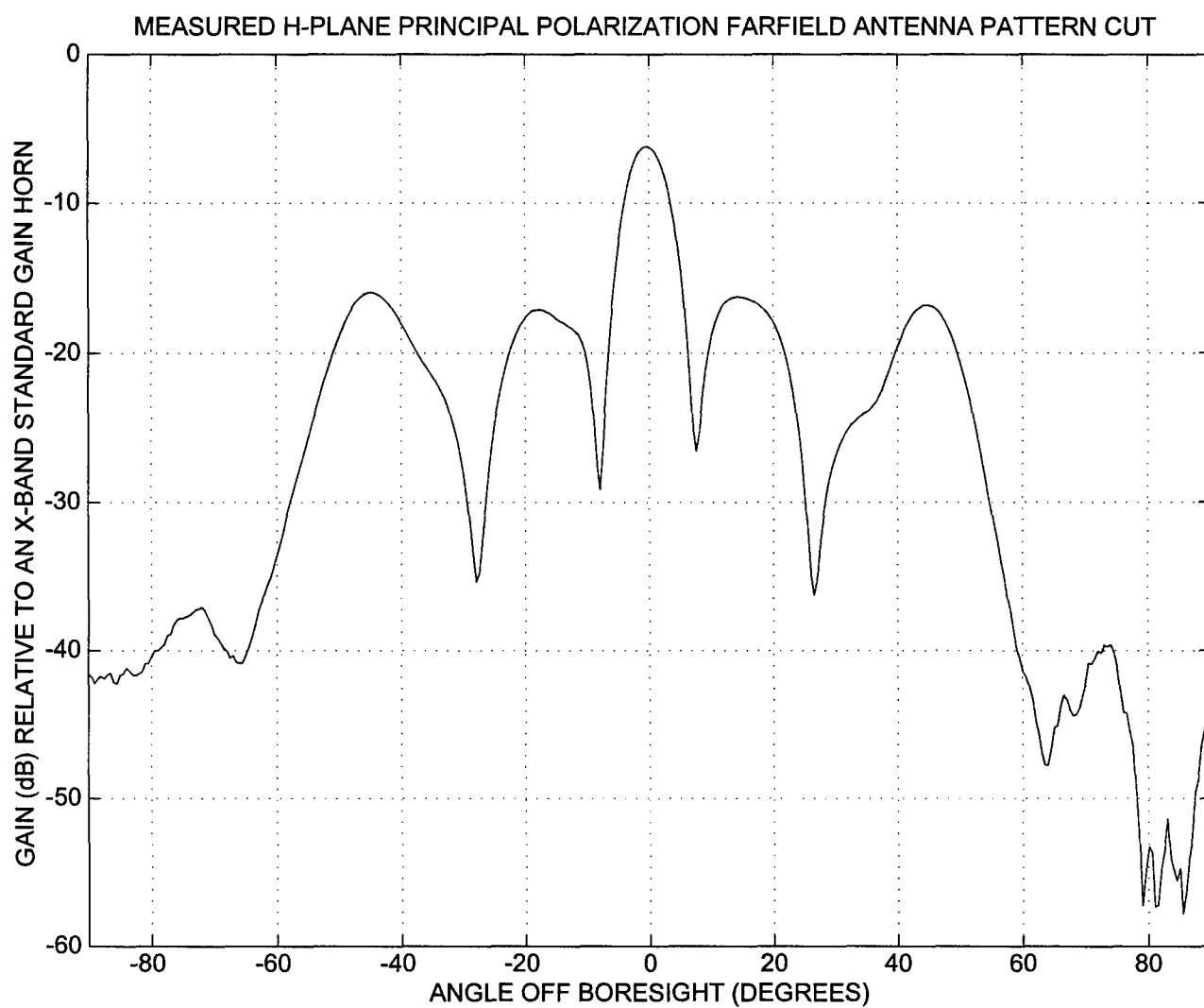


Figure 54. Measured H-Plane Principal Polarization Farfield Antenna Pattern Cut For An Array Of TMM-3 Rectangular Microstrip Patch Elements With Inset Feeds Arrayed In The H-Plane, Frequency = 9.830 GHz

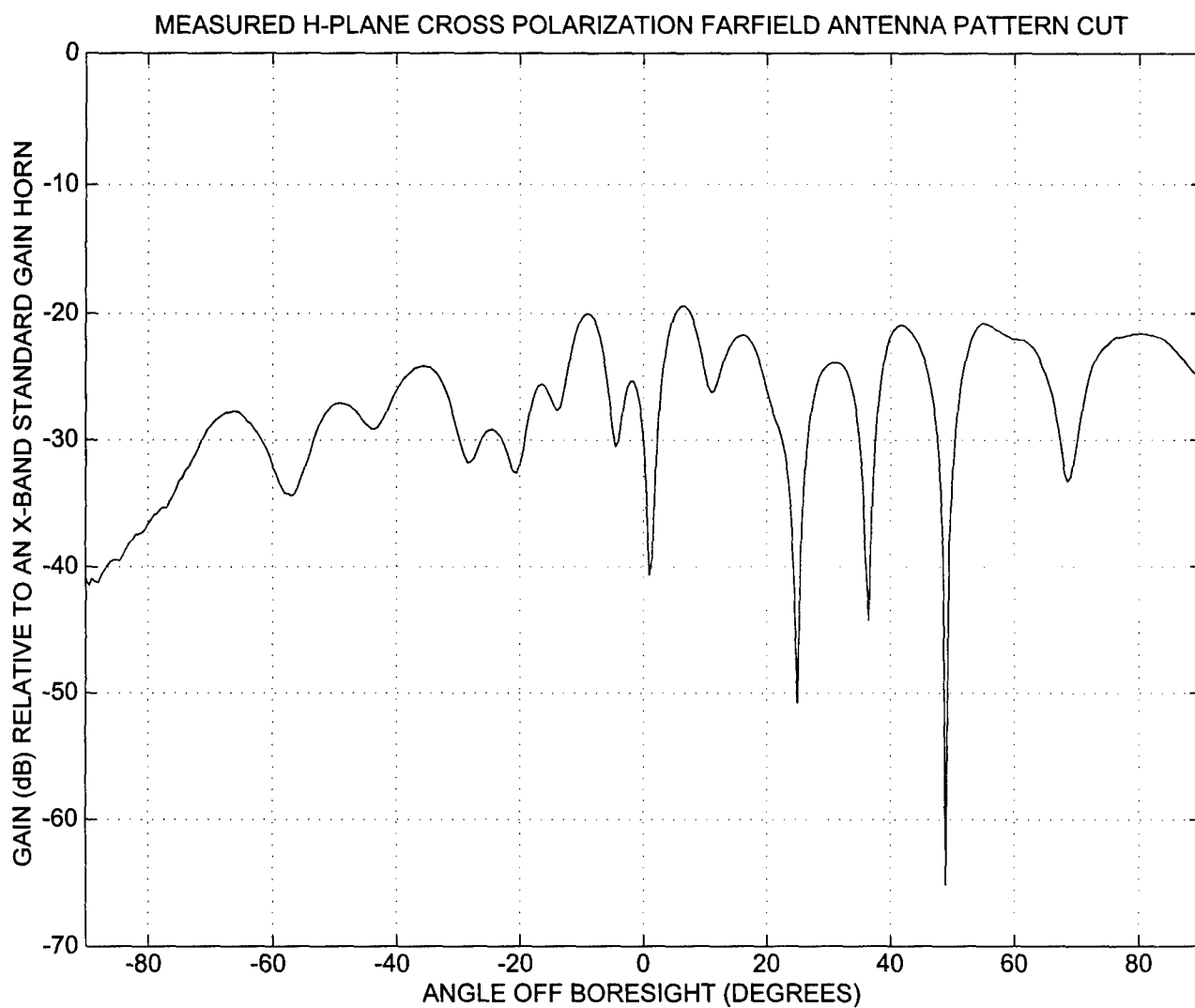


Figure 55. Measured H-Plane Cross Polarization Farfield Antenna Pattern Cut For An Array Of TMM-3 Rectangular Microstrip Patch Elements With Inset Feeds Arrayed In The H-Plane, Frequency = 9.830 GHz

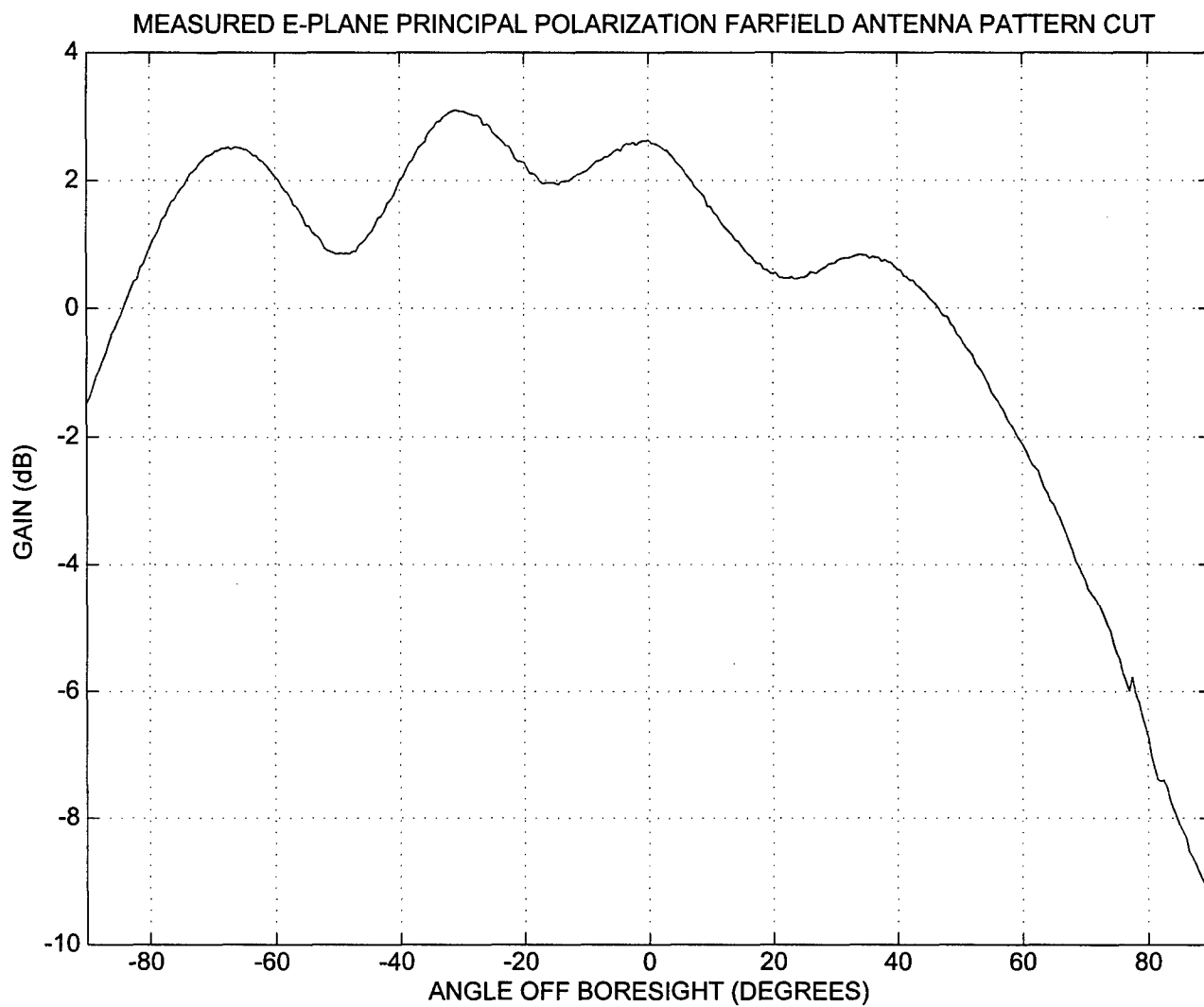


Figure 56. Measured E-Plane Principal Polarization Farfield Antenna Pattern Cut For An Array Of TMM-3 Rectangular Microstrip Patch Elements With Inset Feeds Arrayed In The H-Plane, Gain Not Calibrated, Frequency = 10.000 GHz

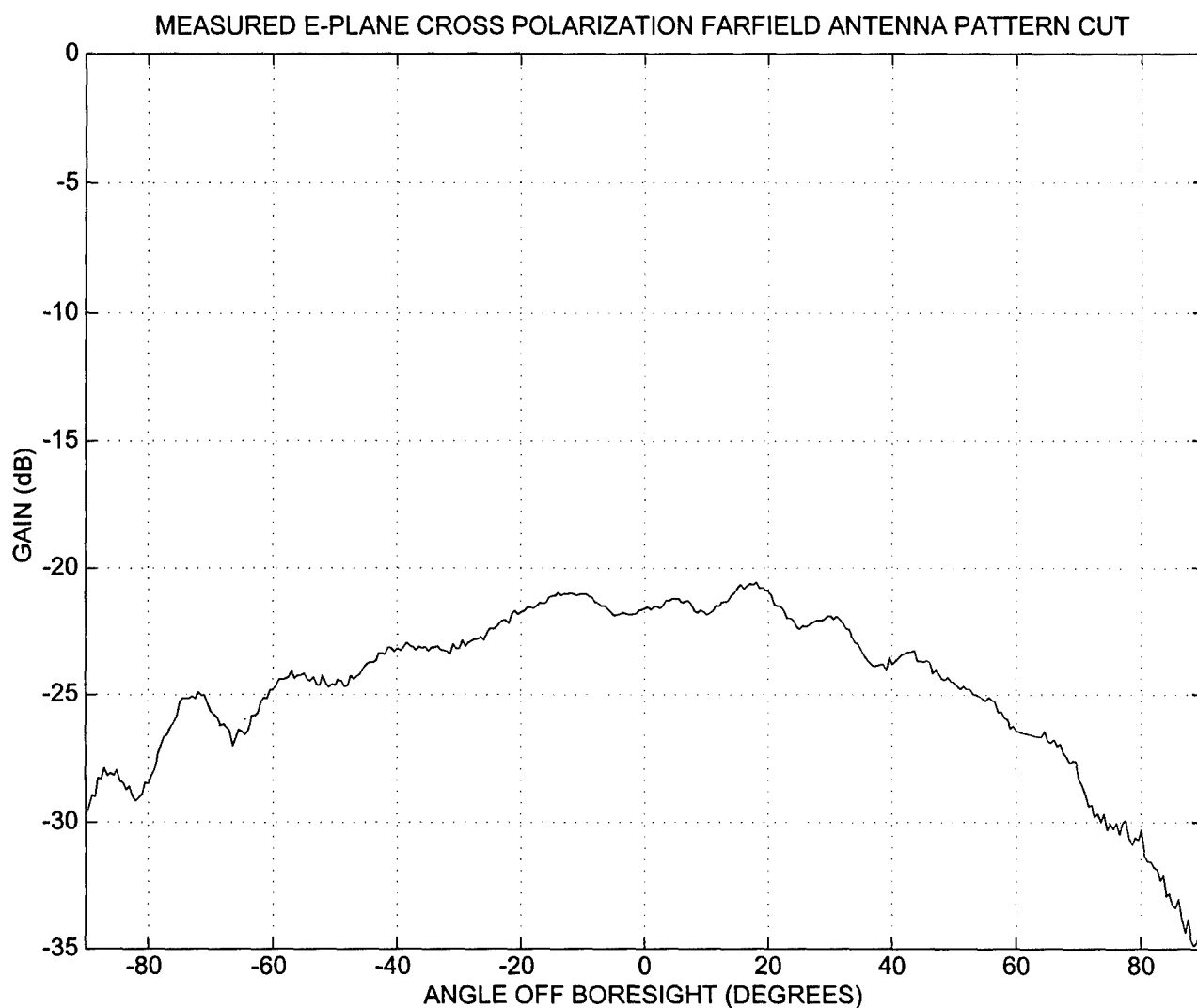


Figure 57. Measured E-Plane Cross Polarization Farfield Antenna Pattern Cut For An Array Of TMM-3 Rectangular Microstrip Patch Elements With Inset Feeds Arrayed In The H-Plane, Gain Not Calibrated, Frequency = 10.000 GHz

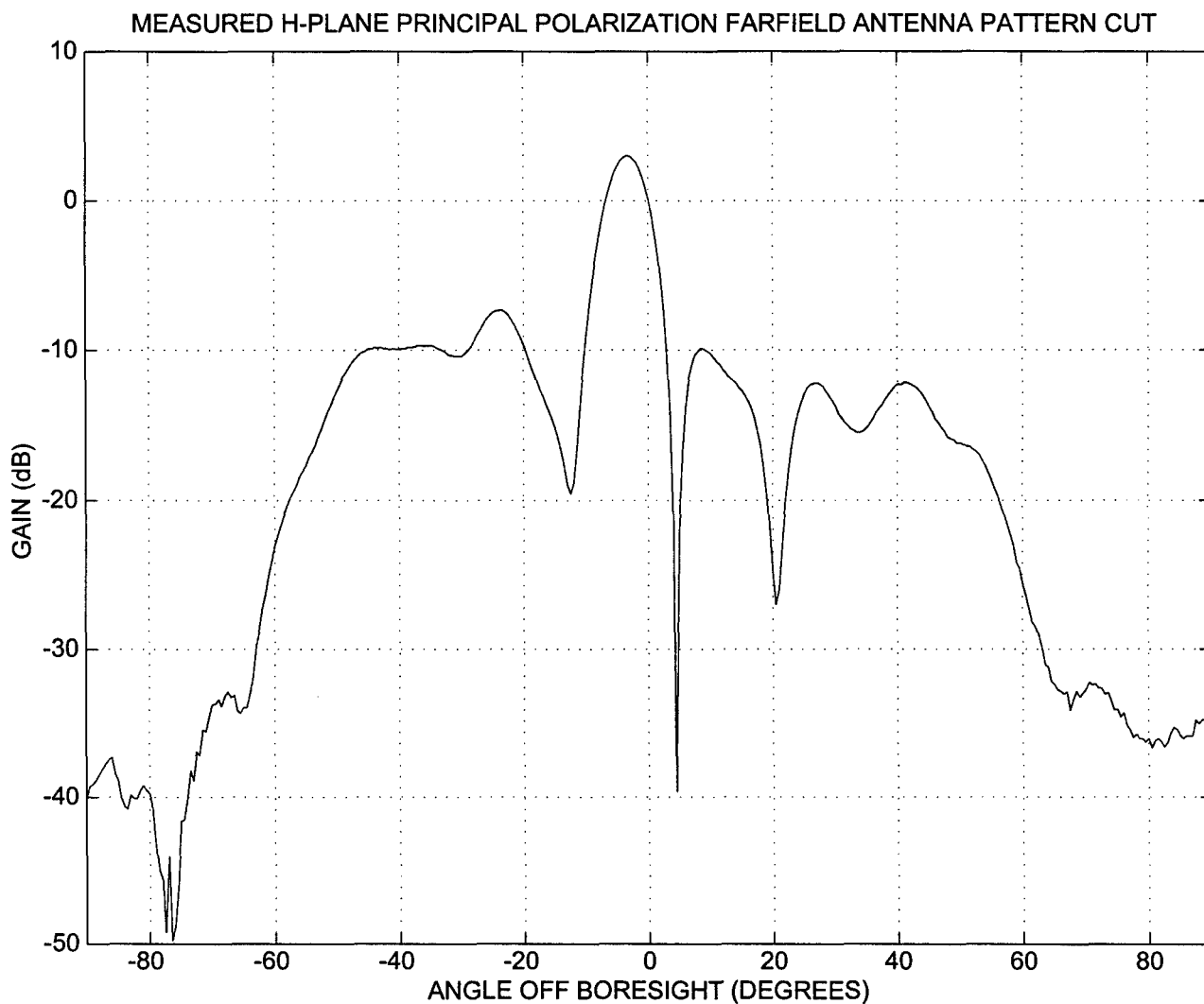


Figure 58. Measured H-Plane Principal Polarization Farfield Antenna Pattern Cut For An Array Of TMM-3 Rectangular Microstrip Patch Elements With Inset Feeds Arrayed In The H-Plane, Gain Not Calibrated, Frequency = 10.000 GHz

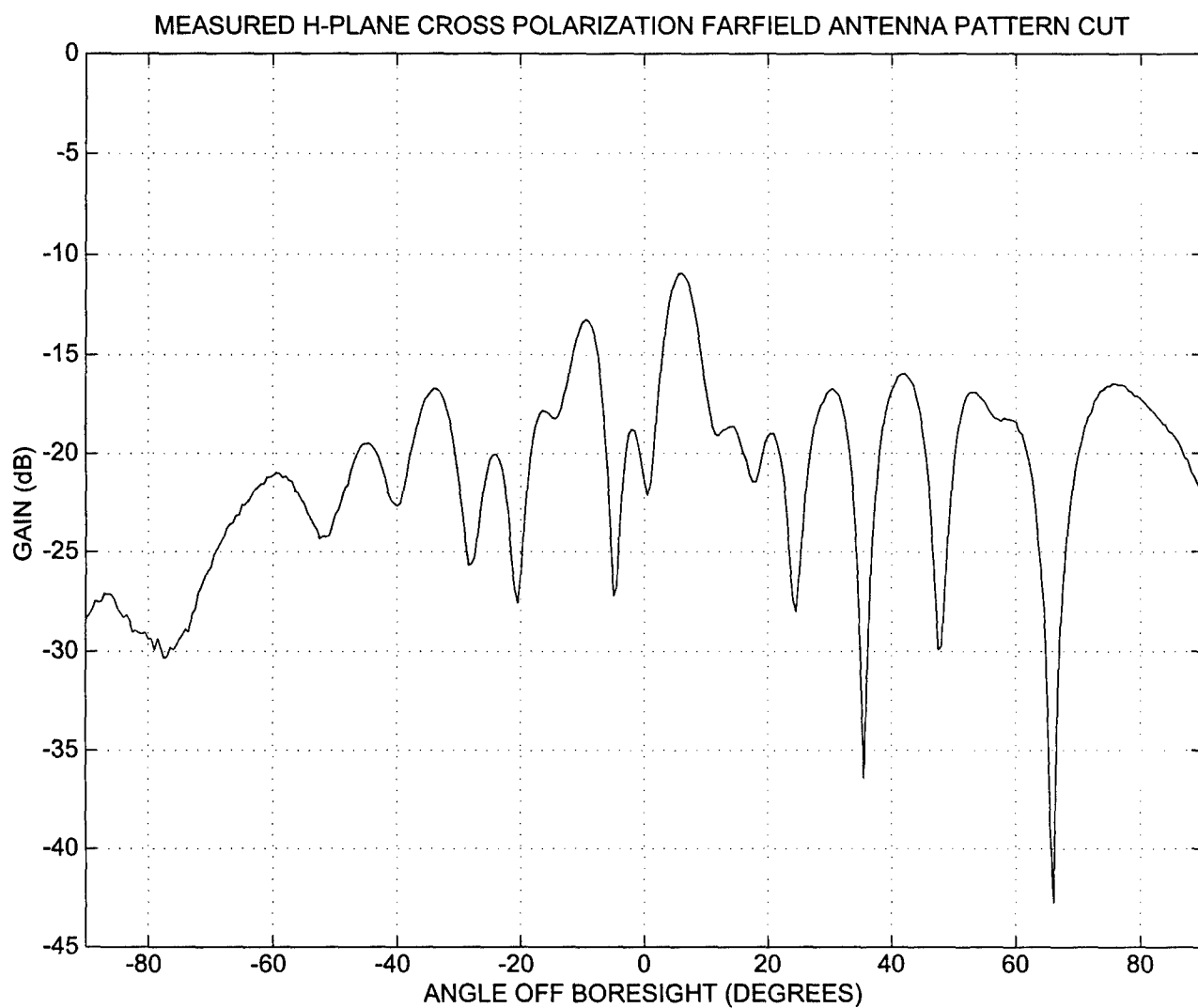


Figure 59. Measured H-Plane Cross Polarization Farfield Antenna Pattern Cut For An Array Of TMM-3 Rectangular Microstrip Patch Elements With Inset Feeds Arrayed In The H-Plane, Gain Not Calibrated, Frequency = 10.000 GHz

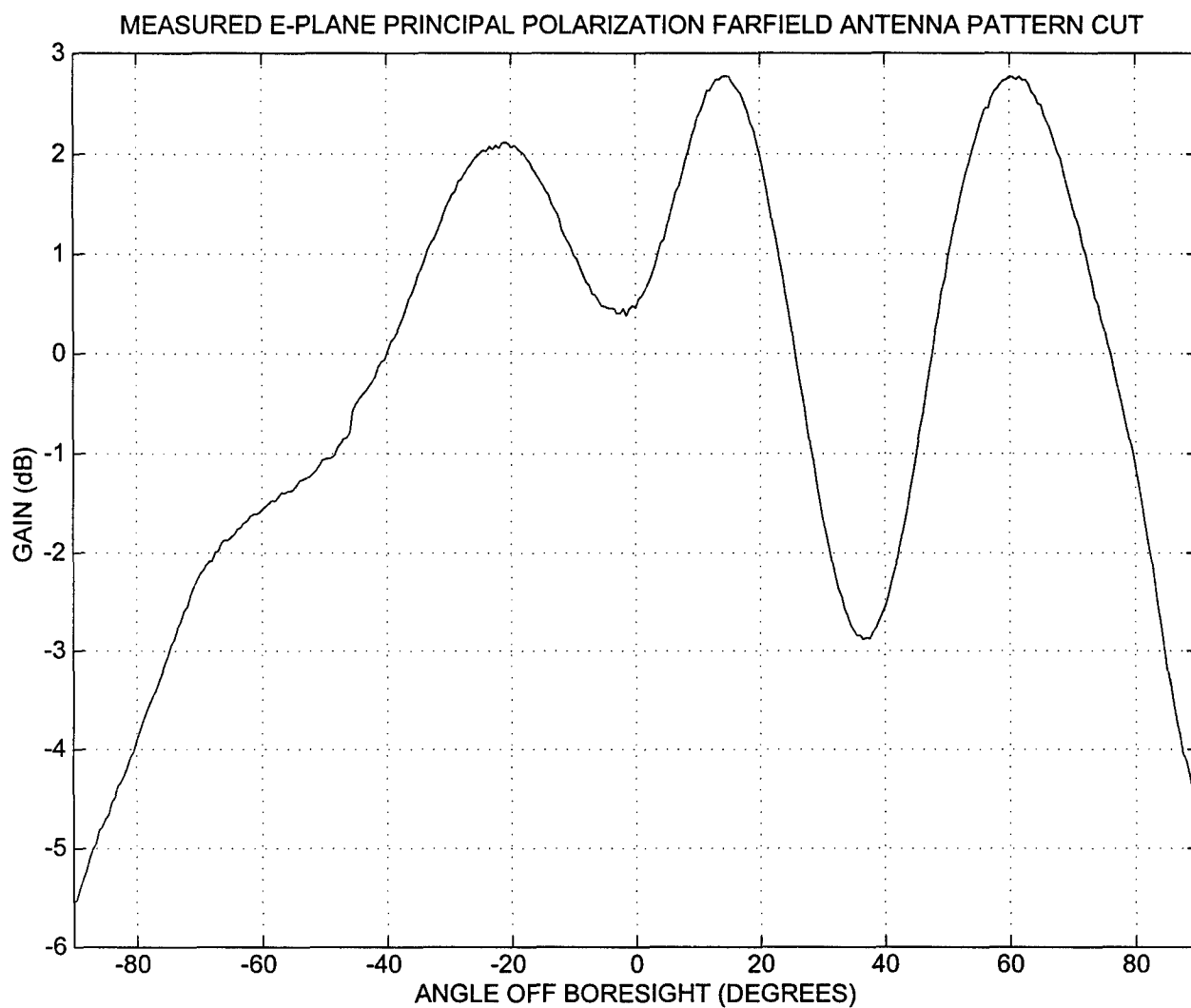


Figure 60. Measured E-Plane Principal Polarization Farfield Antenna Pattern Cut For An Isolated, Trimmed And Painted TMM-3 Rectangular Microstrip Patch Element With An Inset Feed, Gain Not Calibrated, Frequency = 9.975 GHz

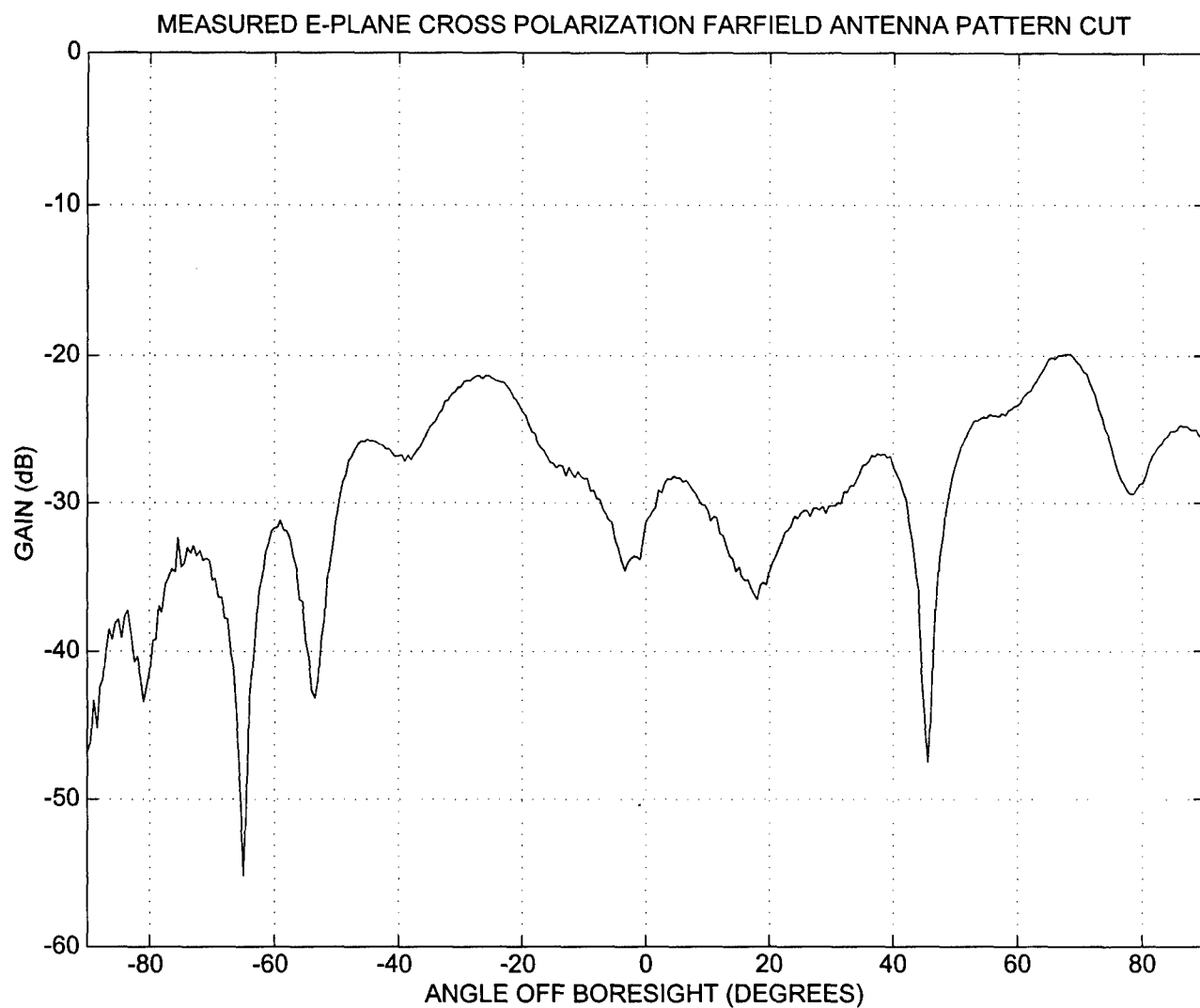


Figure 61. Measured E-Plane Cross Polarization Farfield Antenna Pattern Cut For An Isolated, Trimmed And Painted TMM-3 Rectangular Microstrip Patch Element With An Inset Feed, Gain Not Calibrated, Frequency = 9.975 GHz

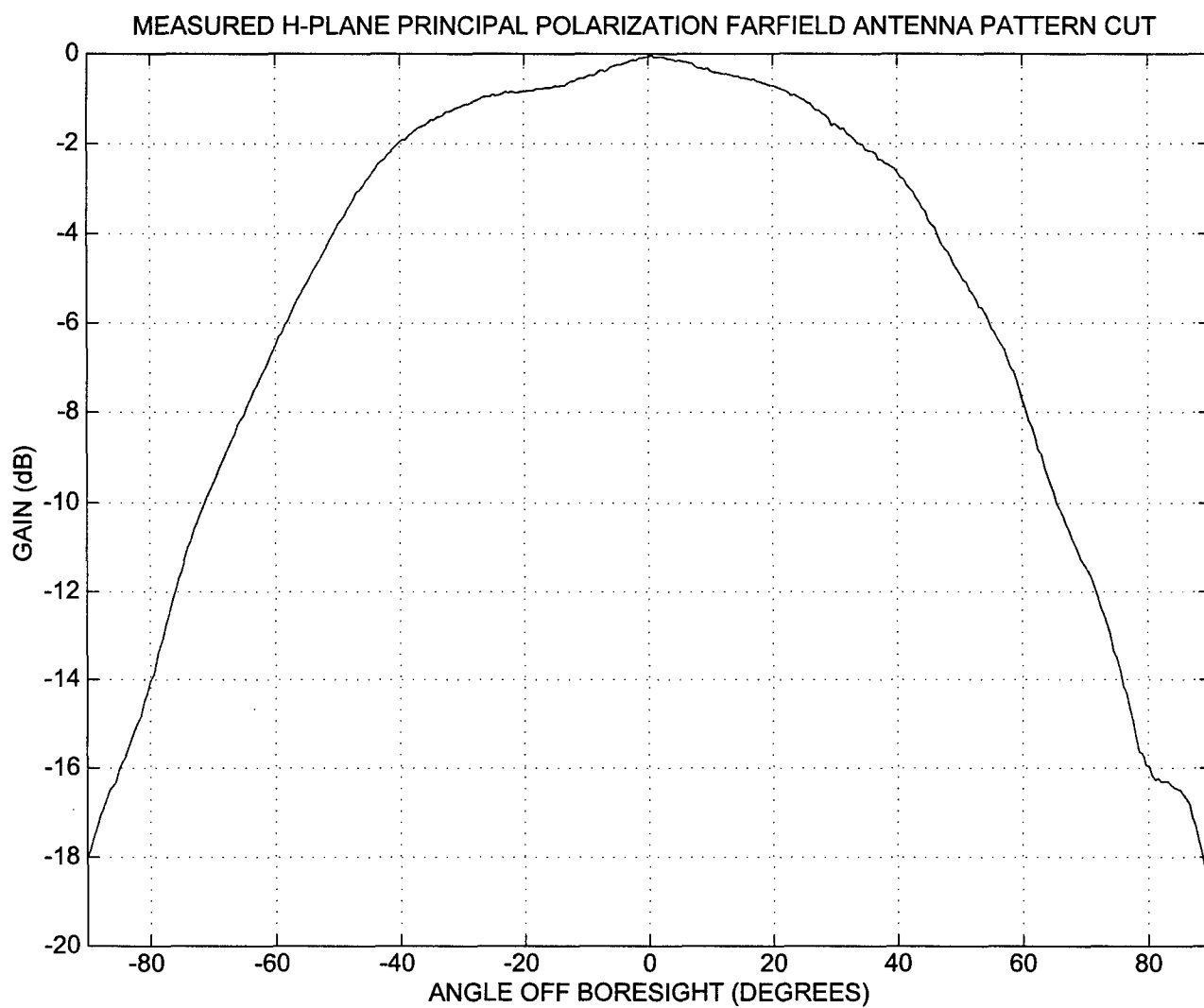


Figure 62. Measured H-Plane Principal Polarization Farfield Antenna Pattern Cut For An Isolated, Trimmed And Painted TMM-3 Rectangular Microstrip Patch Element With An Inset Feed, Gain Not Calibrated, Frequency = 9.975 GHz

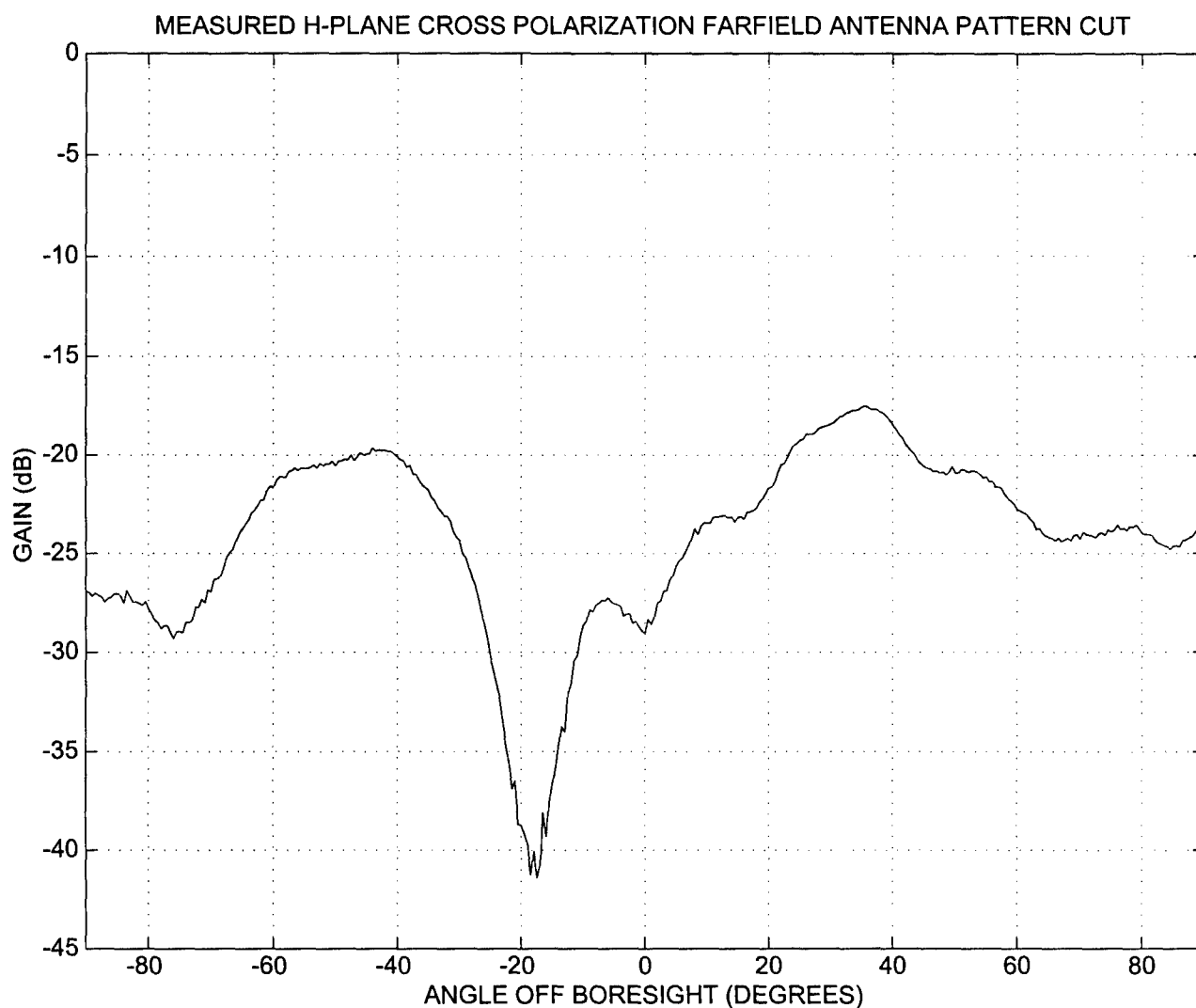


Figure 63. Measured H-Plane Cross Polarization Farfield Antenna Pattern Cut For An Isolated, Trimmed And Painted TMM-3 Rectangular Microstrip Patch Element With An Inset Feed, Gain Not Calibrated, Frequency ≈ 9.975 GHz

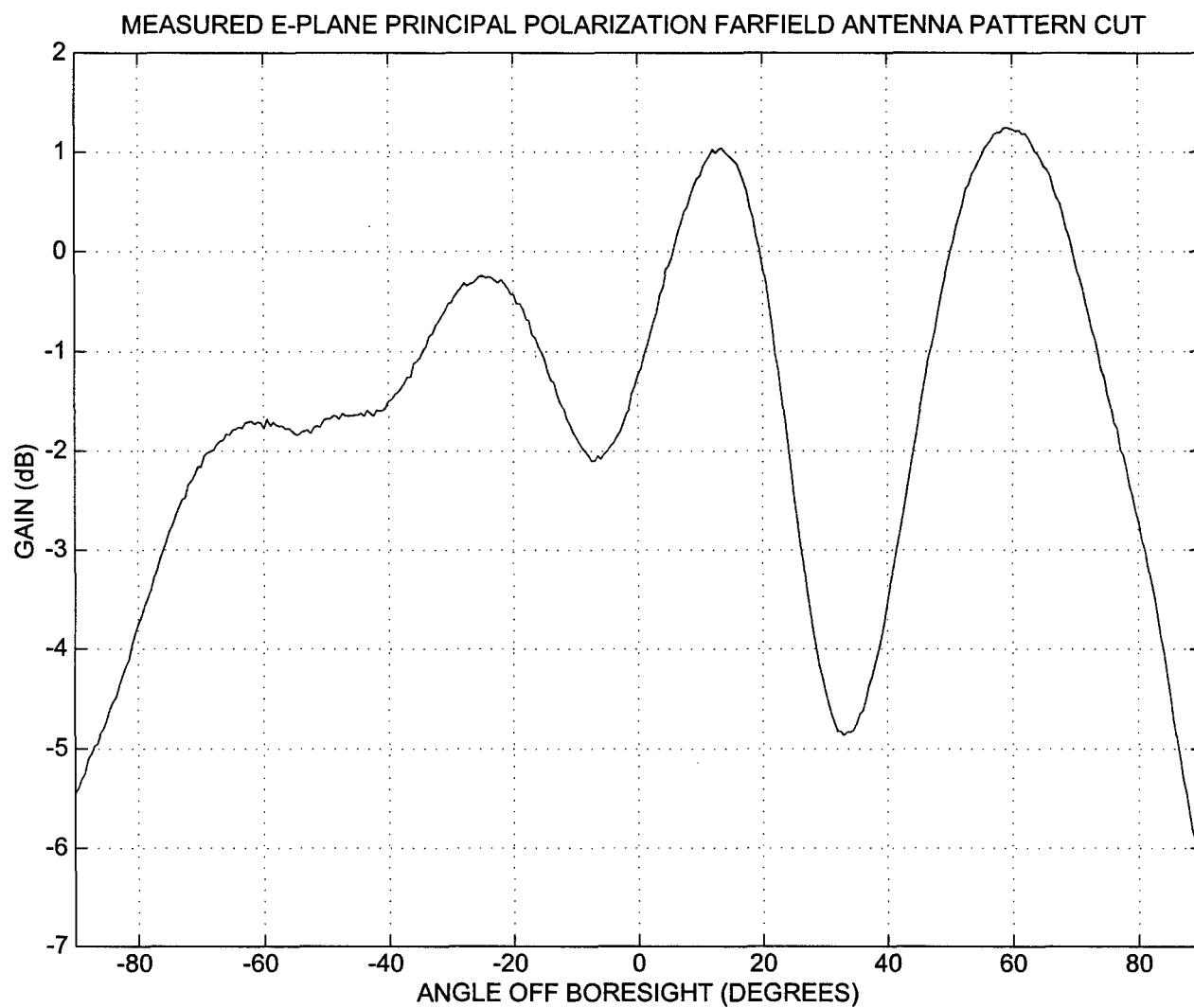


Figure 64. Measured E-Plane Principal Polarization Farfield Antenna Pattern Cut For An Isolated, Trimmed And Painted TMM-6 Rectangular Microstrip Patch Element With An Inset Feed, Gain Not Calibrated, Frequency = 10.135 GHz

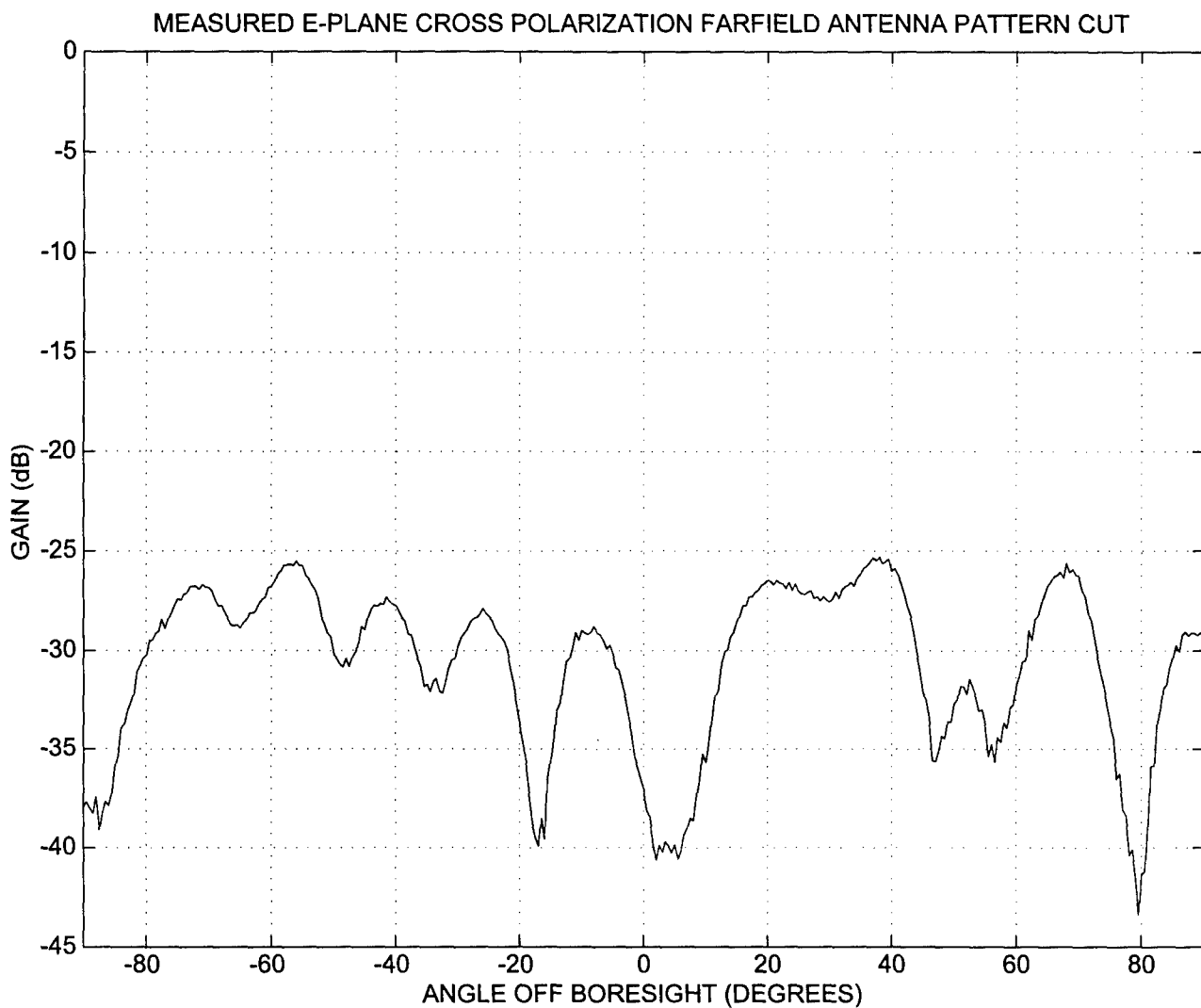


Figure 65. Measured E-Plane Cross Polarization Farfield Antenna Pattern Cut For An Isolated, Trimmed And Painted TMM-6 Rectangular Microstrip Patch Element With An Inset Feed, Gain Not Calibrated, Frequency = 10.135 GHz

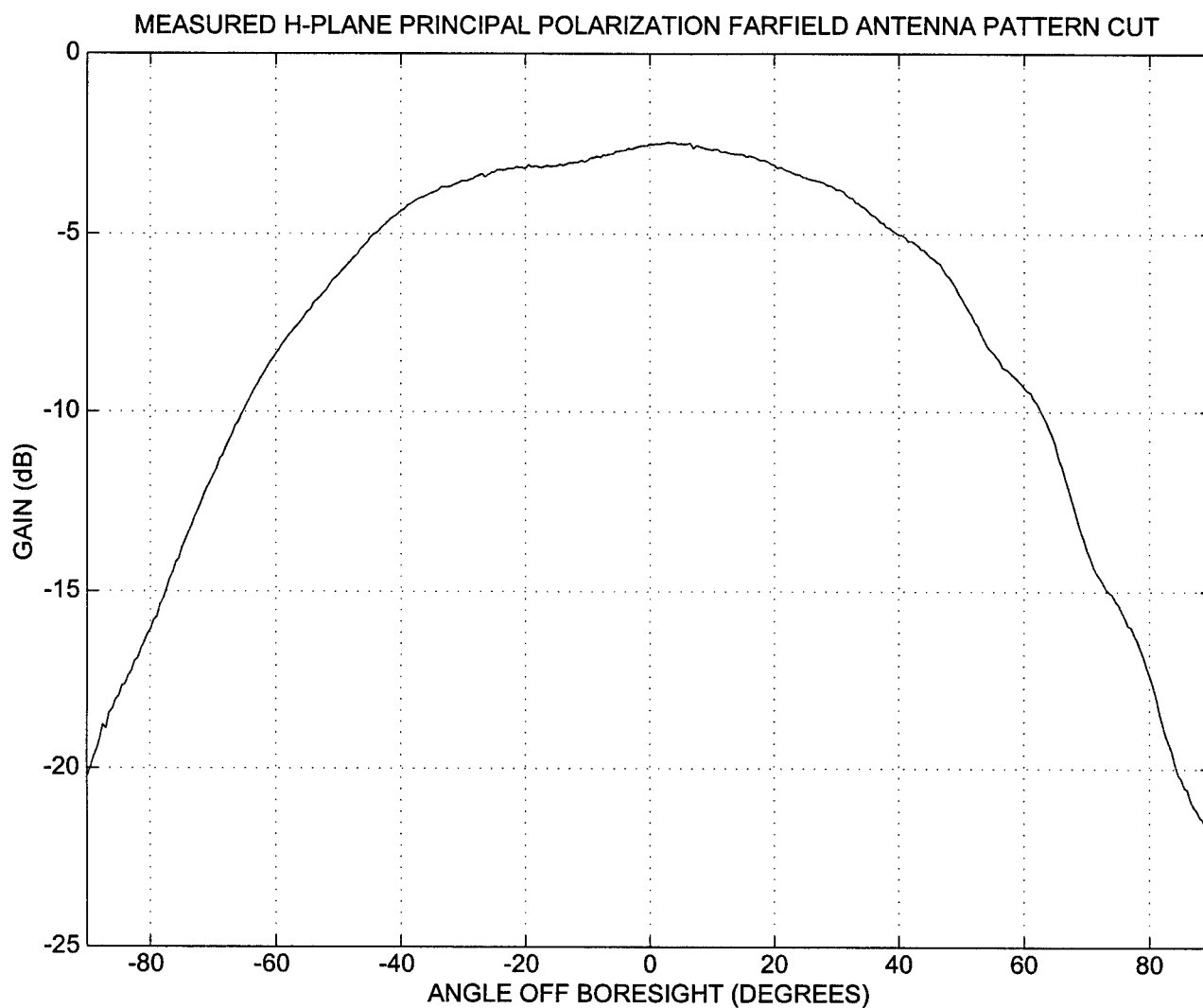


Figure 66. Measured H-Plane Principal Polarization Farfield Antenna Pattern Cut For An Isolated, Trimmed And Painted TMM-6 Rectangular Microstrip Patch Element With An Inset Feed, Gain Not Calibrated, Frequency = 10.135 GHz

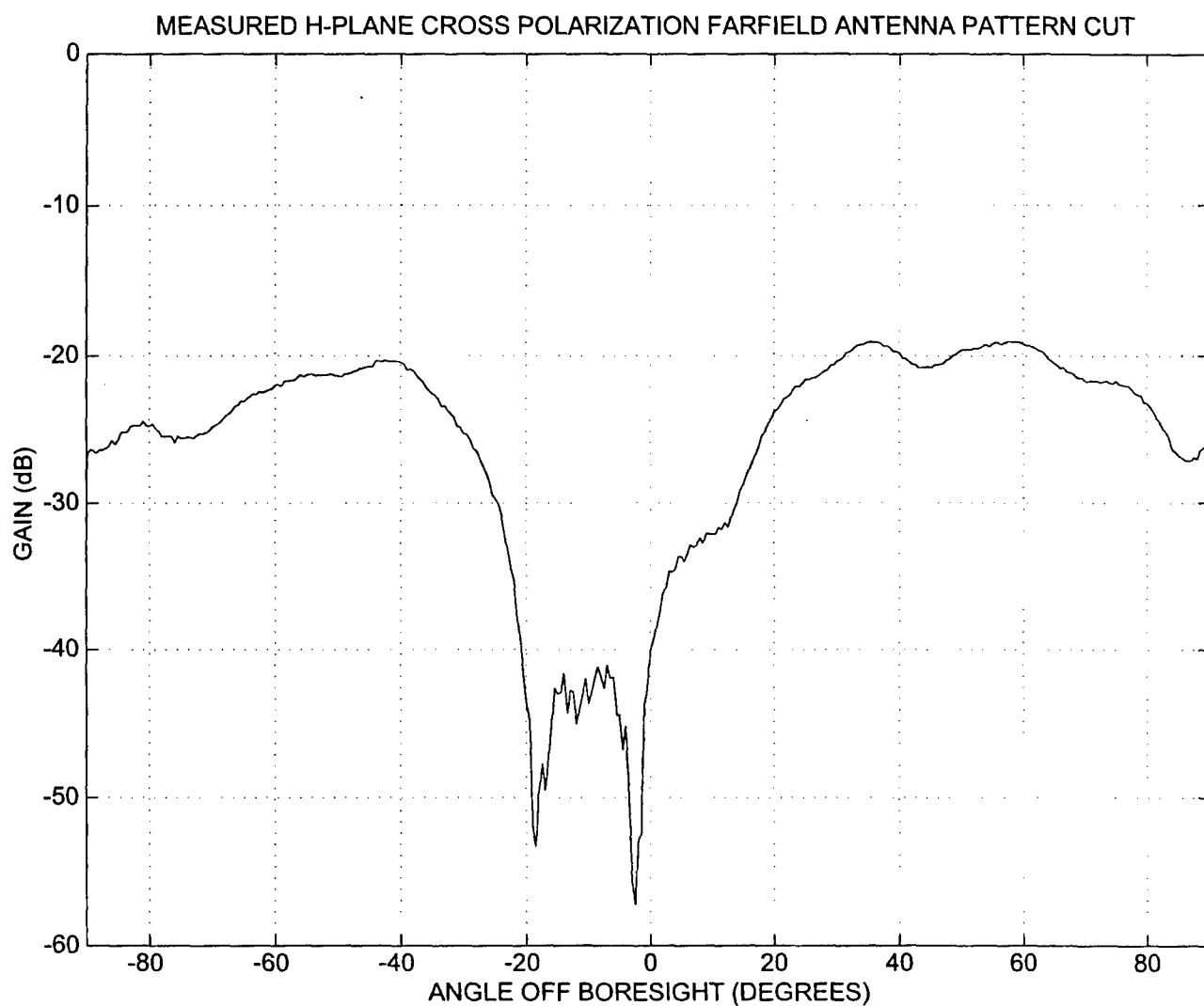


Figure 67. Measured H-Plane Cross Polarization Farfield Antenna Pattern Cut For An Isolated, Trimmed And Painted TMM-6 Rectangular Microstrip Patch Element With An Inset Feed, Gain Not Calibrated, Frequency = 10.135 GHz

APPENDIX L MODELING AN ISOLATED, RECTANGULAR, INSET FED TMM-6 MICROSTRIP PATCH AND ITS FEEDLINE BY MEANS OF TRIANGULAR BASIS FUNCTIONS PREDICTED LARGE VSWR VALUES (GROSS IMPEDANCE MISMATCH BETWEEN THE FEEDLINE AND THE PATCH)

Crude modeling of a 100 ohm microstrip feedline and an isolated, inset fed rectangular microstrip patch on TMM-6 substrate with one oz Cu metallization was performed using triangular basis functions long after the test circuits had been designed and built and the data collected. There were insufficient resources available on the computer system being used to model a whole subarray of patches and their feedlines. Therefore, attention was confined to a single isolated patch and its feedline. Very disturbing results were computed that, had they been available to us when we were designing the patches, would have caused us to do a complete redesign.

The computed voltage standing wave ratio (VSWR) values were very large at the frequencies where modeling was performed:

- at least 378.1 at 10.000 GHz
- at least 64.7 at 9.680 GHz

The above numbers were arrived at by dividing $\text{mag}(\text{max longitudinal current})$ by $\text{mag}(\text{min longitudinal current})$ as computed along the feedline. The numbers are inaccurate due to the coarse modeling employed. It is difficult to say whether current at a peak or a trough of the standing wave on the feedline was sampled in each case. The VSWR values were probably worse than what are listed here.

The microstrip patch input impedance differs markedly from the feedline characteristic impedance (100 ohms) at the frequencies where the modeling was performed.

- the microstrip patch input impedance roughly equals $-j22.5$ ohms at 10.000 GHz.
- the microstrip patch input impedance roughly equals $+j95.0$ ohms at 9.680 GHz.

The above numbers are inaccurate due to the coarse modeling employed. Z_0 for the microstrip feedline equals 100 ohms. The isolated TMM-6 microstrip patches are clearly not matched to their feedlines. Of course, the presence of the other patches and their feedlines markedly changes the electromagnetic environment due to coupling, but the effect of adjacent conductors on the matching between the patches and their feedlines was not investigated.

Below are shown two plots (Figures 68 and 69) illustrating the longitudinal current (that component of the current travelling down the length of the feedline) computed at various points along the feedline for two X-band frequencies.

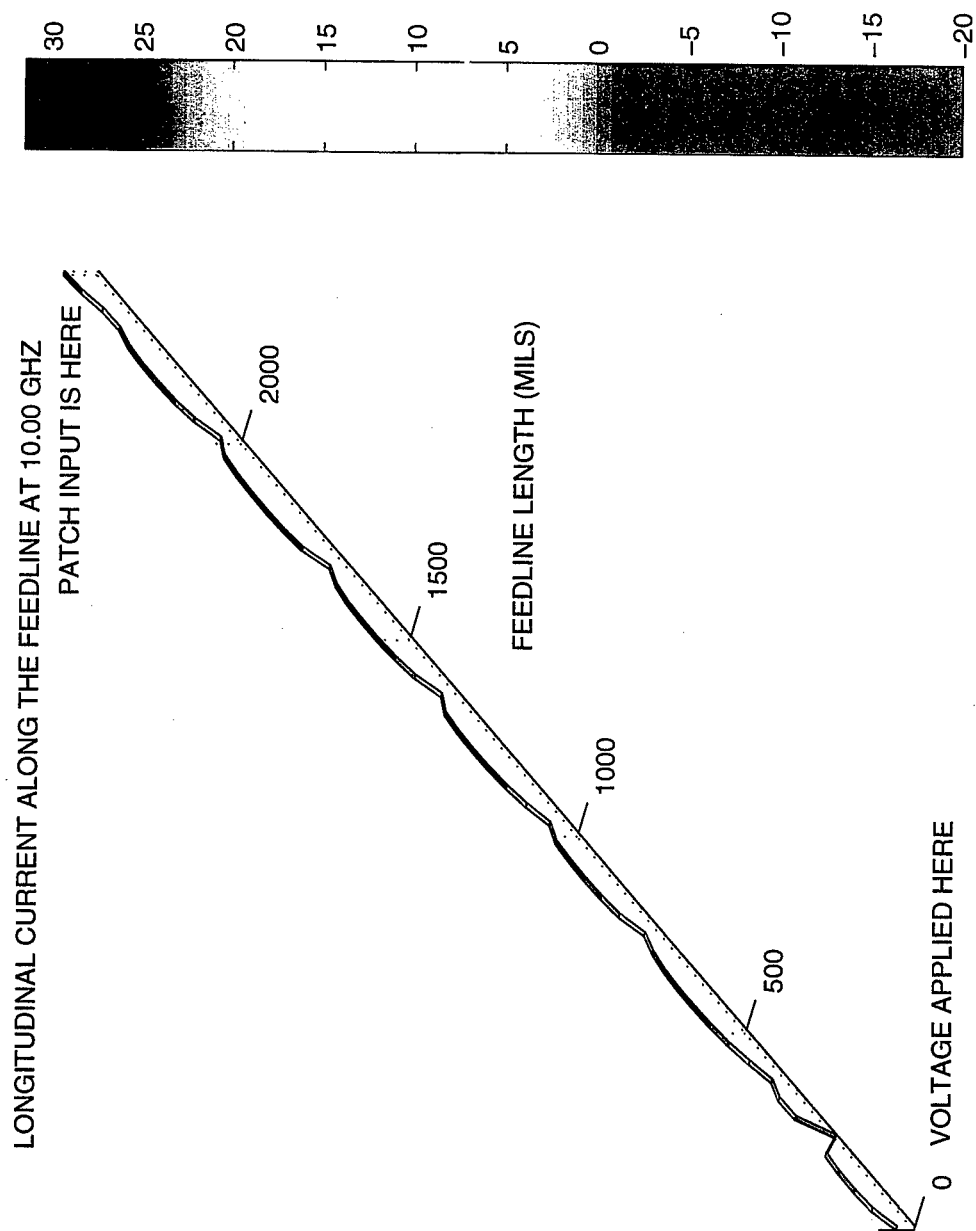


Figure 68. Longitudinal Current Along The 100 Ohm Feedline Leading Up To An Isolated Microstrip Patch With An Inset Feed. Fabricated On TMM-6 Substrate At 10.00 GHz

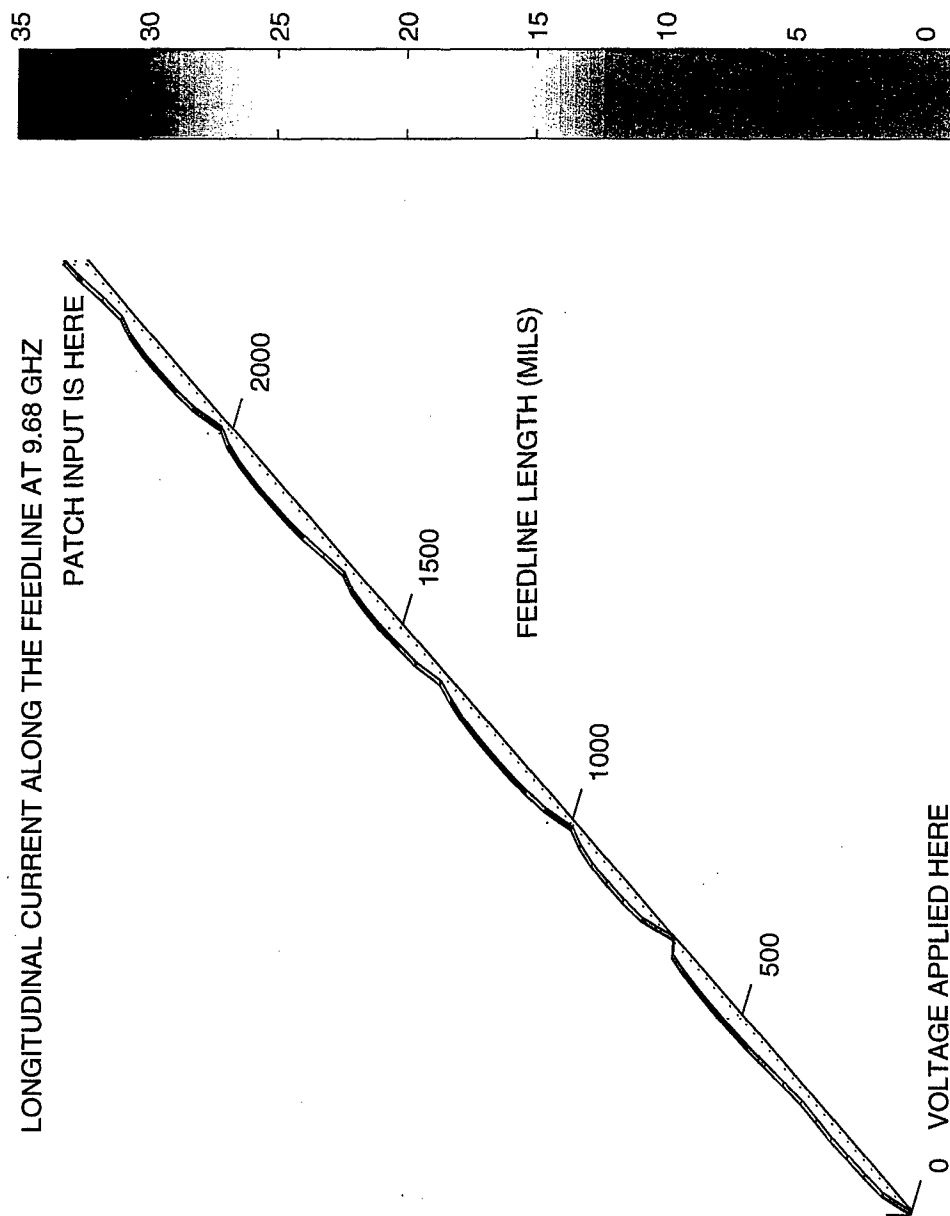


Figure 69. Longitudinal Current Along The 100 Ohm Feedline Leading Up To An Isolated Microstrip Patch With An Inset Feed Fabricated On TMM-6 Substrate At 9.68 GHz